Development and Analysis of SARS-CoV-2 Spike Receptor Binding Domain-Targeting Aptamers

by

Rose Chan

A thesis submitted to the Faculty of Graduate Studies of

The University of Manitoba

In partial fulfilment of the requirements of the degree of

Master of Science

Department of Medical Microbiology and Infectious Diseases

University of Manitoba

Winnipeg

Copyright © 2025 by Rose Chan

Abstract

The severe acute respiratory syndrome coronavirus 2 (SARS-CoV-2) pandemic has highlighted the need for developing both diagnostic and therapeutic tools for emerging diseases. Development of aptamers, nucleic acid-based ligands that bind to target molecules, has become an increasingly popular field in the context of drug discovery and diagnostics. Due to its simplicity, low-cost, and rapid synthesis, aptamer-based diagnostic tools have shown to be on par with antibody-based lateral flow assays and RT-qPCR, which make aptamers a potentially powerful and flexible tool to respond to future outbreaks. The SARS-CoV-2 viral surface receptor Spike protein is a prime candidate target for both diagnostic and therapeutic purposes. Through the process of systematic evolution of ligands by exponential enrichment (SELEX), receptor binding site (S-RBD)-specific aptamers were screened and developed over multiple cycles of SELEX. Amplified binding sequences from each round of selection were collected and assessed using Bio-layer interferometry (BLI), electrophoretic mobility shift assay (EMSA), and qualitative polymerase chain reaction (qPCR) melt curve analysis. The final mature heterogeneous aptamer pool (10R) was then purified and sequenced on the Illumina next generation sequencing (NGS) platform. Samples from intermediate heterogeneous pools showed increasing target affinity as selection cycles progressed, indicating affinity maturation as stronger binding aptamers were retained and amplified while the weaker sequences were removed from the selection pool. After identifying the top candidates with NGS, they were evaluated with BLI assay, and the best four sequences were assessed with capture aptamer linked immobilized sorbent assay (ALISA). Phophorothioate-modified aptamers were able to retain sequence integrity after 48 hours of incubation in near-physiological environment. However, the phosphorothioate-modified aptamers were not able to neutralize Spike-presenting lentiviral pseudovirus in a surrogate neutralization assay. In conclusion, the study evaluated the viability of aptamer development as a response to the Coronavirus disease 2019 (COVID-19) pandemic. Throughout the process of developing and characterizing SARS-CoV-2 S-RBD aptamer binders, the study identified the benefits and pitfalls of the approach, and suggested that the aptamer platform could be a powerful therapeutic and diagnostic tool for rapid pandemic response once the major challenges have been considered and addressed.

Acknowledgements

I would like to take this opportunity to thank my supervisor Dr. Darwyn Kobasa. The project would never be completed without his support and guidance throughout my Master of Science program. I am grateful to work under his mentorship and supervision.

I would also like to thank my committee members, Dr. Sean McKenna, Dr. Shawn Babiuk, and Dr. Xiao-jian Yao for their insights and advices through these years.

To the past and present members of the HCRV group at the National Microbiology Laboratory, especially Nathan, Marnie, Bryce, Aaron, Thang, and Rob, thank you for the help and kindness that you have showed me. I could not finish my thesis without the support and comradery that you have provided. I am also thankful for the training and support from the Special Pathogen Group, especially Jonathan, Michael, Guodong, Zachary, and Lisa. I owed a big part of the thesis to all these wonderful people.

I would like to thank the academic and administrative support from the Department of Medical Microbiology and Infectious Diseases at UofM, thank you Angie for always being responsive and helpful. To all the friends that I have made during my years in graduate studies, thank you for making my program more meaningful and bearable.

Finally, I would like to thank my family for their love and support. Thank you for always being there for me. I could not do this without you all.

List of Tables

Table 1. Spike RBD binding aptamer controls, Bank40 ssDNA library, SELEX amplification and NGS sequencing primers.

Table 2. SELEX parameter of 10 selection cycles.

Table 3. Quantification of ssDNA generated from each round of SELEX cycle.

Table 4. Top ten most abundant sequences in 10R PCR pool.

Table 5. Sequences that were synthesized and tested.

List of Abbreviations

SARS	Severe Acute Respiratory Syndrome
WHO	World Health Organization
2019-nCoV	novel coronavirus 2019
SARS-CoV-2	Severe Acute Respiratory Syndrome Coronavirus-2
ICTV	International Committee on Taxonomy of Virus
COVID-19	Coronavirus disease 2019
RNA	Ribonucleic acid
mRNA	Messenger Ribonucleic Acid
ssRNA	Single stranded RNA
gRNA	genomic RNA
sgRNA	subgenomic RNA
VOC	Variant of Concern
ACE2	Angiotensin-converting enzyme 2
hACE2	Human ACE2
RBD	Receptor binding domain
IL	Interleukin
TNF- α	Tumor necrosis factor- α
ARDS	Acute respiratory distress syndrome
PASC	Post-acute sequelae of COVID-19
S	Spike protein
M	Membrane protein
E	Envelope protein
NP	Nucleocapsid proteins
FP	Fusion peptide
TMPRSS2	Transmembrane serine protease 2
ORF	Open reading frame
pp	Polyprotein
nsp	Non-structural protein

RTC	Replicase-transcriptase complex
RdRp	RNA-dependent RNA polymerase
L	Leader sequence
TRS	Transcription-regulating sequences
DMV	Double membrane vesicles
CM	Convoluted membrane
ER	Endoplasmic reticulum
ERGIC	ER-to-Golgi intermediate compartment
PCR	Polymerase chain reaction
qPCR	Quantitative PCR
RT-qPCR	Reverse transcription qPCR
ePCR	Emulsion PCR
aPCR	Asymmetric PCR
DNA	Deoxyribonucleic acid
cDNA	complementary DNA
ssDNA	Single stranded DNA
dsDNA	Double stranded DNA
Ct	Cycling threshold
LAMP	Loop-mediated isothermal amplification
RT-LAMP	Reverse transcription LAMP
CRISPR	Clustered Regularly Interspaced Short Palindromic Repeats
Cas	CRISPR-associated protein
RAT	Rapid antigen tests
POC	Point of care
Ig	Immunoglobulin
mAb	Monoclonal antibodies
MERS-CoV	Middle East respiratory syndrome–related coronavirus
LNP	Lipid nanoparticle
VLP	Virus-like particle

NMR	Nuclear magnetic resonance
XNA	Xenonucleotides
SELEX	Systematic Evolution of Ligands by Exponential enrichment
A	Adenine nucleobase
C	Cytosine nucleobase
T	Thymine nucleobase
U	Uracil nucleobase
G	Guanine nucleobase
EMSA	Electrophoretic mobility shift assay
DiStRO	Diversity standard of random oligonucleotides
T_m	Melting temperature
HTS	High-throughput sequencing
NGS	Next-generation sequencing
ELISA	Enzyme-linked immunosorbent assay
ALISA	Aptamer-linked immobilized sorbent assay
FLAA	Fluorescence-linked aptamer assay
HRP	Horseradish peroxidase
SPR	Surface plasmon resonance
BLI	Biolayer interferometry
PEG	Polyethylene glycol
miRNA	Micro RNA
siRNA	Small interfering RNA
Vero E6	African green monkey kidney clone E6
HEK	Human embryonic kidney cells
IF	Immunofluorescence
$TCID_{50}$	Median tissue culture infectious dose
BSL	Biosafety level
VLP	Virus like protein
VSV	Vesicular stomatitis virus

HIV	Human immunodeficiency virus
nt	Nucleotide (unit)
NML	National Microbiology Laboratory
LV	Lentivirus/Lentiviral
DMEM	Dulbecco's modified Eagle medium
FBS	Fetal bovine serum
PBS	Phosphate-buffered saline
DPBS	Dulbecco's PBS
BSA	Bovine serum albumin
RPM	Revolution per minute
EDTA	Ethylenediaminetetraacetic acid
UV	Ultraviolet
NTC	No template control
UMI	Unique molecular identifier
EPM	enhancement PCR mix
SPRI	Solid-phase reversible immobilization
TBE	Tris/Borate/EDTA
ANOVA	Analysis of variance
Ala/A	Alanine
Arg/R	Arginine
Asn/N	Asparagine
Asp/D	Aspartic acid
Cys/C	Cysteine
Gln/Q	Glutamine
Glu/E	Glutamic acid
Gly/G	Glycine
His/H	Histidine
Ile/I	Isoleucine
Leu/L	Leucine

Lys/K	Lysine
Met/M	Methionine
Phe/F	Phenylalanine
Pro/P	Proline
Ser/S	Serine
Thr/T	Threonine
Trp/W	Tryptophan
Tyr/Y	Tyrosine

List of Figures

Figure 1. Frequencies and phylogeny data of mutation and variants of SARS-CoV-2 from 2020 to 2022.

Figure 2. Mapping of functional sites on SARS-CoV-2 Spike monomer.

Figure 3. Schematics of SARS-CoV-2 cell cycle and potential antiviral targets.

Figure 4. Schematic of Aptamer folding and binding to target.

Figure 5. SELEX cycle workflow for anti-S RBD ssDNA aptamer development.

Figure 6. Common aptamer nucleotide modification.

Figure 7. Schematics of SARS-CoV-2 Spike presenting pseudotype virus production.

Figure 8. Vectors used in pseudotype LV production.

Figure 9. SELEX PCR optimization.

Figure 10. dsDNA characterization of 1R-10R with HS DNA bioanalyzer system (A) and qPCR melt-curve analysis (B).

Figure 11. BLI association and dissociation of 2R, 6R, 10R aptamer in serial dilution.

Figure 12. Gel electrophoresis of 10R aPCR amplicon and 10R gel extract visualized with small RNA bioanalyzer chip.

Figure 13. Gel electrophoresis of Liu 1a and SELEX aptamer candidates after incubation with SRBD.

Figure 14. Capture ELISA of biotinylated aptamers.

Figure 15. BLI association and dissociation sensorgram of biotinylated aptamers.

Figure 16. Predicted secondary structure of aptamer candidates.

Figure 17. Liu 1a Molecular Docking Simulation.

Figure 18. Gel electrophoresis of phosphorothioate-modified S2Rev-B40 at 0, 24, 48 hours DMEM incubation.

Figure 19. Luciferase signal of LV pseudovirus infected cells after mAb or aptamer treatment.

Figure 20. Effects of spinoculation on HEK293T-ACE2/TMPRSS2 cell morphology and pseudotype lentivirus transduction efficiency.

Table of Contents

Abstract 2
Acknowledgements 3
List of Tables 4
List of Abbreviations 5
List of Figures 10
Table of Contents 11
Chapter One: Introduction 14
1.1 SARS-CoV-2 14
1.1.1. COVID-19 Pandemic and Epidemiology 14
1.1.2. Transmission and Clinical symptoms 17
1.1.3. Viral structure and life cycle 18
1.1.4. Diagnostic Approaches for SARS-COV-2 22
1.1.5. Therapeutic Approaches for SARS-CoV-2 24
1.1.6. Vaccination for SARS-COV-2 26
1.1.7. Community Surveillance for SARS-CoV-2 28
1.2. Aptamer 30
1.2.1. Molecular structure 30
1.2.2. Aptamer Selection Approach 32
1.2.3. Aptamer Sequencing 36
1.2.4. Aptamer-Target Binding Analysis 37
1.2.5. Aptamer Synthesis and Modification 38
1.2.6. Aptamer Applications 39
1.3. In-vitro infection assay for the Detection and Propagation of SARS-CoV-2 42
1.3.1. Authentic Virus Models 42
1.3.2. Pseudotype Virus Model 43
Chapter Two: Research Goal 46
2.1. Rationale 46
2.2. Hypothesis 46
Chapter Three: Materials and Method 47
3.1. Reagents for Aptamer Selection 47

3.2. Cells and Pseudovirus Preparation 49
3.3. Systematic Evolution of Ligands by EXponential enrichment (SELEX) 51
3.3.1 Target Selection 51
3.3.2 SELEX PCR Optimization 52
3.3.2. Binding sequence Amplification 56
3.4. Asymmetric PCR for ssDNA Amplification 57
3.5. ssDNA pool binding enrichment assessment 57
3.5.1. Qualitative Polymerase Chain Reaction (qPCR) melt-curve analysis 57
3.5.2. Aptamer Pool Bio-layer Interferometry (BLI) Assay 58
3.6. Next Generation Sequencing (NGS) 59
3.6.1. Library Purification and Preparation 59
3.6.2. Data Processing 61
3.7. Candidate Binding Assessment 62
3.7.1. Single-Sequence Gel Electrophoresis 62
3.7.2. Aptamer Linked Immobilized Sorbent Assay (ALISA) 62
3.7.3. Single-Sequence BLI assay 63
3.8. *In vitro* Pseudotype Virus Microneutralization Assay 64
3.8.1 Determining lentivirus pseudovirus working titer 64
3.8.2 Aptamer microneutralization assay 65
3.9. Aptamer Biostability Assay 66
3.10 Liu 1a Molecular Docking Simulation 67
3.11. Statistical Analysis 67
Chapter Four: Results 68
4.1. Aptamer Candidate Selection 68
4.1.1 SELEX Optimization 68
4.1.2. Monitoring SELEX Selection 70
4.1.3. Evaluation of S-Binding Aptamer Pool 71
4.1.4. Identify Binding Sequence Using HTS 74
4.2. Aptamer Characterization 79
4.2.1. Seq2Rev form DNA-SRBD Complexes in Gel Electrophoresis 79
4.2.2. Weak Candidate-SRBD Binding was Detected in ALISA 79
4.2.3. Seq2For, Seq2ForB40, Seq2Rev and Seq2RevB40 Showed Weak Binding Activity in BLI Analysis 81

4.2.4 Secondary Structure Prediction of Aptamer Candidates 84
4.2.5 Liu 1a Molecular Docking Simulation 84
4.3. Biostability of Modified Aptamers in Physiological Environment 87
4.4. *In vitro* Microneutralization of Pseudotype Virus with Aptamers 87
Chapter Five: Discussion 93
5.1. SELEX and Aptamer Selection 93
5.2. Aptamer Characterization 97
5.3. *In vitro* Microneutralization of Pseudovirus by Aptamers 102
5.4. Aptamer Applications and Their Role in COVID-19 Diagnostics and Therapeutics 105
Chapter Six: Concluding Remarks and Future Direction 109
Chapter Seven: References 111
Chapter Eight: Appendix 137
8.1. R codes for NGS data quality assessment and processing 137
8.2. Printed Cutadapt NGS data processing summary 141
8.3. Buffer formula 142
Chapter Nine: Copyright Permissions 143

Chapter One: Introduction

1.1 SARS-CoV-2

1.1.1. COVID-19 Pandemic and Epidemiology

In December of 2020, the Chinese public health officials reported that clusters of an outbreak of a severe pneumonia disease was spreading in Wuhan, Hubei province, central China. The origin of the outbreak was believed to be a local seafood market located in Wuhan [1, 2]. Within a month, the novel disease had caused more than 5900 confirmed cases in China alone, and Chinese scientists had successfully isolated the pathogenic agent of the emerging pneumonia-causing respiratory disease [3]. It is speculated that the virus might have originated as a bat-derived SARS- like coronavirus, which spilled over to animal hosts that were sold at the seafood market, or directly to humans [1–4]. By January of 2020, cases were confirmed in travelers outside of China, such as in Thailand, Japan, Korea, and United States [5, 6]. Many countries started to screen passengers for symptoms of the novel coronavirus in passengers on direct and connecting flights from China. The city of Wuhan was placed under lockdown, and travel restrictions, testing, and self-quarantine measures were implemented to control the spread of the emerging disease [5–7]. The World Health Organization (WHO) declared that novel coronavirus 2019 (2019-nCoV) as a Public Health Emergency of International Concern on January 30, 2020 [1, 6–8]. On February 11, 2020, the novel virus was renamed as ”Severe Acute Respiratory Syndrome Coronavirus-2 (SARS-CoV-2)” by the International Committee on Taxonomy of Virus (ICTV) [1, 9]. By mid-2020, many countries experienced unprecedented numbers of Coronavirus disease 2019 (COVID-19) cases and associated deaths which greatly stressed national public health systems, leading to workplace and school shutdowns, international trade and supply chain interruptions, stock market crashes, mass layoffs, retail, food, and manufacturing crises, and global recession [7]. Emergency funds were allocated to speed-up the research and development of COVID-19 diagnostics and therapeutics, and soon, multiple expedited clinical trials of promising vaccine and drug candidates were conducted simultaneously, and pharmaceutical companies were competing to release the first effective antiviral and prophylactic vaccine against COVID-19 [6, 10]. On December 2, 2020, a messenger ribonucleic acid (mRNA)-based vaccine that was developed by Pfizer and BioNTech became the

first fully tested COVID-19 vaccine to be approved for emergency use [10, 11]. Soon, other pharmaceutical companies such as Moderna and AstraZeneca also announced successful development of prophylactic vaccines against SARS-CoV-2 infection [10].

As the pandemic progressed, emerging mutations and variants of SARS-CoV-2 were reported (Fig. 1). By mid-2020 emergence of a non-synonymous Spike protein mutation at position 614 (Aspartic acid (D) replaced by Glycine (G)) quickly overtook the pre-existing Wuhan type and became the main circulating strain. In late 2020, the B1.1.7 lineage (Alpha), a Variant of Concern (VOC), was detected and quickly became the dominating COVID-19 linage in United Kingdom, and soon, globally [12, 13]. The Alpha variant was shown to exhibit enhanced transmissibility compared to the ancestral Wuhan lineage due mutations that facilitated better binding between the Spike protein and the human receptor, angiotensin-converting enzyme 2 (hACE2) [12, 14]. In May, 2021, the WHO announced that a new SARS-CoV-2 VOC, B.1.617.2 lineage (Delta), believed to be originated from India, was rapidly replacing the Alpha variant, and becoming a VOC that dominated circulating lineages [15]. As the population developed immunity against SARS-CoV-2 either through infection or immunization, cases of re-infection were rising as Delta variant was shown to carry mutations that facilitated immune evasion against neutralizing antibodies [15–17] In November, 2021, the WHO declared another emerging variant, BA 1.1.529 (Omicron), as a VOC [18]. Compared to previous variants, the Omicron virus carried more mutations, especially at antigenic sites such as the Spike receptor binding domain (RBD), driven by the selective pressure caused by immune response of the population due to natural infection and the vaccination program. The risk of re-infection greatly increased even for those who were previously immunized [13, 17, 19, 20]. It was advised to take the COVID-19 booster vaccine shots to strengthen waning immunity and provide sufficient protection against the circulating Omicron variant [6, 13, 17, 19]. Throughout 2022, more subvariants of Omicron emerged, such as BA.1 to BA.5, and Omicron remained as the only circulating VOC in 2023 [21]. WHO declared that COVID-19 was no longer a public health emergency on May 5, 2023, as the severity of the pandemic had been declining [22]. As of January 2025, there were 7.1 million cumulative deaths and over 777 million cumulative cases worldwide [23].

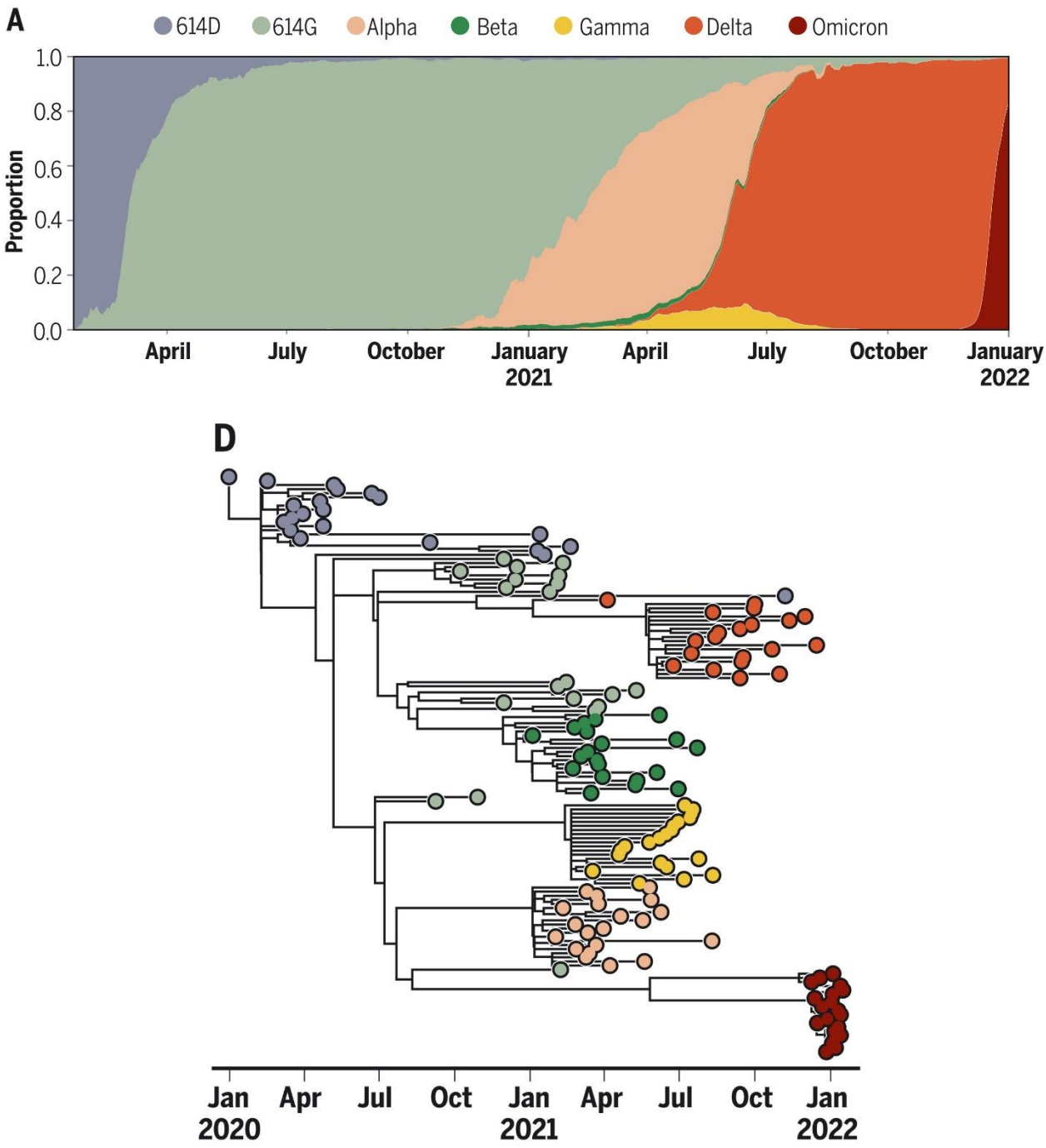


Figure 1. Frequencies and phylogeny data of mutation and variants of SARS-CoV-2 from 2020 to 2022. (A) The frequencies of SARS-CoV-2 variants of concern, as calculated based on sequence data deposited in Global Initiative for Sharing Avian Influenza Data (GISAID). (D) Phylogeny tree derived from SARS-CoV-2 sequence data, representing evolutionary relationship of variants shown in (A). This figure was reprinted with permission from Koelle K et al [13] under the license of Creative Commons Attribution (CC BY 4.0).

1.1.2. Transmission and Clinical symptoms

SARS-CoV-2 is commonly transmitted through close contact, fomites, and contaminated surfaces [1, 24, 25]. There are concerns that virus can be transmitted through small airborne aerosol particles in closed indoor environments like aircrafts, hospitals, public transportation, schools, apartments, and bathrooms, yet the exact risk is still under debate [26–28]. A wide range of animals are also susceptible to SARS-CoV-2 infection, as animal surveillance studies have detected SARS-CoV-2 in wildlife, livestock, house pets, and animals in captivity [29–32]. Animal-to-human and human-to-animal transmission are possible and can pose a threat to further virulent mutation [29, 31].

The presymptomatic incubation period varied from variant to variant, ranging from 1 to 10 days [33, 34]. Epidemiological data shows that Omicron variant has a shorter incubation period than previous lineages [33, 35]. Infected presymptomatic and asymptomatic individuals can still shed viruses and be contagious [34]. Studies have suggested that about 18-37% of infected population are asymptomatic, and Omicron infections are more likely than its ancestral strains to be asymptomatic or cause milder symptoms [13, 36, 37].

Common mild to moderate COVID-19 symptoms include sore throat, dry cough, fever, muscle pain, shortness of breath, diarrhea, fatigue, and anosmia (impaired or loss of smell) [38]. In severe cases of COVID-19 that requires hospitalization, patients presented with elevated neutrophils, D-dimer, blood urea, and creatinine levels, which are associated with systemic metabolic and cardiovascular distress. Patients in critical condition may develop cytokine storm, a cascade of dysregulated inflammation, in which the excess secretion of inflammatory factors such as interleukin 6 (IL-6), IL-10, tumor necrosis factor- α (TNF- α) can cause more damage than protecting the host [39–43]. Immunothrombosis caused by hypersecretion of coagulation factors disrupts the alveolar-capillary barrier, reducing gas exchange efficiency and exacerbates tissue hypoxia [43]. As disease progresses, patients developing acute respiratory distress syndrome (ARDS) present with extensive lung injury caused by macrophage and neutrophil infiltration of alveoli and bronchi on chest X-ray, resulting in lowering blood-oxygen levels and accelerating metabolic acidosis, multiple organ

failure, and even death [42–45]. The prognosis and mortality rate of COVID-19 is associated with multiple factors including virus strain, host sex, age, comorbidity, immunization status, medical history (obesity, diabetes, hypertension, cardiovascular disease, immunodeficiency), and host demographic background (income, education) [46–48].

It is reported that about 10% of infected individuals experienced post-acute sequelae of COVID-19 (PASC or "Long COVID") symptoms including chronic fatigue syndrome, memory loss, cognitive impairment or "brain fog", depression, irregular sleeping pattern, diabetes, autoimmunity, and cardiovascular disorders. These symptoms can persist for more than two years after first acquiring the infection [49–51]. The mechanism of long COVID is not fully understood. It is suggested to be caused by tissue inflammation and damage [49], reinfection or possible SARS-CoV-2 persistence in tissue reservoirs [52], or reactivation of Epstein Barr virus (EBV) or herpesviruses due to a dysregulated immune system after SARS-CoV-2 infection [53].

1.1.3. Viral structure and life cycle

SARS-CoV-2 is an enveloped positive-sense single stranded RNA (+ssRNA) virus, which belongs to the subgenus of sarbecovirus (SARS Betacoronavirus), in the genus of Betacoronavirus, of the family of Coronaviridae [54]. The coronavirus virion has an outer lipid envelope with three surface proteins: membrane protein (M), envelope protein (E), and Spike protein (S). The average diameter of the virion is 80-120 nm. Within the membrane envelope, the helical nucleocapsid proteins (NP) are attached to the viral RNA genome, which is about 29.9 kilobases in length [55, 56].

The S protein is the primary surface protein of SARS-CoV-2 virus, which is crucial for transmission, mediating attachment, and entry to host cells. The S protein is about 180-200kDa in size, with 1273 amino acid residues [57]. It has a club-like geometry, and protudes about 16-21 nm from the virion lipid envelope [55]. The S protein is a trimeric glycoprotein with two subunits: S1, which contains the receptor binding domain (RBD, residues 333-526); and S2 (Fig. 2) [58]. SARS-CoV-2 S protein targets the angiotensin converting enzyme 2 (ACE2) of the host [58]. The S trimers of a free virion can adopt a closed or partially opened RBD conformation,

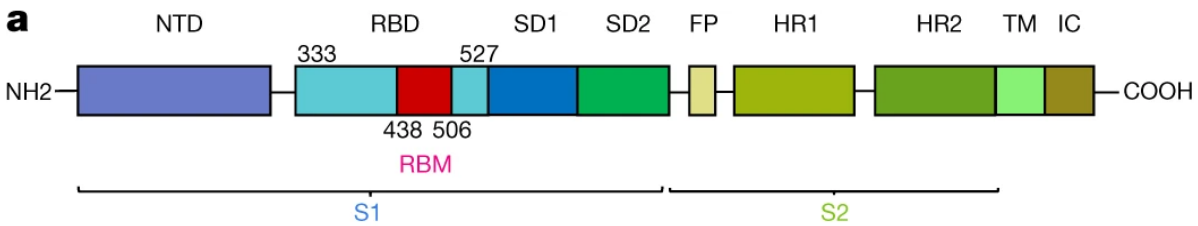


Figure 2. Mapping of functional sites on SARS-CoV-2 Spike monomer. NTD: N-terminal domain; RBD: receptor binding site; RBM: receptor binding motif; SD1: subdomain 1; SD2: subdomain 2; FP: fusion peptide; HR1: heptad repeat 1; HR2: heptad repeat 2; TM: transmembrane region; IC: intracellular domain. Reprinted with permission from Springer Nature: Lan J *et al.* [58].

which restricts exposure of RBD to ACE2 [59, 60]. Once the ACE2 binding occurs, S1 undergoes a conformational change and furin-mediated proteolytic cleavage at the S1/S2 junction, to permit a more-open conformation of RBD [57, 58, 60]. The multiple RBD-ACE2 bindings pull the virion envelope membrane and cellular membrane closer, which then promote clathrin-mediated endocytosis or membrane fusion [60]. The S2 cleavage site (S2') of most coronaviruses needs to be cleaved by a cellular protease to expose the fusion peptide (FP) to initiate membrane fusion [55, 61, 62]. For SARS-CoV-2, the S2' can either be cleaved by cathepsin L in the cellular endosome after endocytosis, or by host membrane-bound transmembrane serine protease 2 (TMPRSS2) [61, 63].

After membrane fusion and uncoating, the core NP and viral genome are released into cell cytoplasm for viral genome replication. To achieve this, open reading frame 1a (ORF1a) and ORF1b of the virus genome is first translated into polyproteins 1a (pp1a) and pp1ab (Fig. 3). After post-translational modification, the polyproteins are processed into about 16 non-structural proteins (nsp) to facilitate viral genome replication [55, 64]. The nsps assemble and form a replicase-transcriptase complex (RTC), which has multiple functions including RNA-dependent RNA polymerase (RdRp), helicase, interferon inhibitor, immune evasion, polyprotein processing, endoribonuclease, mRNA capping and terminal processing [64]. The RTC then attaches to the positive-strand viral genomic RNA (gRNA) and starts transcribing multiple copies of full-length negative gRNA as the template for generating progeny viral gRNA. The RTC also transcribes a nested set of discontinuous negative-strand subgenomic RNAs (sgRNAs) from the original positive-strand gRNA [64, 65]. These sgRNAs all carry a common leader sequence (L), located at the 5' end of the positive strand gRNA and various nsp and structural protein ORFs, located at 3' end of the gRNA. To generate these sgRNAs, transcription-regulating sequences (TRS) are scattered upstream of most ORFs and at the 3' end of the L sequence on the gRNA. TRS plays an important role of interrupting RTC transcription (to generate sgRNA) and attaching the L sequence to the incomplete negative sgRNA [55, 65]. The RdRP transcribes negative gRNA and sgRNA to positive-strand gRNA and viral mRNA. The RTC synthesizes sgRNA and gRNA in

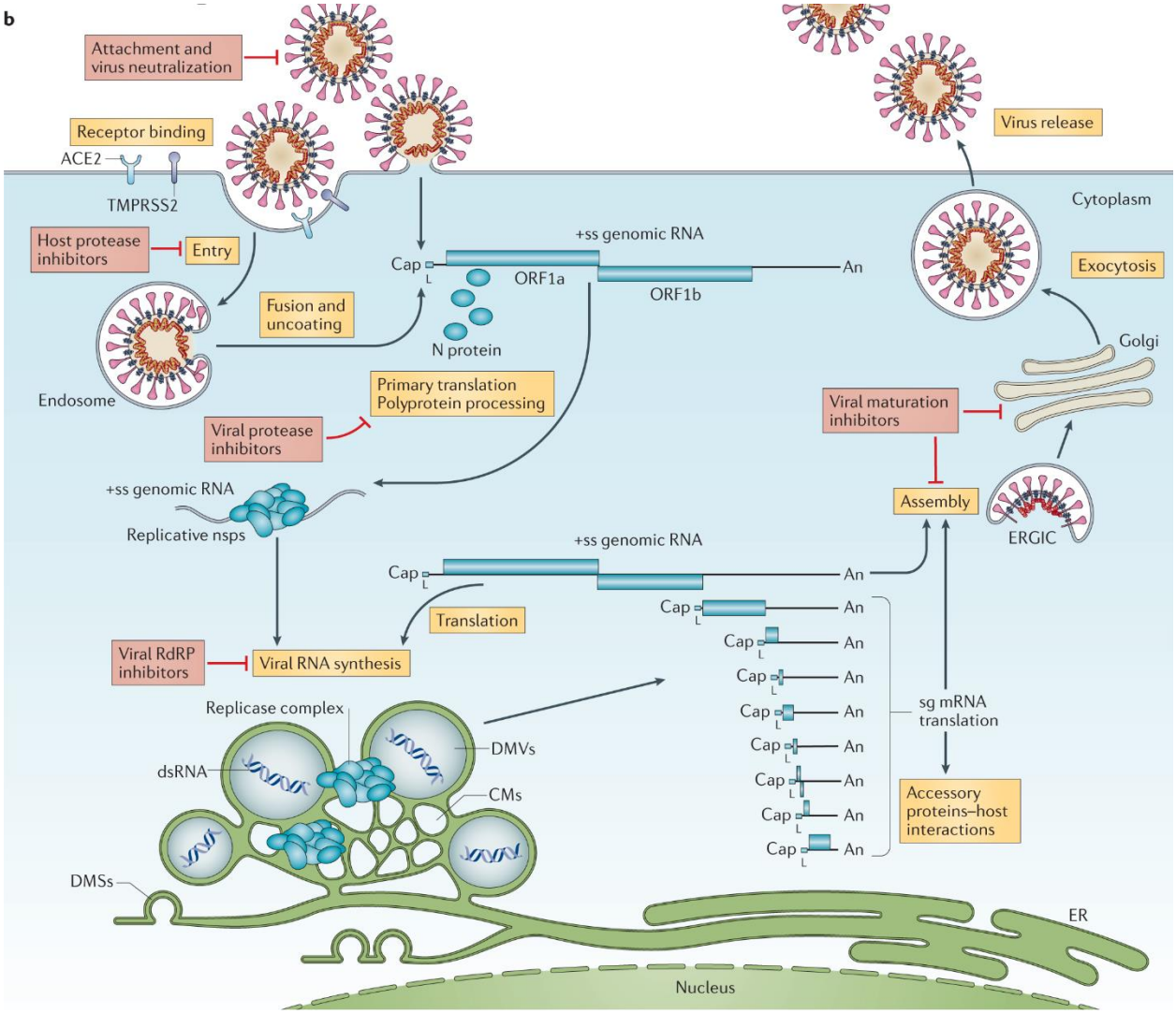


Figure 3. Schematics of SARS-CoV-2 cell cycle and potential antiviral targets. SARS-CoV2 virion attaches and enters host cell after S protein binging with ACE2 receptor. The virion then uncoats and releases N protein and viral positive gRNA for nsp translation. The nsps form replicative complex (RTC) and start synthesizing copies of gRNA and sgRNA. The RTC forms replication organelles (DMVs and CMs) at cellular ER to create stable microenvironment for viral RNA synthesis. The viral mRNAs are translated into accessory and structural proteins and are then transported to ERGIC for assembly and budding. Mature viral particles are released via exocytosis. Image reprint with permission of Springer Nature: *V'kovski P et al.* [64]

remodeled vesicles (double membrane vesicles, DMV) and folded membrane (convoluted membrane, CM) structures at the cellular endoplasmic reticulum (ER), shielding the viral RNA synthesis from intracellular antiviral elements (Fig. 3) [55].

The viral mRNAs are translated at the ER and proteins are transported to the Golgi apparatus through the ER-to-Golgi intermediate compartment (ERGIC) for secretion. The positive-strand gRNA is encapsulated by newly translated N protein. The S, M, and E proteins are assembled and integrated into the phospholipid membrane of the ERGIC vesicle, budding and forming progeny virus particle which contains the NP encapsulated gRNA. The mature virus particles exit the host cell by exocytosis (Fig. 3) [66].

The SARS-CoV-2 structural proteins have been targeted for antiviral and vaccine development to block viral attachment and cell entry. The Spike protein is a hotspot for viral mutations to enhance human ACE2 binding and immune evasion, as recorded over the course of the pandemic. The Omicron variant, the dominant circulating variant as of writing, has about 50 cumulative amino acid mutation in comparison to the ancestral Wuhan strain, and over half of them occur on the S protein [67]. Some mutations, such as the D614G that was reported as early as April 2020 (figure 1) [13], in which the aspartic acid at 614 residue is replaced by glycine, are shown to stabilize S protein expression and enhance incorporation into the virion envelope [68, 69]. Mutations in S protein RBD enhance the binding affinity of human ACE2 by forming new molecular interactions between receptor-virus residues [70]. Antigenic shift of the Omicron lead to weakened antibody neutralization (either from prior immunization, infection, or monoclonal antibody treatment), which greatly increased the transmissibility and chances of reinfection [13, 20, 67, 69–71].

1.1.4. Diagnostic Approaches for SARS-COV-2

There are two main types of diagnostic tests: the molecular test which targets viral genetic material; and the antigen test that targets viral proteins. The gold-standard for COVID-19 screening is reverse transcription quantitative polymerase chain reaction (RT-qPCR) [72]. Typically, samples are collected via saliva, nasal, nasopharyngeal, or oropharyngeal swabs. The

samples are then sent to laboratories for further processing and analysis. The viral RNA is extracted, reverse transcribed into complementary DNA (cDNA), and then amplified with gene-specific primers for detection with fluorescent probes. The virus titer of the sample is estimated by comparing the cycling threshold (Ct) value of the real-time amplification step to the Ct standard curve derived from known virus titers [73]. Virtually any SARS-CoV-2 gene region can be targeted for qPCR amplification, however, genetically conserved sites such as RdRP, E, and NP proteins are popular gene targets [72]. The test is highly specific and sensitive, but requires specialized reagents and laboratory instruments. The RT-qPCR test is also relatively time consuming, the collection-to-result turnover time ranges from 4 hours to a week, depending on the logistics and capacity of the testing facilities [74, 75]. Recently, another nucleic acid amplification diagnostic approach, the reverse-transcription loop-mediated isothermal amplification (RT-LAMP) test shortened the technological barrier by removing the need for a thermocycler and shortens the turnover time to less than an hour with comparable sensitivity and specificity to the conventional RT-qPCR method [76, 77]. Clustered Regularly Interspaced Short Palindromic Repeats (CRISPR) and CRISPR-associated protein (Cas) are also proposed as a promising COVID-19 diagnostic tool. Combined with various reporter systems (e.g. colorimetric, fluorescent, electrochemical), novel virus detection platforms that utilize CRISPR-Cas technology can achieve single-molecule sensitivity and specificity with comparable turnover time as traditional RT-qPCR approach. [78–80].

COVID-19 Rapid antigen tests (RAT) were distributed for at-home and point-of-care (POC) testing. They were designed to be portable, end-user friendly, and provide rapid results within 15 to 30 min. A typical RAT kit includes a ready-to-use lateral flow immunoassay strip that can detect the presence of SARS-CoV-2 antigen in a given sample [81, 82]. For POC and at-home rapid diagnosis, self-collected nasal or throat swab are submerged in the collection tube with pre-mixed assay buffer before loading onto the designated well of the testing strip. In most of the commercially available kits, the RAT antibodies target viral N protein since it is one of the more genetically conserved structural proteins of SARS-CoV-2 [83]. The convenience and availability of RAT kits helped mitigate the stress on medical providers, health facilities, and test sites during the pandemic by providing at-home testing for symptomatic patients.

Throughout the clinical course of the infection, the sensitivity and accuracy of both molecular and RAT change due to differences in host immune response, viral load, and affected tissue types. The limit of detection of various tests depended on sample type, handling, and virus variants. Typically, the viral load at the beginning (exposure) and the end of the infection cycle (convalescence) were usually below the limit of detection [81, 84–86]. RAT positive results have been shown to correlate to symptom onset, with peak sensitivity of 73% to 84% after symptom onset, confirmed with RT-qPCR [84, 87]. RT-qPCR is able to detect viral genome earlier than the RAT approach, and the PCR positive signal persists even when the individual was no longer producing infectious virus [85, 86]. As the host immune response reacts to the viral infection, IgG and IgM antibodies could be detected weeks to months after the initial infection in serological tests which could be used for population-wide surveillance. Serological surveillance was used to track the spread of virus in both symptomatic and asymptomatic populations, virus variants, and evaluate the effectiveness of the SARS-CoV-2 immunization program [85, 88].

1.1.5. Therapeutic Approaches for SARS-CoV-2

Due to the severity of the COVID pandemic, the pharmaceutical race to develop effective viral therapeutics was fierce. Governments were issuing emergency deployment of novel drugs, and fast tracking of the research pipeline to expedite promising therapeutic candidates for clinical trials. There were two major approaches to COVID-19 treatments: antiviral drugs that target a viral component, and immunomodulatory therapies that regulate immune response to prevent extensive damage cause by dysregulated inflammation [89]. Since the start of the pandemic, thousands of small molecule drugs and monoclonal antibodies were tested, and a handful of those were deployed under emergency circumstances.

The anti-SARS-CoV-2 antibodies were derived from convalescent donors or humanized mice. Neutralizing monoclonal antibodies (mAb) that target S protein block viral attachment to hACE2 to prevent cell entry [90]. Some monoclonal antibodies that target the S protein can block the cleavage and exposure of S fusion domain [91]. Neutralizing antibodies also facilitate

host viral clearance to limit the spread of infection [90]. Nanobodies, a functional heavy-chain fragment that has a smaller molecular weight (~15 kDa) can reach cryptic epitopes that were previously inaccessible to full mAb [92, 93]. Cocktail formulas composed of several different classes of antibodies can target different viral components to avoid immune escape [94] However, due to the emergence of variants, many health authorities have revoked the emergency use authorization of existing anti-SARS-CoV-2 monoclonal antibody therapies, with few exceptions [94, 95].

Synthetic protein and small molecule drugs that target viral components are designed to disrupt viral lifecycle mechanisms such as RNA replication (helicase, RdRp), polyprotein cleavage and post translational modification (viral protease), or viral proteins that are involved in immune evasion or pathogenicity (nucleocapsid and other non-structural proteins) [89]. Antivirals that target RNA viruses, such as remdesivir and ritonavir, were tested and approved for emergency use [96, 97]. A novel oral coronavirus protease inhibitor, nirmatrelvir, was co-packaged with another antiretroviral, ritonavir, as one of the first SARS-CoV-2-specific therapeutic drugs, sold under the brand name Paxlovid. SARS-CoV-2 drugs are more effective when administered in early infection stages as they reduce viral load, virus shredding, and shorten recovery time [98, 99]. Unconventional approaches that target host components are also being explored. For example, ACE2 derivatives can block viral attachment *in vitro*, and may provide protection against angiotensin II-dependent hypertension, however their clinical efficacy against COVID-19 is still not clear [100, 101].

In addition to vaccination, pre-exposure prophylactic monoclonal antibodies may be given to high-risk groups with severe immunodeficiency [89, 102–104]. In the context of clinical management, patients with mild to moderate COVID-19 symptoms do not typically require hospitalization. According to Public Health Agency of Canada guidelines, severe and critical COVID-19 patients with lower respiratory tract infection are put on supplemental oxygen therapy (ventilators) to stabilize their blood oxygen level. Supportive care that treats specific COVID-19 related complications is administered when needed, such as antibiotics to treat secondary infections [105]. Inpatients with acute respiratory distress syndrome (ARDS) and immune hyperactivation presentations are given corticosteroids such as dexamethasone,

cytokine-, kinase- and complement-inhibitors, and other immunotherapies that target the host immune mediators [43, 89, 102, 105, 106]. Immunomodulation therapy has been shown to lower mortality in patients on ventilators [89, 105, 106].

1.1.6. Vaccination for SARS-COV-2

During the 2020 outbreak, investors and governments were greatly incentivized to expedite development and testing of promising vaccine candidates. The vaccine development pipeline was streamlined and stages of clinical trials were carried out in parallel as experimental data emerged. The fast-track approach shortened the development-to-distribution timeline from 4-10 years, to just under a year [107]. The first SARS-CoV-2 vaccines were approved for emergency use authorization in December of 2020 [10], which became the fastest vaccines ever developed in the history of medicine. The unprecedented speed of vaccine development relied on pre-existing studies, including experimental SARS-CoV and MERS-CoV vaccine candidates, the mRNA vaccine platform, and lipid nanoparticle (LNP) vehicles [107, 108].

The two mRNA-based vaccines developed by Moderna and Pfizer-BioNTech were approved for emergency use by the Canadian federal government in December 2020 [109]. Both vaccines contain a synthetic mRNA sequence that encodes the SARS-CoV-2 S glycoprotein [110, 111]. The synthetic mRNA is encapsulated in a LNP that stabilizes and protects the nucleic acid from environmental degradation, and it also promotes cellular uptake [112]. Upon intramuscular administration, the LNP vehicles attach to host cells, and mRNAs are released into the cytoplasm. To increase stability and antigen expression, the mRNA sequence is synthesized with modified nucleotides and translation-optimization features such as human-optimized codons, 3’ capping and a poly-A-tail. Both the engineered LNP and exogenous mRNA can act as adjuvants to trigger innate cellular responses through the binding of pattern recognition receptors, which lead to downstream cytokine release and recruitment of neutrophils, dendritic cells, and monocytes [113]. The recombinant SARS-CoV-2 S antigen is translated within the host cell, which triggers B cells to produce protective anti-Spike antibodies and induces differentiation of memory B cells [114]. The advantage of a mRNA vaccine is that

that it greatly shortens the turnover time from virus detection to vaccine production by utilizing virus RNA sequencing and the simplicity of mRNA synthesis. Furthermore, mRNA immunization elicits both innate and humoral immune response, thus providing a strong protection against intracellular pathogens.

Another approach for developing a COVID-19 vaccine was replication-defective viral vector vaccines. Viral vectors are selected based on their ability to deliver target genes into target cells, permitting and transgene expression [115]. A popular SARS-CoV-2 vaccine vector is the adenovirus, where its early genes (E1 and/or E3) are deleted and replaced by a dsDNA sequence encoding the SARS-CoV-2 S glycoprotein. Due to the deletion, the viral vector is unable to replicate, but is still capable of targeting a broad range of cell types to express antigen and trigger innate and humoral immune responses [116]. To overcome pre-existing immunity that may interfere with the vaccine delivery, non-human or low seroprevalence adenovirus serotypes are chosen as viral vectors [117]. AstraZeneca and Janssen adenovirus-vector COVID-19 vaccines were approved for Canadian emergency use authorization at the beginning of 2021 [109].

Virus-like particle (VLP) Covifenz vaccine was designed to package recombinant SARS-CoV-2 glycoproteins in empty virions, imitating authentic virion without genetic material [118]. For VLP production, a plasmid carries a modified SARS-CoV-2 S glycoprotein gene, which is transfected into a VLP production platform, such as tobacco plant, insects or mammalian cells, yeast, or bacterial culture [118, 119]. Usually, the transformation plasmid also carries a platform-adapted signaling peptide to facilitate protein expression, post-translation modification, intracellular transportation, VLP assembly and budding [118]. VLPs that are produced by the transfected cells are then harvested and purified. When injected, the VLPs are taken up by antigen presenting cells, which activate both innate and humoral immune response [118, 120]. The plant-derived VLP Covifenz vaccine (Medicago) was granted emergency use authorization February of 2022in Canada [109].

Conventional vaccine platforms, such as viral subunit and inactivated-virus were also used by vaccine manufacturers. The Nuvaxovid SARS-CoV-2 S RBD subunit vaccine, (Novavax)

was authorized by Health Canada in February of 2022 [109]. As a subunit vaccine, recombinant SARS-CoV-2 S glycoprotein was expressed and produced in insect cell bioreactors. The glycoprotein was then harvested, purified, and administered with a LNP adjuvant [120]. Outside of Canada, the inactivated virus CoronaVac vaccine (SinoVac) uses virus samples collected from infected patients. The authentic viruses are then cultivated in large-scale African green monkey kidney cells bioreactors for production and purification, followed by inactivation of infectivity using β-propiolactone [121, 122]. Although the inactivated virus vaccine is non-infectious and has a long shelf life, the virus inactivation process may alter the native antigen conformation, diminishing its antigenic potential [123]. To compensate for their weak innate immune activation, both subunit and inactivated-virus vaccines are administered with an immune-stimulating adjuvant to elicit a stronger immune response [120, 124].

Most of the vaccines were initially designed to be administered in two doses (prime-boost vaccination regimen) to generate long-lasting protective immunity against wild-type SARS-CoV-2 infection. Unfortunately, the SARS-CoV-2 S protein, the go-to vaccine antigen, is highly susceptible to mutation, driven by virus-host adaptation and immune escape [13]. Neutralizing antibodies that are derived from prior vaccinations provide reduced protection against VOCs [13, 125]. As the protection of the vaccine waned overtime, health authorities and vaccine manufacturers recommended additional booster shots to enhance and prolong the existing protection [126]. Bivalent vaccines that targeted the original Wuhan strain and emerging variants were also manufactured and authorized in late 2022 [109].

1.1.7. Community Surveillance for SARS-CoV-2

During the first wave of the pandemic, most of the suspected cases in North America were international travelers who had visited regions with reported outbreaks. Screening sites were set up at airports and international borders to monitor potential imported cases. Starting from March 2020, inbound travelers entering Canada were requested to submit personal information for contact tracing purposes [127]. Close contacts and passengers of the affected flight were asked to quarantine and complete a COVID-19 test if there was a confirmed case

[128]. However, as the pandemic progressed, health authorities adapted more practical and manageable surveillance approaches as the pressure on the healthcare system had greatly increased. Mass qPCR testing sites were set up all over the nation to collect nasopharyngeal swab samples from communities to monitor the spread of SARS-CoV-2 [129]. At the peak of the pandemic, testing facilities switched to high capacity population screening strategies such as sample pooling and priority testing (e.g. symptomatic patients, healthcare workers) [130, 131]. Many countries, including Canada, started to explore wastewater testing to monitor SARS-CoV-2 prevalence in communities [132]. In Canada, sewage sample were collected bi-weekly at water treatment plants, and were sent to municipal laboratories for sample processing and RT-qPCR screening. Health authorities could use the wastewater data to better pinpoint and support affected communities even before the rise of symptomatic cases due to pre-symptomatic viral shedding [133]. The procedure was sensitive enough to pick up as low as five infectious cases per 100,000 population [134, 135], and was capable of tracking circulating variants [136]. The increased accessibility to RAT made home testing and self-reporting quicker and more convenient, which greatly relieved the stress on community testing sites and the healthcare system [137, 138]. Testing data was submitted to federal, provincial and territorial health authorities, which was then complied and released to the public. The information was utilized by the local government to implement respective social distancing measures (e.g. lockdown, restricting venue capacity) and decision making [139].

Population serology surveillance was an important epidemiology tracker before and after the COVID-19 vaccines become available [88]. Pre-vaccination seroprevalence data showed that the actual number of infected cases were under-reported as anti-SARS-CoV-2 antibodies were detected in a higher proportion of the population than reported cases, especially in less economically developed communities [140]. To study vaccine effectiveness, biological samples from vaccinated volunteers, COVID-19 in- and out- patients, healthcare workers, community members from vulnerable sectors such as those from long-term care homes and immunosuppressed patients were taken for serological assessment. Longitudinal studies were set up to assess the progression of neutralizing antibody production after vaccination. As most of the vaccines were initially designed to be administered in a prime-boost

regimen, studies have compared serology of people of different vaccination statuses (non-vaccinated, single dose, boosted etc.) [141–144]. Furthermore, the serological data served as a pointer for evaluating vaccine protection against severe COVID-19 symptoms and hospitalization [145, 146]. The presence of neutralizing antibodies, the duration of antibody production, and neutralizing ability against VOCs have become crucial evidence when discussing implementation of extended vaccination schedule [144–146].

1.2. Aptamer

1.2.1. Molecular structure

Aptamers are short synthetic single-stranded nucleic acids (ssDNA or ssRNA) that can bind to target molecules due to their secondary and tertiary structure (Fig. 4A). The three-dimensional structure of the aptamer is determined by its sequence, specifically, the bases. The biochemical properties of the bases, including ionic bonds, hydrogen bonds, and other electrostatic forces affect the intramolecular folding, thus influencing the tertiary structure of the sequence. The molecular structure of an aptamer determines its function. Aptamers can bind to a range of molecules including small molecules like drugs [147, 148], hormones [149, 150], metal ions [151], proteins (e.g. Fig. 4B) [152, 153], viruses [154], cells and living organisms [155, 156]. It has a small molecular weight, which is advantageous for targeting hidden binding sites that might not be sterically accessible to conventional mAbs [157].

Aptamers can be synthesized with ssDNA or ssRNA, each with slightly different properties. It was once believed that an RNA aptamer was superior to a DNA aptamer because of the diversity of well-known functional motifs of RNA found in nature [158, 159]. However, the field gradually recognized the versatility and improved stability of DNA aptamers. DNA aptamers are more chemically and thermally stable than RNA aptamers due to the removal of 2’-hydroxyl group [159, 160]. Chemical substitution, modification, and the inclusion of xenonucleotides (XNA) bases have also been explored to further increase structural diversity and stability [160–162].

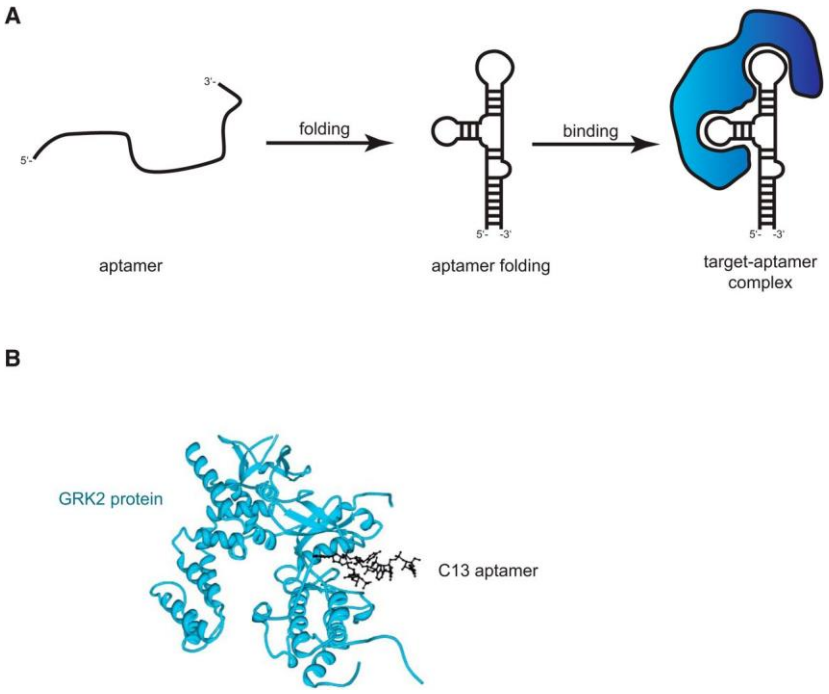


Figure 4. Schematic of Aptamer folding and binding to target. (A) Single stranded RNA or DNA aptamer forming secondary structures. The folded aptamer can interact and bind to target molecule based on intermolecular forces. (B) 3D model of G protein-coupled receptor kinase 2 (GRK2) and C13 RNA aptamer, as determined by X-ray diffraction (PDB: 3UZT [153]). This figure was reprinted with permission from Wolter O & Mayer G [163] under the license of Creative Commons Attribution (CC BY 4.0).

An aptamer assumes its secondary structure based on intermolecular interactions, including the Watson-Crick and non-Watson-Crick base parings, self-hybridization, hairpin loops, branching arms or multiway junctions, and square planer structure formed by four spatially adjacent guanine bases regardless of sequential distance (G-quadruplex) [164, 165]. Because of the size of the aptamers, experimental approaches to analyze the structure of aptamers have been proven to be difficult [166]. Experimental small molecule analyses such as X-ray crystallography and nuclear magnetic resonance (NMR) were able to resolve the structure of ligand-bound aptamers [166–168]. As modern computational simulations become more powerful, atomistic simulations were developed to model and predict the structure of ligand binding interactions of DNAzymes, riboswitches, and aptamers [165, 169, 170]. By factoring various biophysical properties such as temperature, pH, presence of ions and water molecules, *in silico* aptamer molecular analyses such as molecular docking and molecular dynamics can provide multiple structural possibilities and rank them based on predicted stability and binding affinity [169–172].

1.2.2. Aptamer Selection Approach

The conventional way of developing aptamers is through the process of Systematic Evolution of Ligands by Exponential enrichment (SELEX) (Fig. 5). Briefly, the process includes steps of exposing antigen to a single-stranded nucleic acid library (step 1) with randomized sequences (step 3). Non-binding, or weak-binding sequences are washed off after incubating with targeted antigen, and strong binding aptamers are retained and collected (step 4). These binding sequences are then amplified through PCR (step 5), and single-stranded sequences are re-generated and re-introduced to the cycle (step 6) for another round of selection [173]. At the end of each cycle, non-binding and weak binders are eliminated from the pool, while the strong binders are retained and amplified. Ideally, the remaining sequences that are retained in the pool are strong candidates that exhibit high binding affinity towards the target antigen.

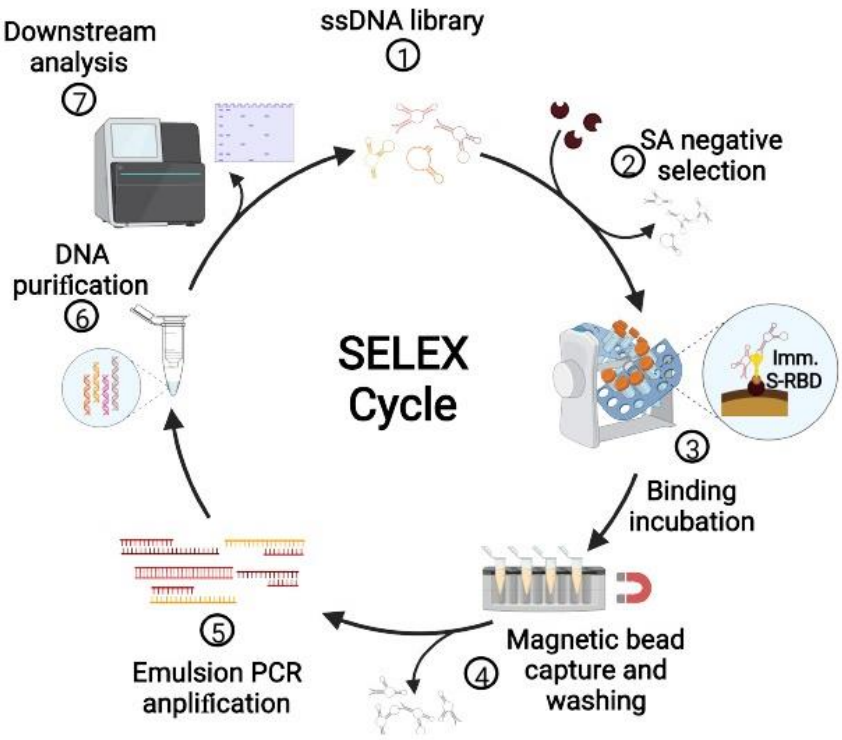


Figure 5. SELEX cycle workflow for anti-S RBD ssDNA aptamer development. Binding aptamer sequences are selected and amplified through multiple SELEX cycles, a process that eliminates weak binding sequence, and amplifies strong binders. Image created with BioRender.com.

There are many considerations and parameters to optimize SELEX to increase the success chance of generating a high-binding aptamers. From the beginning of the selection process, choosing a suitable starting library is crucial for generating a good binder. The design of the starting library dictates the complexity of the secondary structure, which affects the target binding affinity and specificity of the candidate. The starting nucleic acid library usually consists of a randomized region, which is 25-50 nucleotides (nt) long, flanked by two constant PCR primer regions for amplification [162]. If the library is truly randomized, with 4 nucleotides (A, C, T/U, G), the library can hold 4^{25} ($\approx 10^{15}$) to 4^{50} ($\approx 10^{30}$) unique sequences. Ideally, the constant PCR primer region of the library should not interfere with the secondary structure formation of the functional region, to avoid introducing PCR bias during selection and amplification steps. Suboptimal primer region design can sabotage the selection process if they sterically interfere with proper aptamer-target binding. Amplification biases can accumulate over multiple SELEX cycles, which can skew the chance of selecting a strong binding candidate [162]. Although a library with a longer randomized region can form complex motifs, long randomized sequences are prone to self-aggregate, which can block ligand-target interaction, and increase the chance of primer annealing to a random region (off-target), which can cause amplification of unwanted PCR by-products [174].

Based on the purpose of the aptamer, the antigen could be metal ions, a chemical compound, a protein, whole cell, virus, bacteria, and tissues. Live cells expressing native state biomarkers and membrane proteins can be carriers for selecting aptamers that can bind to target molecules in a physiological environment, which is a popular approach for cancer diagnostic and therapeutic application [175]. For protein targets, the conventional approach is to immobilize the protein target to a matrix, such as a nitrocellulose membrane, affinity chromatography column, or coated magnetic beads so that binding aptamer sequence can be retained while washing off non-binders using eluting buffer (Fig. 5, step 3 and 4)[162, 176]. By utilizing the differences in weight and electrochemical charge, through gel or capillary electrophoresis, binding-oligonucleotides-target complexes could be separated from the non-binding sequences through a process called electrophoretic mobility shift assay (EMSA) [176–179].

In addition to positive selection, negative selection or a counterselection step eliminates non-binding or off-target sequences from the nucleic acid pool by incubating the library with a non-target (Fig. 5, step 2). Negative selection using structurally similar non-targets, such as the same viral antigen from another serotype, can generate highly specific aptamers, down to subspecies specificity [180, 181]. Non-targets such as common biomarkers and serum proteins are also able to increase the target specificity species and remove off-target binding sequences [182].

One of the most important steps of SELEX is the PCR step. To retain all binding sequences from previous steps, every unique species in the recovered aptamer pool must be equally amplified to properly represent the binding enrichment progress [183]. In some cases, mutations and alterations are encouraged during the PCR step to introduce diversity to the aptamer pool. Point mutations, homologous, and nonhomologous recombination caused by an error-prone or mutagenic polymerase can potentially increase the chance of generating high affinity sequences that are not recovered by previous SELEX steps [184, 185]. The problem with such an approach is that sequences that are difficult to amplify, such as those with GC-rich regions or complex secondary structures, can promote biased amplification, potentially introducing unwanted by-products to subsequent selection steps [162, 183]. Off-target hybridization of primers with the aptamer functional region can result in truncated or incomplete sequences, long sequences with repetitive primer daisy chains, or sequences where the primers are disrupting the functional region [186]. The over-amplification of these by-products can overload and dominate the aptamer pool for subsequent cycles of SELEX, decreasing the chance of generating an ideal binding sequence, therefore stringent quality control measures are required in every step of the amplification.

After PCR amplification, single-stranded oligonucleotides are regenerated to re-enter the next cycle of SELEX selection. Conventional PCR amplification results in a new complementary strand for each existing sequence, doubling the combination of sequences. The forward and reverse strands are hybridized and must be separated for proper intramolecular folding to take place. For RNA aptamers, the reverse strand of the dsDNA can be used as a

template to regenerate ssRNA through transcription, removing the additional DNA strand that is created during the amplification step [173].

In silico SELEX is another aptamer selection approach that utilizes computational power to screen and predict binding sequences for a given target. With the assistance of molecular modelling software, the starting library can be "pre-screened" by including sequences with predicted binding activity [169, 187–189]. Molecular modelling simulations can predict 3D structures and ligand-sequence interaction based on physiochemical properties. *In silico* aptamer design and selection can greatly shorten the aptamer development time by removing experimental selection steps [171]. However, the challenge of *in silico* SELEX is that the current simulations have limited accuracy when predicting structures and interactions due to technological constraints, therefore experimental validation is still crucial for aptamer development [190].

1.2.3. Aptamer Sequencing

At the end of SELEX, the strong binding sequences should have emerged and dominate the aptamer population within the pool. For quality assurance, the diversity standard of random oligonucleotides (DiStRO) assay can be used to quickly access the sequence convergence and compare the melting curve of the aptamer pools over the rounds of selection. The collective melting curve of the late-selection-stage aptamer pool is expected to have a high melting temperature (T_m) and a narrow peak in comparison to early stage aptamers [191].

After SELEX, individual sequences are then isolated and identified, which can be achieved by traditional molecular cloning-Sanger sequencing technique, or through high-throughput sequencing (HTS). The short aptamer sequences have to be adapted to corresponding platforms before the sequencing process. For the cloning-Sanger sequencing method, the pool of nucleic acid is ligated into plasmid vectors and transformed into competent cells for culturing. Theoretically, each bacterial colony is a clonal population that grows on the selective medium and carries the same copy of plasmid with the same unique inserted aptamer sequence. For a typical SELEX workflow, usually 30-100 colonies are picked, amplified, and the

plasmids are then extracted and purified for Sanger sequencing [183]. As the aptamer pool is most likely to be dominated by the strongest binding sequences after rounds of SELEX enrichment, multiple colonies might contain the same strong binding sequences because they are the most abundant at the end of the selection. The recovered sequences are ranked based on frequency, and candidates with the highest frequencies are selected for subsequent characterization and testing [192]. The cloning-Sanger sequencing method is relatively inexpensive and simple; however, it is time consuming and labour intensive. Furthermore, many potential binding sequences could be lost due the low throughput approach [193].

The HTS or the Next Generation Sequencing (NGS) approach is currently the most popular method for identifying binding sequence after the selection steps. In comparison, NGS has a shorter preparation time and requires smaller amount of sample for analysis, which is especially helpful for monitoring sequence enrichment in-between cycles of selection [194]. A sample of each cycle of selection can be sequenced in parallel on a multiplex platform after being labeled with a unique sequencing index [195]. Bioinformatics tools that are specifically designed to assist the data analysis of aptamer sequencing are capable of compiling sequencing data from multiple selection rounds, performing cluster analysis, and tracking the emergence of binding sequences over the course of the selection process. Such an approach can be used to reduce the number of cycles needed to generate a promising candidate [194, 196, 197].

1.2.4. Aptamer-Target Binding Analysis

Binding analysis is crucial for determining the endpoint of the selection process and to evaluate the specificity and affinity of the aptamer against the target molecule. In between rounds of SELEX, samples of generated aptamers are collected and analyzed. Promising aptamer candidates are isolated and tested individually. Both labelled and label-free aptamers can be evaluated via different approaches.

Conventional protein-protein analytical approaches can be adapted for aptamer purposes. Aptamer-linked immobilized sorbent assay (ALISA) and fluorescence-linked aptamer assay (FLAA) utilize a labeled aptamer sequence to quantify binding affinity of the aptamer to

the target [198, 199]. Captured aptamers can be detected by using ssDNA dye, or through enzyme-linked approaches such as biotin-streptavidin-horseradish peroxidase (HRP) interaction [200–202]. For visualization, electrophoretic mobility shift assay (EMSA) or gel shift assay separates the bound aptamer-target complex from free non-binding aptamers in a non-denaturing native gel matrix [162, 203]. In the last two decades of aptamer research, surface plasmon resonance (SPR) or biolayer interferometry (BLI) technologies are the go-to molecular assays to measure the association and dissociation rate of an aptamer-target complex in real-time. The instrument detects the shift in reflected light caused by the molecule interactions, and generates a sensorgram that shows the change in light wavelength. The data is then used to model the interaction kinetics, and to calculate the association and dissociation constant of the binding target and the aptamer with good precision, down to sub-nanomolar concentration [204–206].

In silico molecular modelling predicts the structure and binding kinetics of aptamers by simulating the intra- and intermolecular forces. 3D aptamer geometry is modelled based on the predicted secondary structure of a given sequence [207–209]. Linear nucleotides are base-paired based on Watson-Crick complementary pairing, forming secondary hairpin and loop structures [210]. Aptamer folding software would generate several possible folding conformation with suggested Gibb's free energy according to the given experimental parameters. *In silico* analysis can also predict specific interacting atoms between the target and the aptamer, however such processes require high computational power. Without supporting experimental data, the accuracy of the predicted structure and binding kinetics are questionable [209].

1.2.5. Aptamer Synthesis and Modification

Once the ideal aptamer candidate is identified and isolated, further modification can enhance the binding efficiency and functionality of the sequence according to its intended application. For aptamer biosensor and diagnostic purposes, the main application considerations are the shelf life and stability of nucleic acid. Although a DNA aptamer is

relatively more stable than its RNA counterpart, it is still susceptible to nuclease digestion or heat denaturation [211–213]. For *in vivo* therapeutic use, renal filtration, physiological environment (biological salinity, acidity, and ionic concentration), immunogenicity, cell toxicity, and the presence of ubiquitous nucleases pose a challenge to develop long-lasting, effective aptamer-based therapeutics [161, 211, 214].

Compared to native RNA and DNA aptamers, modified aptamers have higher stability, and higher resistance against the ambient and physiological environment [161] (Fig. 6). Xeno-nucleic acid (XNA), with chemical modification on its sugar (e.g. 2'-amino, 2'- fluoro, Locked and Unlocked Nucleic Acid, 2'-O-methoxy-ethyl), base, or backbone can provide protection against nuclease digestion, and potentially increase binding functionality that may exceed natural nucleotides (Fig. 6) [161, 162]. One of the common modifications, oxygen-to-sulphur substitution at the ribose subunit or at the phosphodiester linkage generates thioaptamers with higher nuclease resistance (Fig. 6), and improved target binding when compared to natural DNA sequences [215, 216]. Conjugation of innate molecules -- such as addition of methyl groups, biotin, PEGylation, cholesterol conjugation (Fig. 6) -- onto the 3'- and 5'- terminals of the sequences enhances the resistance against exonucleases, overcomes renal filtration, and can be used as a biomarker for aptamer synthesis and analysis [161, 214, 215, 217]. Another strategy is to synthesize bivalent aptamers where two sets of aptamers are fused together, forming a circular sequence that can resist exonuclease digestion, and bind two targets at once [218, 219].

1.2.6. Aptamer Applications

Aptamer technology is gaining popularity in diagnostic, biosensor, and therapeutic development. Based on its intended purpose, aptamers can be customized to perform various tasks including visual (bioluminescent, fluorescent, and visible light) and electrical signaling, target capturing, and inhibiting protein function [211–213].

Fluorogenic RNA aptamers (e.g. Spinach RNA aptamer, a green fluorescent protein mimic) are used as a reporter tool to track and quantify tagged RNA expression of a transfected

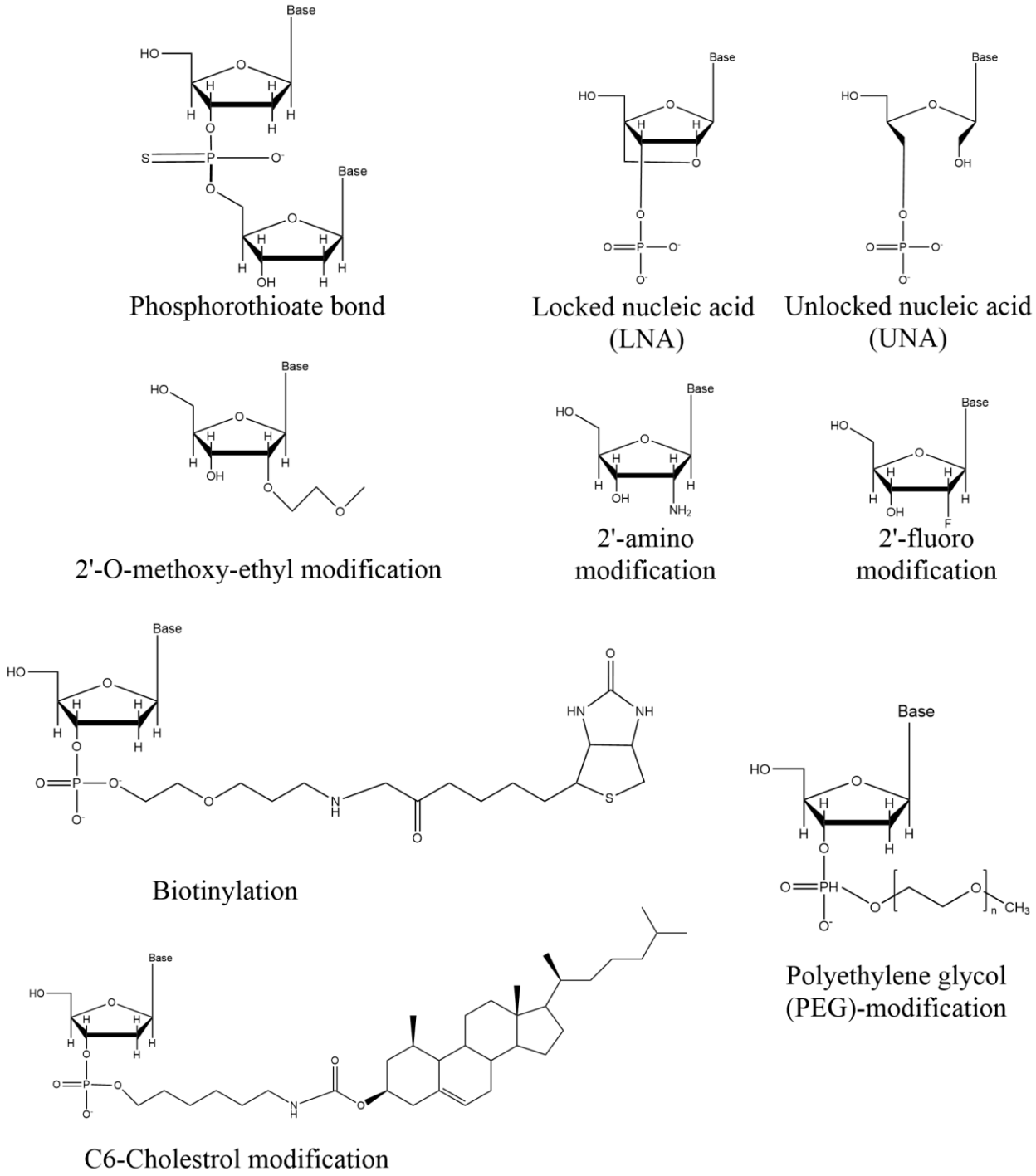


Figure 6. Common aptamer nucleotide modification. Post-selection aptamer nucleotide modification with add-on functionality, reduced renal filtration, and increased nuclease resistance. Figure created with ChemDraw.

living cell, whether the target sequence is a coding or non-coding RNA [220, 221]. For diagnostics, aptamers can be synthesized onto chips and membranes just like mAb. Since aptamers can be selected against live cells, there is research to detect cancer cells using modified aptamers for the flow cytometry platform [222, 223]. To overcome the small molecular mass and susceptibility to nuclease degradation, aptamer-functionalized gold or carbon nanoparticles can improve nucleic acid stability and amplify signal [211, 224, 225]. In recent years, aptamer-based SPR optical biosensors are gaining popularity due to their sensitivity and convenience [226]. Outside of the laboratory setting, there is an interest in developing POC devices based on electrochemical or colorimetric aptamer assays like microfluidic chips, paper or nitrocellulose membrane-based chromatography, dot blot, and lateral flow strips [227]. Such technology can be deployed in the field where access to laboratory instrumentation is limited. This is particularly useful in illicit drug screening [227–229], rapid pathogen detection [230–232], or even clinical cancer diagnosis [233].

SOMAscan, developed by the company SomaLogic, is an emerging high throughput proteomic and biomarker discovery platform that utilizes modified aptamers for detecting and quantifying biomarkers in a given sample. The platform is based on slow off-rate modified aptamer (SOMAmer) technology, which contains modified deoxyuridine nucleotides that provides enhanced nuclease resistance, structural complexity, and target affinity [234, 235]. The SOMAscan platform has a library of unique SOMAmer sequences that can bind to specific protein biomarkers, and acts as a surrogate for protein quantification. Depending on the version of the platform, the multiplex system is able to identify more than 7000 human protein analytes simultaneously [236].

For therapeutic purposes, aptamers have been explored as carriers for targeted drug delivery. Due to the high specificity of aptamers, studies have developed sequences that recognize specific oncogenic biomarkers on the cell surface through cell-SELEX (selecting aptamers using live-cells as target) [194, 237, 238]. Aptamer-coated vesicles, such as liposome or gold nanoparticles are able to deliver and release chemotherapeutic agents to selected cancer cells with reduced cytotoxicity in mouse models [239–241]. Aptamer-conjugated

therapeutics (such as miRNA, siRNA, peptides, and cancer drugs) show greater cell-specificity and drug permeability than the therapeutic agent alone [237, 242–244].

As of writing, pegaptanib (brand name Macugen) is the only therapeutic aptamer approved by Canada and US health authorities. Pegaptanib antagonizes vascular endothelial growth factor, which slows the progression of age-related macular degeneration by suppressing new blood vessel growth and vascular leakage in the eye [245]. The main hurdles of therapeutic aptamer application are the short *in vivo* half-life, rapid renal filtration, and limited biodistribution, however these can be addressed through post-selection modification [232, 246, 247]. Even though there are many on-going research efforts to develop novel therapeutic aptamers, most of them are still in stages of animal testing and clinical trials due to efficacy and toxicology concerns [211, 247]. The incentive to develop therapeutic aptamers is also curbed by notable cases of severe allergic reaction associated with aptamer PEGylation [248] and the market domination of conventional antibody therapies [247].

1.3. In-vitro infection assay for the Detection and Propagation of SARS-CoV-2

1.3.1. Authentic Virus Models

Authentic SARS-CoV-2 virus can be used to develop virus neutralizing small molecules, such as antivirals, mAb, and aptamers *in vitro*. Replication-competent SARS-CoV-2 viruses are collected and propagated from contaminated material, clinical samples, infected livestock and wildlife [249]. Cell lines that are susceptible to SARS-CoV-2 infection are utilized for evaluating infectivity of the virus *in vitro*, which is useful for screening therapeutic drugs and developing diagnostic platforms. Immortalized cell lines, such as African green monkey kidney clone E6 (Vero E6) and human embryonic kidney cells HEK293, have been modified to express the necessary ACE2 receptors and TMPRSS2 protease that enable viral attachment and entry [250]. Another *in vitro* infection model is to use primary human cells and tissues. Studies have developed human lung alveolar type 2 trans-well and 3D (organoid) cell models to mimic the air-liquid interface in human airway, which is more physiologically relevant than 2D cell culture models. The viral infection can be visualized through immunofluorescence (IF) staining, and

viral load can be quantified in harvested cells by conventional virology assays such as the median tissue culture infectious dose ($TCID_{50}$) assay and RT-qPCR [251–253]. These models are great for investigating the cellular response to virus infection in a controlled laboratory setting. Infectious SARS-CoV-2 virus has to be handled in a biosafety level 3 (BSL-3) containment laboratory.

1.3.2. Pseudotype Virus Model

Biosafety Level 2 (BSL-2)-safe SARS-CoV-2 pseudotype virus was designed to overcome the required use of a BSL-3 containment laboratory for handling and propagation of live viruses. A pseudotype virus, or a pseudovirus, is a virus like particle (VLP) that presents a foreign viral surface protein that is not encoded in its engineered genome. The pseudovirus genome is replication-incompetent and is only capable of one-round of infection in susceptible cells [254]. To produce a pseudoviruses with SARS-CoV-2 S protein, a cloned -- and often codon optimized --SARS-CoV-2 S gene in a plasmid-expression vector is transfected into cells along with a replication defective carrier virus vector and other auxiliary plasmids (e.g. reporter gene, transfer vector) that facilitate the expression, packaging, and release of Spike coated non-replication competent pseudoviruses for downstream experiments (Fig. 7) [255]. As of writing, vesicular stomatitis virus (VSV) [256–258], human immunodeficiency virus (HIV-1) (lentivirus) [259–261], murine leukemia virus (retrovirus) [262] , influenza A virus [263], measles virus [264], and adenovirus [265–267] have been explored as packaging systems for SARS-CoV-2 pseudotype viruses.

The main consideration in designing a pseudotype virus is its application. A viral vector that expresses SARS-CoV-2 S protein can be a vaccine candidate, as it is capable of binding to SARS-CoV-2 host receptors and stimulating the production of anti-S antibodies. Additionally, the viral vectors are highly immunogenic, often due to strong adjuvant properties that enhance the immune response and increase neutralizing antibody titers [264]. The reduced containment requirements for handling pseudoviruses made drug screening and antibody neutralization experiments more accessible and flexible [268]. Furthermore, pseudoviruses can be modified to express reporter genes for enhanced assays readouts. For example, luciferase and green

fluorescent protein reporter genes can be inserted into the viral backbone vector and packaged in pseudoviruses so that reporter protein can be expressed and detected in infected cells to signify viral entry, and transcription and translation of viral proteins and the reporter protein [269]. Mutations of S protein are easily incorporated into the platform just by modifying the gene within the S-expression plasmid. Subsequent *in vitro* procedures can be conducted in BSL-2 containment setting, which greatly lowers the training and equipment barriers for many labs [268]. Although a pseudotype virus is not able to simulate the native viral pathogenicity and complete life cycle of authentic SARS-CoV-2 virus, it is still a great surrogate infection model to study S protein attachment and cell entry.

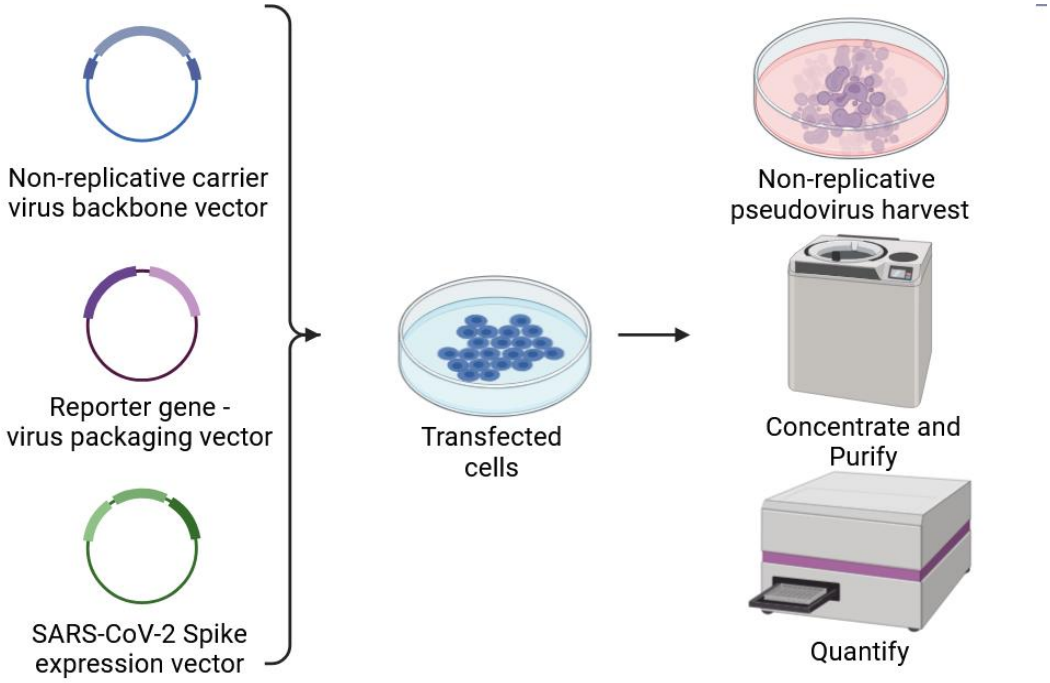


Figure 7. Schematics of SARS-CoV-2 Spike presenting pseudotype virus production. Replication non-competent pseudoviruses are harvested after transfecting competent cells with SASRS-CoV-2 Spike expression vector, packaging vector with reporter gene, and replication defective carrier virus vector (or backbone vector). The infected cell culture is harvested, and SARS-CoV-2 presenting virus-like particles are concentrated and purified using ultracentrifuge. The titer of the progeny pseudovirus is measured and quantified by fluorescence or luminescence plate reader. Figure created with BioRender.com.

Chapter Two: Research Goal

2.1. Rationale

The COVID-19 pandemic has highlighted the need for swift development of diagnostics and therapeutics for emerging diseases. The development of diagnostics and therapeutics is usually time consuming and very expensive. This study aims to utilize the aptamer technology to discover and develop SARS-CoV-2 targeting sequences as potential diagnostic tool and antiviral candidate. Since April 2020, multiple groups have developed aptamers that recognize viral S protein, even exhibit cross-reactivity against other SARS-CoV-2 VOC. Aptamers that target components of the viral infection and life cycle can be great therapeutic candidates. In previous *in vivo* studies, anti-S protein aptamers were able to neutralize authentic SARS-CoV-2 viruses and S-presenting pseudoviruses. Aptamer have high specificity and affinity to target molecules, and can be easily synthesized and manipulated, with a wide range of modifications for flexible applications. Furthermore, the selection and development of aptamers are relatively quick, convenient, and cost-effective, which makes it a great tool for rapid pandemic response.

2.2. Hypothesis

Aptamers that are selected using S-RBD recombinant protein will show binding activity and specificity towards SARS-CoV-2 virus and will block and neutralize infection in a pseudovirus model of *in vitro* infection.

Chapter Three: Materials and Method

3.1. Reagents for Aptamer Selection

Streptavidin coated magnetic beads (Invitrogen, Cat# 65001) used in SELEX for Biotinylated RBD conjugated protein was purchased from Thermo Fisher Scientific. Biotinylated RBD of SARS-COV-2 Spike protein (40592-V27H-B), His-tagged RBD of SARS-CoV-2 Spike Protein (40592-V08B), rabbit SARS-CoV-2 Spike monoclonal Antibody (40592-R190) were purchased from Sino Biological Inc. Peroxidase labeled anti-rabbit IgG antibody (074-1506) is purchased from Kirkegaard & Perry Laboratories, Inc. Streptavidin (S888) for aptamer binding negative control is purchased from Thermo Fisher Scientific. D-Biotin for bio-layer interferometry biosensor blocking (BP232-1) was purchased from Fisher Scientific.

All DNA sequences including individual aptamers, primers, and modified nucleic acids were synthesized by Integrated DNA Technologies, Inc. Spike RBD binding positive control aptamer sequences were synthesized based on existing literature (Table 1). The ssDNA 40mer Bank40 library, streptavidin-targeting positive and negative aptamer control, DNA selection, emulsion, DNA purification, DNA diversity analysis columns and reagents were included in the XELEX DNA Core Kit (E3650) (EURx Ltd, distributed by Roboklon GmbH). Bank40 (5' - TGACACCGTACCTGCTCT - N40 - AAGCACGCCAGGGACTAT - 3') has a random 40mer sequence (N40), flanked by 2 constant 18 nucleotide (nt) primer region at its 5' and 3' ends. The primer regions can be targeted by PCR amplification with SELEX Forward and Reverse primer (Table 1). 1X SELEX buffer (140mM NaCl, 2mM Cl, 5mM $MgCl_2$, 2mM $CaCl_2$, 20mM Tris pH7.4, 0.05% Tween® 20, EURx) was used for aptamer selection and characterization.

For microneutralization assays, poly-L-lysine coated, clear 96-well plates (FisherScientific, Cat# 0877293) were used for cell seeding, infection, and incubation. Black clear-bottom plates (FisherScientific, Cat# 1256607) were used for luciferase assays. For ALISA and aptamer biostability assay, clear 96-well plates (Corning #3690) were used. For BLI assays, black, flat bottom plates (Corning #3915) were used.

Table 1. Spike RBD binding aptamer controls, Bank40 ssDNA library, SELEX amplification and NGS sequencing primers.

Name	Abbreviation	Length (nt)	Sequence (5' → 3')
Streptavidin aptamer controls [195]	SA Pos Ctrl	40	ATCTCCGATTGCCCCACG**ACGC**AGTGGT**CG**G**A**GTTACTTT
	SA Neg Ctrl	40	TGACACCGTACCTGCTCTATGCCTATCATGGGCAACCACG
Spike RBD binding aptamer controls [270]	Liu 1	76	ATCCAGAGTGACGCAGCATCGAGTGGCTTGTTTGTAATGTAGGGTTCCGGTCGTGGGTTGGACACGGTGGCTTAGT
	Liu 1a	40	TCGAGTGGCTTGTTTGTAATGTAGGGTTCCGGTCGTGGGT
Biotinylated aptamer control	Biot-Liu1a	40	Biotin - TCGAGTGGCTTGTTTGTAATGTAGGGTTCCGGTCGTGGGT
Phosphorothioated aptamer controls	PhosThio Liu1a	40	TCGAGTGGCTTGTTTGTAATGTAGGGTTCCGGTCGTGGGT
	PhosThio PhiX	60	GGATGGTGTTAATGCCACTCCTCTCCCGACTGTTAACACTACTGGTTATATTGACCATGC
Bank40 ssDNA library		76	TGACACCGTACCTGCTCT - (N40) - AAGCACGCCAGGGACTAT
SELEX amplification primer	Bank40 FWD	18	TGACACCGTACCTGCTCT
	Bank40 RVS	18	ATAGGTCCCTGGCGTGCTT
NGS sequencing primer	Bank40 NGS FWD	60	CGTCGGCAGCGTCAGATGTGTATAAGAGACAG –(N10)- TGACACCGTACCTGCTCT
	Bank40 NGS RVS	60	CTCGTGGGCTCGGAGATGTGTATAAGAGACAG –(N10)- ATAGTCCCTGGCGTGCTT
	Illumina index 1 read PCR primer	48	CAAGCAGAAGACGGCATACGAGAT[i7]GTCTCGTGGGCTCGG
	Illumina index 2 read PCR primer	52	AATGATACGGCGACCACCGAGATCTACAC[i5]TCGTCGGCAGCGTC

Known streptavidin binding motif is bolded. Phosphorothioate backbone nucleotides is underlined. For NGS sequencing, Bank40 NGS primers were designed to have 10 random nucleotides (N) as unique molecular identifiers. Illumina index 1 & 2 read PCR primers carried a unique 8 nucleotide ([i7] and [i5]) index (for multiplex sequencing purposes).

3.2. Cells and Pseudovirus Preparation

HEK293T/ACE2-TMPRSS2 cells (SL222) that were susceptible to SARS-CoV-2 Spike lentivirus pseudotype virus were obtained from GeneCopoeia. SARS-CoV-2 Spike pseudotype lentivirus was provided by Dr. Heidi Wood's group at the National Microbiology Laboratory (NML). The pseudovirus development and preparation was as previously reported [261]. Briefly, a luciferase-ZsGreen transfer vector, an empty HIV packaging vector, and a SARS-CoV-2 Spike envelope expression vector were used to transfect HKE293T cells (Fig. 8). Replication-incompetent lentiviral particles with SARS-CoV-2 Spike envelope protein were harvested, clarified, and concentrated for surrogate neutralization assay.

The HEK293T/ACE2-TMPRSS2 cells were cultured in Dulbecco's modified Eagle medium (DMEM) supplemented with 10% heat inactivated (56^{o}C, 30 minutes) fetal bovine serum (FBS, HyClone), 100 units/mL penicillin, 100 units/mL streptomycin, 6mM L-glutamine, 1mM sodium pyruvate (referred to as DMEM10 medium as it contained 10% FBS). For routine passaging, additional 100µg/mL hygromycin and 1µg/mL puromycin were added as selection antibiotics. All experiments were done using cells under 25 passages. For the surrogate neuralization assay, HEK293T/ACE2-TMPRSS2 cells were cultured in DMEM without phenol red (HyClone), supplemented with 5% heat inactivated FBS, 100 units/mL penicillin, 100 units/mL streptomycin, 2mM L-glutamine, 1 mM sodium pyruvate (DMEM without phenol red). The pseudotyped virus stock was diluted in Dulbecco's phosphate-buffered saline (DPBS, Gibco), supplemented with 5mM of $MgCl_2$ for optimal aptamer folding and stability (DPBS/Mg). Cells were grown in a 5% CO_2 incubator at 37^{o}C.

Passaging of cells was performed by first discarding old DMEM10 medium, then gently rinsing the cells with DPBS. 2mL of 0.25% trypsin-EDTA (Gibco) was then added, and cells were trysinized at 37^{o}C for 5 min. The cells were resuspended with 8mL of fresh DMEM10 medium. 10µL of cell suspension were mixed with 10µL of 0.4% trypan blue stain (Invitrogen) and loaded onto a cell counting chamber slide and counted with the Countess^{TM} automatic cell counting system (Invitogen). Resuspended cells were transferred to a new T150 flask (Corning) and fresh DMEM10 medium was added to a final cell density of 4x10^{3} cells/mL. Cells were passaged when they reached 80-90% confluency.

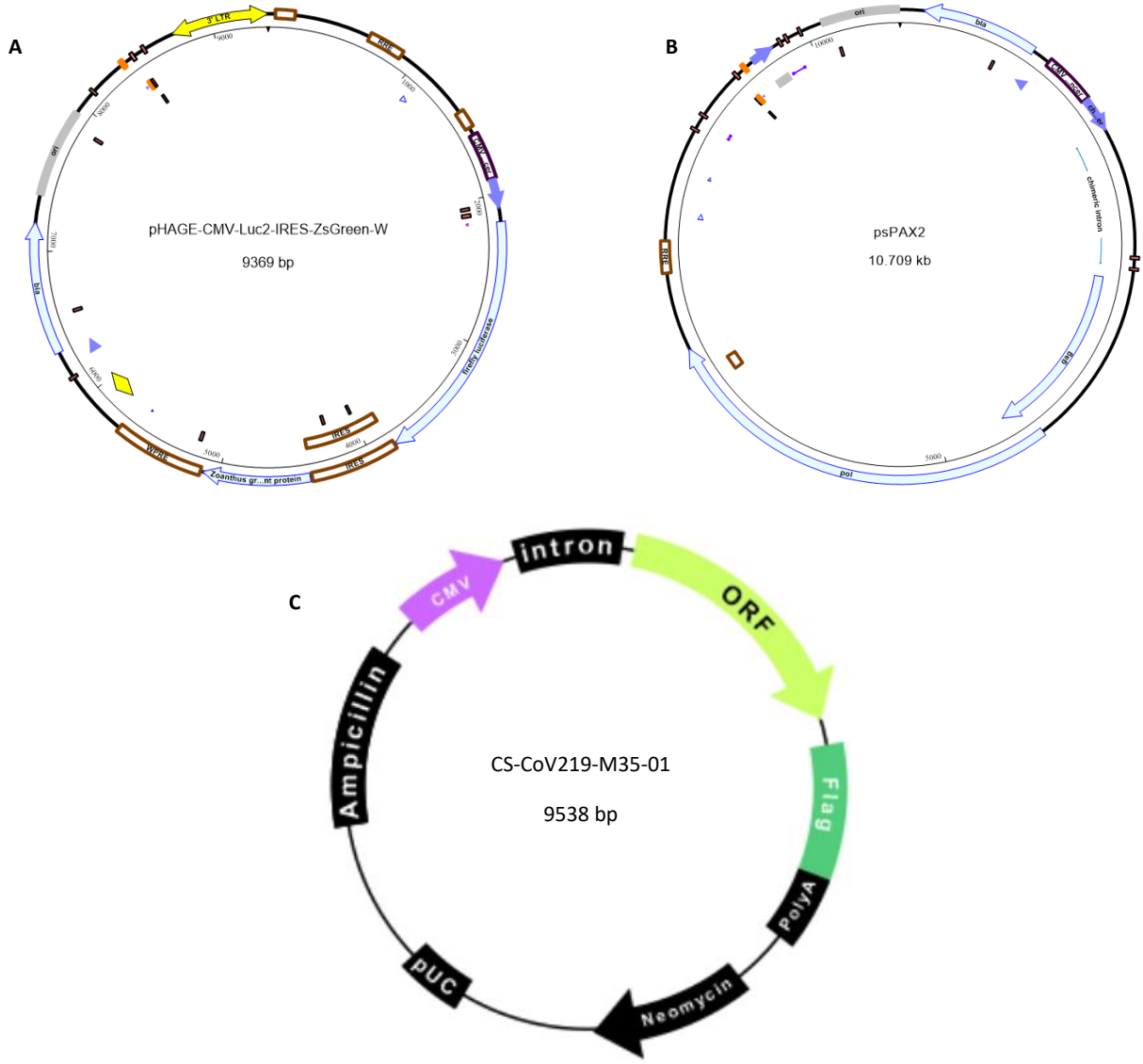


Figure 8. Vectors used in pseudotype LV production. Transfer vector, pHAGE-CMV-Luc2-IRES-ZsGreen-W (A), empty HIV packaging vector, PsPAX2 (B), and SARS-CoV-2 Spike envelope expression vector, CS-CoV219-M35-01 (C). pHAGE-CMV-Luc2-IRES-ZsGreen-W and PsPAX2 could be purchased from AddGene (Cat# 164432, 12259), and CS-CoV219-M35-01 were synthesized by GeneCopoeia or generated in-house.

3.3. Systematic Evolution of Ligands by EXponential enrichment (SELEX)

3.3.1 Target Selection

To select binding sequences in the aptamer pool, the Bank40 ssDNA library was first exposed to the target antigen, the RBD region of SARS-CoV-2 S protein. To do this, biotinylated S RBD (S-RBD) recombinant protein was immobilized on streptavidin-coated magnetic beads. The streptavidin-coated beads were washed 3 times with 1X SELEX buffer before immobilization. For the first round of selection, 1000µg of streptavidin-coated magnetic beads were resuspended in 100µL of 1X SELEX buffer in a clean 1.5mL tube, and 7.5µg of biotinylated S-RBD was added. To make sure the beads were fully saturated, the amount of biotinylated-SRBD needed was determined by testing fixed amount of magnetic beads against increasing concentration of protein until the beads could no longer bind to additional protein as determined by Nanodrop (IgG setting). The mixture was set on an orbital tube shaker at 300 RPM and incubated for 30 min at room temperature. The protein coated beads were then separated by magnet and washed four times with 1mL of 1X SELEX buffer to remove residual buffer and unbound protein and resuspended to 100µL in 1X SELEX buffer. Twenty micromolar Bank40 ssDNA library, which was included in the XELEX core kit (EURx), was used for the first round of SELEX selection. To promote secondary structure formation and proper folding, Bank40 ssDNA library was heated to 94^{o}C for three min and immediately chilled on ice for 10 min, then slowly brought back to room temperature. Then, 500pmol of heat-denatured Bank40 library, diluted in 1X SELEX buffer, was added to the protein-coated beads and incubated for 90 min at room temperature, gently agitated on a tube rotator. After incubation, the beads were immobilized with magnet, and washed one to three times with 500µL of 1X SELEX buffer. The bound sequences were then eluted on a heated block with 50µL of nuclease-free water which was preheated to 94^{o}C. The eluted supernatant was quickly transferred to a clean 0.5mL screw cap tube. The elute was stored in –30^{o}C freezer until amplification step.

A counter selection step was implemented at the beginning of 2nd cycle and onwards. In a 1.5mL tube, the nucleic acid pool (2 – 10th round of SELEX, 2-10R) from previous SELEX cycle was heat denatured (incubated at 94^{o} for 3 min, then immediately chilled on ice for 10 min, and slowly brought back up to room temperature). The regenerated ssDNA pool was then mixed

with 50ul of 10X SELEX buffer, and diluted with molecular-grade nuclease-free water to a final volume of 500ul. 200µg of streptavidin-coated magnetic beads was added to the diluted ssDNA pool, and incubated on a tube rotator for 1 hour at room temperature (Fig. 5, step 2). After incubation, the tube was transferred to a magnet stand and the sequence-bound beads were separated and discarded, removing off-target anti-streptavidin sequences from the ssDNA pool. The supernatant was collected and quantified with Nanodrop.

The stringency of the selection process was increased in later SELEX cycles. For stricter selection, the amount of S-RBD protein and streptavidin-coated beads were gradually reduced from 7.5µg to 1.5µg; the binding incubation time was shortened from 90 min to 15 min; and the amount of post-incubation 1x SELEX buffer washes increased from one to three times to remove weaker binders (see Table 2 for detail breakdown for each SELEX round).

3.3.2 SELEX PCR Optimization

Ideally, the amplified PCR product should maintain a high level of diversity with minimal non-specific amplification. An optimization experiment was set up to compare different PCR polymerase kits to determine the optimal PCR parameter. Three different kits were tested: Takara PrimeSTAR Max DNA polymerase master mix (Takara Bio, Cat# R045A), iProof High-Fidelity polymerase PCR kit (BioRad, Cat# 1725301), and Phusion U Multiplex PCR master mix (Thermo Fisher, Cat# F562L). For each PCR polymerase kit, a gradient PCR was set up to determine the polymerase-specific optimum annealing temperature for the primer-annealing step. Once the optimal annealing temperature was established, each kit was used to amplify the starting Bank40 ssDNA library through conventional “PCR” and or emulsion PCR (ePCR) separately. To compare PCR specificity and efficiency, the PCR product of each kit was evaluated with quantative PCR (qPCR) melt-curve and gel electrophoresis analyses.

For gradient PCR, 12 PCR reactions were made per DNA polymerase kit. A 600µL master mix was prepared as follow: 103.2µL Bank40 template (stock concentration 1250pmol), 24µL of each Bank40 FWD and RVS primer (stock concentration 100µM), and individual components from each polymerase kit. The individual components as follow: PrimeSTAR polymerase kit:

Table 2. SELEX parameter of 10 selection cycles.

SELEX Cycle #	Protein (μg)	Beads (μg)	Binding incubation time (min)	Washing step (# of washes x buffer volume (μL))	Total number of ePCR cycles*
1	7.5	1000	90	1x500	30 (15+15)
2	3.75	500	60	1x500	27 (15+12)
3	3.75	500	60	1x500	15
4	3.75	500	60	2x500	154
5	3.75	500	45	2x500	15
6	3.75	500	45	2x500	13
7	3	400	45	2x500	11
8	2.625	350	30	3x500	20 (10+10)
9	2.625	350	30	3x500	10
10	1.5	200	15	3x500	10

*Note that the number of ePCR cycles was determined by the concentration of ssDNA recovered from the previous round of selection. The suggested maximum ePCR cycles per emulsion preparation was 15 cycles to prevent overamplification and nucleotide depletion within individual lipid micelles. Therefore, 1R, 2R, and 8R samples were subjected to two sets of ePCR, as denoted by brackets (“set 1”+ “set 2”).

300µL of polymerase mater mix and 148.8µL of nuclease-free water; iProof polymerase kit: 120µL of 5XGC buffer, 12µL of dNTP (10mM, Thermo Scientific, Cat# R0193), 12µL of $MgCl_2$ (50mM), 6uL of polymerase (2U/µL), 18µL of DMSO, and 280.8µL of nuclease-free water; Phusion polymerse kit: 300µL of 2X Phusion master mix, and 148.8µL of nuclease-free water. The master mix of each kit was aliquot into 12 0.2mL PCR tubes and loaded onto Biometra T Gradient Thermocycler, and the following cycling parameter was ran: 95^{o}C for 1 min, then 20 cycles of 95^{o}C for 10 sec, 48-62^{o}C for 30 sec, 72^{o}C for 30 sec, and finally 72^{o}C for 5 min. PCR samples from each kit were loaded onto separate 1% agarose gel (prestained with 1x precast GelGreen Nucleic Acid Gel Stain (Biotium, Cat# 41005)), together with GelPilot 1kb Plus ladder Ladder (Qiagen, Cat# 239095) and ran at 50V for 45 minutes with 1x TAE buffer. The gels were then visualized with gel documentation system (Syngene) under UV light. Annealing temperature that resulted in the sharpest band for each kit was chosen for further PCR optimization.

Then, to compare the specificity of conventional PCR (open PCR) and emulsion PCR (ePCR), each PCR kit was used to set up two different PCRs to determine the optimal amplification approach. The principle of ePCR is to encapsulate individual oligonucleotides in separate micelles to minimize PCR bias. For each kit, 200µL of aqueous PCR mix was prepared as follow: 34.4µL Bank40 template (stock concentration 1250pmol), 8µL of each Bank40 FWD and RVS primer (stock concentration 100µM), and individual components from each polymerase kit. Kit-specific individual components as follow: PrimeSTAR polymerase: 100µL of polymerase master mix and 49.3µL of nuclease-free water; iProof polymerase kit: 40µL of 5XGC buffer, 4µL of dNTP (stock concentration 10mM), 4µL of $MgCl_2$ (stock concentration 50mM), 2uL of polymerase (2U/µL), 6µL of DMSO, and 93.6µL of nuclease-free water; Phusion polymerse kit: 100µL of 2X Phusion master mix, and 49.6µL of nuclease-free water. Half of the master mix was divided into duplicate (2x50µL) open PCR reactions, and the remaining half was divided and reserved for duplicate (2x50µL) ePCR reaction. For each ePCR reactions, an additional oil phase was made with emulsion components provided in the XELEX kit: 220µL of emulsion component 1, 20µL of emulation component 2, and 60µL of emulsion component 3, the mixture was then vortexed thoroughly. 50µL of aqueous PCR mix was then added to the oil

phase, and the mixture was vigorously vortexed for 5 min at 4°C. Both open PCR and ePCR reaction mixes were then loaded onto ProFlex PCR system (Applied Biosystems). The thermocycler parameters were: 95°C for 120 sec, then 20 cycles of 95°C for 30 sec, 55.8°C (PrimeSTAR)/57.5°C (iProof)/59.2°C (Phusion) for 60 sec, 72°C for 180 sec, and finally 72°C for 300 sec. The annealing temperature was set based on the temperature that resulted in optimal band resolution from previous gradient PCR experiment (see Chapter Four: Result). After PCR amplification, 1mL of 1-butanol was added to the ePCR reaction mix and vortexed thoroughly to break the emulsion. For phase separation, 250µL of orange separation SFB buffer (XELEX kit) was added to the opened emulsion solution, and mixed by gentle agitation. After centrifuging the mixture at 16000xg for 2 min, the yellow coloured organic phase was carefully removed from the phase-separated ePCR reaction mix and 275µL of ethanol (100% v/v) was added to the aqueous phase. Both ePCR aqueous phase and open PCR reactions were then purified using the XELEX kit spin columns as per manufacturer instruction, and recovered dsDNA was quantified using Qubit™ 1X dsDNA High Sensitivity assay kit (Invitrogen, Cat# Q33231). To investigate whether the PCR approach would exhibit preferential amplification, a separate open PCR reaction with minimal amplification cycling was set up so that the amplicon would retain the same degree of diversity as the starting Bank40 library, and could be used as a diversity standard. For that, a duplicate open PCR reaction was set up using the iProof PCR kit (same reaction mix formulation, same thermocycling temperature and duration as above). The reaction was amplified with six PCR cycles, the dsDNA PCR product was purified and recovered with the same methods as other PCR samples.

For qPCR melt-curve analysis, 5µL RT^2 SYNR Green ROX qPCR master mix (Qiagen, Cat# 330523) and 10µL of nuclease-free water was added to 5µL of purified PCR amplicons. A no-template-control (NTC) was set up alongside the PCR amplicons. The duplicate samples (3 reaction kits, 2 PCR condition per kit, 2 reactions per condition), additional 2 diversity standard samples, and 2 NTC (16 samples in total) were then loaded onto a qPCR 96-well plate. The samples were analysed on QuantStudio™ 5 Real-Time PCR system (Applied Biosystems) for the following melt-curve analysis parameter: 95°C for 120 sec, then 76 °C for 180 min, take one measurement per minute, 20 °C for 15 sec, heating up to 98 °C with 0.1 °C increment per sec

with continuous data collection, and hold for 15 sec once reach 98 °C. Data was retrieved and processed via QuantStudio analysis software v1.5.1. The melting curve of each sample was visualized and compared side-by-side with the diversity standard.

For gel electrophoresis analysis, 10µL of the purified sample from the previous step was loaded onto a 2% agarose gel (precast stained with 3x GelGreen stain) along with 50bp DNA ladder (Invitrogen, Cat# 10416014), and ran at 50V for 60 min. The gel was then transferred to a gel documentation system (Syngene) and dsDNA bands were visualized and recorded under UV light.

3.3.2. Binding sequence Amplification

Different DNA polymerase mixes were also tested to compare their ability to amplify the highly diverse ssDNA library with sufficient efficiency and minimal byproduct formation.

ePCR reagents were included in the XELEX core kit (EURx). Briefly, in a 1.5mL tube, for the PCR oil phase that generates the encapsulating micelles, mineral oil and emulsifying reagents, specifically 220µL of emulsion component 1, 20µL of emulation component 2, and 60µL of emulsion component 3, were mixed and vortexed thoroughly. For the PCR aqueous phase that contained PCR reagents and oligonucleotides, 1X PrimeSTAR Max Premix (Takara), 200pmol of Bank40 3' and 5' primer, and 0.5µg of ssDNA SELEX elute were mixed and topped with nuclease-free water to the final volume of 50µL. The PCR water phase was then mixed with the PCR oil phase, and the mixture was vigorously vortexed for five min at 4°C. Since the total reaction volume exceeded 0.2mL, the white emulsified ePCR reaction mix was then aliquoted into to 2 0.2mL PCR tubes and loaded onto a ProFlex PCR system (Applied Biosystems). Based on the XELEX kit user manual, the thermocycler parameters were: 95°C for 120 sec, then maximum 15 cycles of 95°C for 30 sec, 55.8°C for 60 sec, and 72°C for 180 sec; then 72°C for 300 sec. The ePCR mixture was then processed and dsDNA was purified using the XELEX core kit clean up procedure as per manufacturer instruction. The recovered dsDNA was then quantified using the Qubit dsDNA kit. Due to the supposed emergence of dominating binding sequences over rounds of SELEX, the number of ePCR cycles was gradually lowered along the selection process (see breakdown of number of ePCR cycles for each SELEX round in

Table 2). If the yield of recovered amplicon fell below 1µg, additional ePCR (for reactions 1R, 2R, and 8R, see Table 2) was set up to generate sufficient dsDNA for subsequent selection steps.

3.4. Asymmetric PCR for ssDNA Amplification

Aptamer pools were amplified with asymmetric PCR (aPCR) [271, 272] before pool-target binding analysis. Five microliters of ePCR dsDNA product from the selected rounds were mixed with 200pmol Bank40 FWD primer and 4pmol Bank40 RVS primer, 25µL of 2X PrimerSTAR polymerase (Takara), and topped with nuclease-free water to constitute 50µL of PCR mix in a 0.2mL PCR tube. PCR mixes were loaded onto the thermocycler and the following parameter were run: 95^{o}C for 120 sec., then 50 cycles of 98^{o}C for 10 sec., 55.8^{o}C for 5 sec., and 72^{o}C for 5 sec. The amplicons were then purified using Monarch® PCR & DNA Cleanup Kit (NEB) with oligonucleotide cleanup protocol. The recovered amplicons were quantified by Quant-iT™ OliGreen™ ssDNA assay (Invitrogen).

3.5. ssDNA pool binding enrichment assessment

3.5.1. Qualitative Polymerase Chain Reaction (qPCR) melt-curve analysis

SELEX pool enrichment qPCR melt-curve analysis protocol was adapted from the Diversity Standard of Random Oligonucleotides (DiStRO) assay [191]. First, both SELEX sample and diversity standards (provided in XELEX kit) were amplified with a brief PCR. 2.5nM of diversity standards (0N, 4N, 6N, 12N), Bank40 starting library, and the SELEX samples (1st – 10th round) were mixed with either 4.5uM forward and reverse DivStd Amplification primers (sequence not provided) or 20uM Bank40 FWD and RVS primers. 1X PrimeSTAR polymerase (Takara) was then added to each mixture to make PCR mix. The PCR mixes were then loaded onto the thermocycler with the following PCR parameter: 95^{o}C for 10 sec., then 6 cycles of 59^{o}C for 15 sec., and 72^{o}C for 5 sec, followed by final extension 72 ^{o}C for 300 sec. The PCR amplicons were then purified with DNA purification set included in the XELEX analysis kit. All the PCR products were quantified using Nanodrop.

Next, RT^2 SYNR Green ROX qPCR master mix (Qiagen) was added to 200-300ng (maximum 10µL) of recovered PCR amplicons, and topped to 20µL with molecular-grade nuclease-free water. A no-template-control (NTC) was set up alongside the PCR amplicons. Samples were then loaded onto a qPCR 96-well plate in triplicates, and mounted to QuantStudio™ 5 Real-Time PCR system (Applied Biosystems) for the following melt-curve analysis parameter: 95°C for 120 sec., then 76 °C for 180 min, take one measurement per minute, 20 °C for 15 sec., heating up to 98 °C with 0.1 °C increment per sec. with continuous data collection, and hold for 15 sec. once reach 98 °C. Melting curve data was processed and visualized via QuantStudio analysis software v1.5.1, the melting temperature (T_m) was exported to excel file and the average value of the triplicates was recorded.

3.5.2. Aptamer Pool Bio-layer Interferometry (BLI) Assay

Aptamer pools were amplified with asymmetric PCR (aPCR) [271, 272] before pool-target binding analysis. The 2nd, 6th, and 10th round (2R, 6R, 10R) were selected for BLI analysis. Aptamer pool BLI assay was carried out using the Octet Red 96 system (ForteBio). Before starting the analysis, the streptavidin (SA) biosensors were hydrated with 1X KB buffer (0.01% BSA, 0.002% Tween 20 in PBS) in the sensor tray for 30 min prior to target immobilization step. 200pmol of recovered ssDNA from aPCR amplification was heat denatured at 94°C for 3 min, and immediately chilled on ice for 10 min. The ssDNA was then serial diluted in 1X KB buffer to the final concentration of 1000, 500, 250, 125, 62.5, and 31.25nM. 1X KB was used for initial baseline calibration, baseline, and dissociation step; 0.93µg/mL biotinylated recombinant SARS-CoV-2 S RBD (Sino Biological) in 1X KB buffer was used for loading step; and serial diluted aptamer samples were tested during the association step. All BLI assays were performed at 30°C with shaking speed of 1000rpm in a black 96-well flat bottom plate with 200µL of respective solutions. First, the hydrated SA biosensors were submerged in 1X KB for 60 sec for the initial baseline calibration, they were then transferred to wells with the biotinylated S-RBD protein mixture for 180 sec for the loading and immobilization step. The loaded SA biosensors were transferred into wells with 1X KB buffer for 120 sec to establish the baseline, then they were dipped into the serial diluted aptamer pool sample for 300 sec to allow protein-aptamer

association. Finally, the biosensor were transferred into 1X KB buffer for 180 sec to let the protein to dissociate from the aptamer-coated biosensors. Data analysis was performed using ForteBio Data Analysis 9.0 software. For BLI assays, after subtracting baseline reading from the raw data, adjusted association and dissociation curves were fitted to 1:1 kinetic model to calculate K_D value, as suggested in ForteBio user guide.

3.6. Next Generation Sequencing (NGS)

3.6.1. Library Purification and Preparation

First, 10R dsDNA was amplified and converted to 10R ssDNA through aPCR (see section 3.4.). The amplicon was heat denatured at 94^{o}C for 3 min, and immediately chilled on ice for 10 min. To re move unwanted aPCR byproducts, the heat-denatured amplicon was loaded onto a 3% agarose gel (precast stained with 3x GelGreen Stain) along with original Bank40 ssDNA library and 50bp DNA ladder (Invitrogen), and ran for 75 min, at 70V and room temperature. After electrophoresis, the gel was transferred to the gel documentation system (Syngene) and bands were briefly visualized and recorded under UV light. The gel was then transferred to Safe Imager Blue Light Transilluminator (Invitorgen), approximately 76nt sized 10R ssDNA bands were excised and purified using QIAEX II® gel extraction kit (Qiagen), following manufacturer instructions. To maximize ssDNA recovery, the final elution step was repeated twice. The ssDNA elute was further concentrated with Monarch® PCR cleanup kit, to a final volume of 20µL. The quality of the extracted ssDNA was evaluated through microfluidic Bioanalyzer system (Agilent) using the small RNA kit (Agilent), and concentration was measured by Nanodrop using the ssDNA setting.

Then, the 76nt 10R ssDNA sample was converted to dsDNA and extended to 150bp for optimal sequencing length for the Illumina iSeq platform. To do so, a short PCR step was implemented to extend the 10R sequence with the Illumina adapter and a randomized (10nt) nucleotide unique molecular identifier (UMI, N10, NGS sequencing primer, Table 1) [197]. The addition of UMI would improve reading sensitivity and reduce misreads caused by the uniformity of the Bank 40 primer region [273]. Briefly, 25ng of 10R ssDNA sample, 0.2µM of

NGS sequencing primers (Bank40 NGS FWD and RVS), 1X Pfu master mix (G-Biosiences), and nuclease-free water was mixed and amplified through PCR. The thermocycling parameters were as follows: 98°C for 60 sec., then 3 cycles of 98°C for 5 sec., 72°C for 15 sec.; and 72°C for 5 min. The amplicon was loaded onto a GelGreen prestained 3% agarose gel for electrophoresis (60 min, 70V, room temperature) along with a 50bp DNA ladder. Double stranded DNA bands were visualized, imaged, and 150bp bands were excised. The excised gel was then purified using QIAEX II® gel extraction kit and concentrated with Monarch® PCR cleanup kit.

Finally, Illumina enhancement PCR mix (EPM) and PCR master mix were added to the concentrated 150bp 10R dsDNA, extending individual sequences to ~200bp with another PCR step. The thermocycling parameters were as follows: 98°C for 60 sec., followed by 16 cycles of 98°C for 5 sec., 72°C for 15 sec.; and 72°C for 5 min. For PCR clean up, the amplicon was incubated with AMPure XP solid-phase reversible immobilization (SPRI) Beads (Beckman Coulter). The 1:1.3 amplicon-to-bead volume ratio was empirically determined to remove oligonucleotides that were smaller than 200bp. Briefly, 30µL of AMPure beads and 35µL of AMPure buffer were added to 50µL of PCR amplicon and mixed thoroughly with pipette. The mixture was incubated at room temperature for 5 min, and was then transferred to magnetic plate for 2 min to allow the beads to be separated from the solution. The clear solution was aspirated carefully, without touching the immobilized beads. Then, the immobilized beads were washed with 150µL of 80% ethanol. After the ethanol wash was aspirated, the beads were removed from the magnetic plate and briefly centrifuged, returned to the plate, and dried for 2-5 min. Purified dsDNA was eluted after mixing the dsDNA-bound beads with 25µL of elution buffer (0.1X TE buffer) and incubation at 70°C for 5 min. The beads were separated by using a magnetic stand and supernatant with 200bp NGS-ready 10R dsDNA (NGS-10R) was recovered. NGS-10R was quantified using Qubit dsDNA Kit and the sample quality was assessed with the Bioanalyzer HS DNA kit (Agilent). NGS-10R, and a 50bp DNA ladder, were then loaded onto a GelGreen prestained 2% agarose gel. After electrophoresisl for 1.5 hours at 70V, room temperature, 200bp bands were excised and purified with gel extraction kit. After purification, NGS-10R was quantified with Quibit™ dsDNA HS kit and diluted with Illumina resuspension buffer (RSB) to a final concentration of 200pM. 100µL of NGS-10R diluted sample was mixed

with 15µL of 200pM PhiX control library (Illumina). The mixture was then sequenced on iSeq platform (Illumina). For sequencing parameters, the read type was set as paired end, both read 1 and read 2 (forward and reverse reads) were set to 151 read cycles, to cover the entire length of the ~150bp 10R NGS-adapted extended dsDNA.

3.6.2. Data Processing

Raw NGS data processing workflow was done using R 4.1.1 and cutadapt 4.2 (accessing bash through R studio and Windows Subsystem for Linux) (See Appendix for complete script). The following R libraries were used: readr, BiocManager, ShortRead, ggplot2, tidyr, dada2 (version 1.2), writexl. Briefly, raw NGS data was converted to FASTQ files. Using the filterAndTrim function, reads with a low filter score were removed and saved in a separate file. To remove PCR byproducts such as overtly short sequences (<35nt) and sequences with accidental primer inserts or primer daisy chains, only sequences with correct primer orientation and random region length (35-45nt) were selected and trimmed using the cutadapt function. The cutadapt function was used to trim Bank40 PCR primers from the reads and discard trimmed reads that were too short (<35nt), or too long (>45nt). The reverse and forward reads were filtered and trimmed separately. The trimmed reads were dereplicated and optimized through the dada2 algorithm prior to merging. Essentially, dereplication greatly reduce the size of the data by removing identical reads and give them a correspnding abundance number. Then, the DADA2 pipeline would estimate the error rate by comparing the optimized reads and merge pair reads [274]. The merged reads were then compiled and converted into a Microsoft Excel file.

The pre-processed sequencing data were also visualized and manipulated using FASTAptamer [196]. Further analysis of the specific sequence, such as estimating secondary structure was determined by Mfold webserver (https://www.unafold.org/mfold/applications/dna-folding-form.php) [210]. For structure prediction, the folding temperature was set as 25^{o}C, Na^{+} concentration as 140mM, Mg^{2+} concentration as 5mM. Other settings were left as default.

3.7. Candidate Binding Assessment

3.7.1. Single-Sequence Gel Electrophoresis

Known SARS-CoV-2 aptamers (see table 2) were used as positive controls and were tested along with the aptamer candidates identified by the previous NGS step.

One micromolar of aptamer in 1X SELEX buffer was mixed with increasing concentrations of biotinylated S-RBD (0, 0.1, 0.5, 1, and 2µM) or 1µM streptavidin, and an orbital tube shaker was used to continuously agitate the mixtures. Eight microliters of sample was mixed with 2µL of 5X Hi-Density TBE sample buffer (Novex) and loaded on to a 6% polyacrylamide DNA retardation gel (Novex), along with the GeneRuler 50bp DNA ladder (Invitrogen) for size reference. The gel was mounted into the Mini Gel Tank (Invitrogen) and submerged in 0.5X TBE buffer (see Appendix for recipe). The gel was electrophoresed for 65 min at 90V at room temperature. The gel was then removed from the casting cassette, and soaked in 3X GelRed PAGE staining solution (Biotium) for an hour in the dark and gently agitated. The free-flowing ssDNA that was not coupled with SRBD protein was stained and visualized in the gel documentation system (Syngene) under UV light.

3.7.2. Aptamer Linked Immobilized Sorbent Assay (ALISA)

For streptavidin coating, 50mM carbonate buffer pH 9.6 (Sigma Aldrich) was used as coating buffer, and 0.1% Tween-20 PBS (PBST) was used as plate washing buffer. For SRBD and mAb dilution buffer, 2% BSA PBST was used. For aptamer dilution buffer, an additional 5mM $MgCl_2$ was added to 2% BSA PBST to stabilize DNA structure. Fresh 5% skim milk with 1% Tween 20 PBS was used as blocking buffer.

A clear half-area 96-well plate was coated with 5µg/mL streptavidin (Invitrogen) diluted in coating buffer overnight at room temperature. The coated wells were then then washed with 150µL/well plate washing buffer three times to remove excess coating buffer. To block nonspecific binding, 100µL of blocking buffer was added to each well and incubated for 1 hour

at 37°C. Biotinylated aptamers (synthesized by Integrated DNA Technologies) were heat denatured, chilled, and diluted in aptamer dilution buffer to make 1000nM solutions. Then, 30µL of aptamer dilution was added to the wells and incubated for 1 hour at room temperature with gentle agitation. After three washes, 150µL of blocking buffer was added to each well and incubated for 1 hour while gently agitated for additional blocking. After washing the plate three times, 30µL of 1µg/mL His-Tagged SARS-CoV-2 SRBD protein (Sino Biological), prepared in protein dilution buffer, was added to aptamer coated wells in triplicates, along with aptamer dilution buffer only as negative control, and was incubated for 1 hour at room temperature with gentle agitation. After three washes, 30µL of 1:2000 rabbit anti-Spike antibodies (Sino Biological) was added to each well and incubated for 1 hour at room temperature with gentle agitation. After three washes, 30µL of 1:2500 goat anti-rabbit Ig-G HRP conjugate protein (KPL) was added to each well, and incubated for 1 hour in room temperature with gentle agitation. After three washes, 50µL of pre-warmed TMB ELISA substrate solution (Fisher Scientific) was added to each well, and incubated for 15 min in the dark at room temperature. To stop the reaction, 50µL of 1M sulphuric acid was added to each well, and the plate fluorescence was read on BioTek Synergy HTX multi-mode plate reader (Agilent) at a wavelength of 450nM.

The Brown-Forsythe and Welch analysis of variance (ANOVA) test was used to analyze mean ALISA fluorescence values between testing aptamer and negative control.

3.7.3. Single-Sequence BLI assay

A BLI assay with the aptamer pool was carried out using the Octet Red 96 system (ForteBio). Before starting the analysis, the streptavidin (SA) biosensors were hydrated with 1X KB buffer (see Appendix) in the sensor tray for 30 min prior to the target immobilization step. Biotinylated ssDNA aptamer (synthesized by Integrated DNA Technologies) was heat denatured, chilled, and diluted in 1X KB buffer to the final concentration of 125nM. 1X KB was used for initial baseline calibration, washing, baseline acquisition step, and dissociation step; His-tagged recombinant SARS-CoV-2 S RBD (Sino Biological) was serially diluted 2-fold from 1000-125nM in

1X KB buffer, and was used for the loading step; 100µM biotin (Fisher Scientific) was used for the blocking step. All BLI assays were performed at 30^{o}C with a shaking speed of 1000rpm in a black 96-well flat bottom plate with 200µL of respective solutions. First, the hydrated SA biosensors were submerged in 1X KB for 60 sec for the initial baseline calibration, then biotinylated aptamer dilution for 180 sec for the loading and immobilization step. The loaded SA biosensors were transferred into wells with 1X KB buffer for 120 sec to wash off unattached aptamers, then transported to the wells with biotin blocking solution to block unbound streptavidin on biosensors. Then, the biosensors were transferred to 1X KB to establish baseline reading, then to serial diluted his-tagged recombinant SARS-CoV-2 SRBD protein for 5 to 30 min. The process was monitored in real-time to allow the association curve to reach a plateau. Finally, the biosensors were submerged in 1X KB buffer for 180 sec to allow ligand dissociation. Data analysis was performed using ForteBio Data Analysis 9.0 software. After subtracting baseline reading from the raw data, adjusted association and dissociation curves were fitted to 1:1 kinetic model to calculate K_D value, as suggested in ForteBio user guide.

3.8. *In vitro* Pseudotype Virus Microneutralization Assay

3.8.1 Determining lentivirus pseudovirus working titer

Prior to the microneutralization assay, lentivirus (LV) pseudovirus was titered using an established protocol to determine the working concentration [261]. To do so, the concentrated pseudovirus stock was thawed and diluted 10-fold, followed by an 8-step 2-fold serial diluted with DMEM without phenol red. One hundred microliters of each dilution was added in duplicates onto HEK293T-ACE2/TMPRSS2 cells (10^5 cell/well by day of infection) that was seeded on a clear 96 well plate a day prior. An additional 100µL of DMEM without phenol red assay media was added to each well, supplemented with polybrene (final concentration 250µg/mL in 200µL per well) to facilitate infection. The plate was incubated at 37^{o}C for 48 hours in a 5% CO_2 incubator. Then, after centrifuging the plate at 200xg for 5 minutes, the media was aspirated, and 30µL of Bright-Glo reagent (Promega) and 30µL of DMEM without phenol red were added to all wells, and thoroughly mixed. Fifty microliters of the mixture was transferred to Nunclon Delta-treated black round bottom 96-well plates. The plates were then

read using a Cytation 1 imaging reader (BioTek) using the luminescence setting. The data was exported into Excel file and the lowest dilution (lowest pseudovirus concentration) that could create a signal at least 1000-fold above the background signal of cell-only control was chosen as working concentration.

3.8.2 Aptamer microneutralization assay

HEK293T-ACE2/TMPRSS2 cells (GeneCopoeia) were seeded at the density of 10^4 cells/well, into clear poly-L-lysine coated 96-well plates, and incubated overnight in 5% CO_2 incubator at 37°C.

Phosphorothioated aptamers were first heat denatured at 95°C for 3 min, then chilled on ice for 10 min, and slowly brought back up to room temperature to favor secondary structure folding.

The samples were serial diluted 2.5-fold (1000-1.6nM) in Dulbecco's phosphate-buffered saline (DPBS) containing 1mM $MgCl_2$ (DPBS/Mg) in clear round bottom 96 well plates (Fisher Scientific). Concentrated SARS-CoV-2 Spike-presenting LV pseudovirus was thawed in a 37°C water bath for 3 min, and diluted in DPBS/Mg to working concentration (1:280 dilution) as determined by prior titration assay. For the aptamer treatment step, 60µL of diluted pseudovirus was added to 60µL of serial diluted aptamer sample in clear round-bottom 96 well plates, with blank DPBS as negative control. Known SARS-CoV-2 binding aptamer, phosphorothioated Liu-1a, and rabbit anti-SARS-CoV-2 Spike antibodies (Sino Biological) were used as positive controls. The plates were incubated at room temperature for 1 hour, and occasionally rocked to facilitate neutralization.

Cell media was aspirated from the cell plates, and the 100µL of sample-pseudovirus mixture from the neutralization plates was transferred onto the cells. To replicate the protocol developed by Liu *et al.*, infection was performed by spinoculation by centrifuging for 30 min at 2570xg [270]. After spinoculation, the plates were incubated in 5% CO_2 incubator at 37°C for 2 hours. After incubation, the plates were aspirated and 200µL of fresh DMEM without phenol red (Gibco) was added to each well. The plates were then incubated in 5% CO_2 incubator at 37°C for 48 hours.

To quantify luciferase expression, the plates were centrifuged at for 5 min at 200 X G. Then, media was aspirated from the cell plates. 30µL of pre-warmed Bright-Glo reagent (Promega) and 30µL of DMEM without phenol red were added to all wells, and thoroughly mixed. Then, 50µL of the mixture was transferred to Nunclon Delta-treated black round bottom 96-well plates. The plates were read using a Cytation 1 imaging reader (BioTek) using the luminescence setting.

The microneutralization data was fitted to four variables non-linear dose-response model provided by the Graphpad Prism program.

3.9. Aptamer Biostability Assay

The phosphorothioate-modified Seq2 ReV-B40aptamer was diluted with DMEM containing 5% FBS (heat inactivated) to final concentration of 1µM. One hundred microliters of the diluted sample was added to each well on a clear half-area 96-well plate. The plate was incubated in a 5% CO_2 incubator at 37^{o}C. Samples were collected at 0, 24, and 48 hour time points and analyzed through gel electrophoresis. Briefly, 8µL of samples were mixed with 2µL of 5X Hi-Density TBE sample buffer (Novex) and loaded onto a 6% polyacrylamide DNA retardation gel (Novex), along with 50 bp DNA Ladder (Invitrogen). The gel was placed in Mini Gel Tank (Life Technologies) and electrophoresed at 80V for one hour in 0.5X TBE buffer. After gel electrophoresis, the gel was removed from the casting cassette and transferred to a clean plastic container with 5X GelRed PAGE staining solution (Biotium). The gel was gently agitated for 90 min at room temperature, protected from light for ssDNA staining. The stained gel was then visualized in the gel documentation system (Syngene) under UV light. The intensity of the band was quantified by using the ImageJ program (version 1.53k), and the corrected band intensity was calculated by subtracting background value from the raw mean grey value of each band.

3.10 Liu 1a Molecular Docking Simulation

The crystal structure of SARS-CoV-2 S monomer protein was obtained from the RSCB PDB data bank (https://www.rcsb.org/structure/6M0J, [275]). The PDB file was originally a crystal structure of SARS-CoV-2 Spike receptor-binding domain bound with ACE2 receptor. For the purpose of aptamer-RBD docking, the PDB file was edited with molecular visualization system PyMol 2.5.2 to remove the binding ACE2 peptide (Chain A, 596 residues), and the remaining S-RBD peptide (Chain B, Arg 319 to Phe 541, 222 residues) was saved as a new PDB file. The secondary structure of the Liu 1a sequences were predicted by using the mFold (DNA) web server with the parameters described above (folding temperature: 25^{o}C, Na^{+} concentration: 140mM, Mg^{2+} concentration: 5mM. Other settings were left as default). The generated 2D ssDNA structures were converted to dot-bracket Vienna format, and were used to generate five ssDNA 3D structures by 3dRNA/DNA 2.0.0 web server (http://biophy.hust.edu.cn/new/3dRNA) [276], with optimized procedure, no constraint type, and the bi-residue loop building method. Each prediction was assigned a 3dDNAscore based on distance- and dihedral-dependent energies [277], and the prediction with lowest 3dDNA score was selected for the subsequent docking simulation.

Molecular docking was performed with the ZDOCK 3.0.2 web server [278] after obtaining the PDB files of the aptamers and the RBD. The output file were extracted and the complexes with best ZDOCK scores were visualized with PyMol.

3.11. Statistical Analysis

All results were expressed as means $\pm$ standard deviation. P-values less than 0.05 were considered statistically significant.

Chapter Four: Results

4.1. Aptamer Candidate Selection

4.1.1 SELEX Optimization

A series of PCR optimizations were set up to establish a working SELEX amplification protocol with optimal efficiency and minimum PCR bias. Three different PCR kits were tested: PrimeSTAR Max polymerase kit, iProof High-Fidelity polymerase kit, and Phusion U Multiplex PCR kit. First, a gradient PCR was set up to determine the optimal primer annealing temperature for each of the kits. Twelve reaction mixes from each kit were subjected to a range (48-62^{o}C) of annealing temperatures for 20 cycles, and the PCR product was then purified and loaded onto 1% agarose gel for dsDNA band visualization (Fig. 9A). Based on the band intensity, amplicon size, and sharpness of the resolve band of each reaction, 55.8 ^{o}C was chosen as the annealing temperature for the PrimeSTAR polymerase, 57.5 ^{o}C for the iProof polymerase, and 59.2 ^{o}C for the Phusion polymerase.

Next, an experiment was set up to compare PCR bias between conventional open PCR and emulsion PCR (ePCR). PCR bias and preferential amplification are known issues that could skew the selection process, increasing the chance of SELEX failure [162, 183]. Therefore it is crucial to find an amplification approach that can maintain the input ssDNA pool diversity, so that the aptamer selection is not affected by factors other than the target-aptamer binding. A diversity standard was generated by amplifying the starting Bank40 ssDNA library using non-emulsifying PCR ("open PCR") with minimum PCR cycles (six cycles) to minimize any potential PCR interference. Theoretically, the diversity standard should be a good representation of the sequence diversity that was present in the original starting Bank40 library. Each tested PCR kit was used to set up two different PCRs, an open PCR and an ePCR. The open PCR approach was able to generate a higher concentration of amplicon across all tested kits with final product concentration of 36.4ng/µL, 32.5ng/µL, 26.3ng/µL for PrimeSTAR, iProof, and Phusion kit, respectively. The ePCR approach, in comparison, was not as effective as the open PCR, possibly due to the encapsulating micelles that restricted over-amplification giving yields of 21.7ng/µL, 3.94 ng/µL, 8.8 ng/µL for PrimeSTAR, iProof, and Phusion kit, respectively.

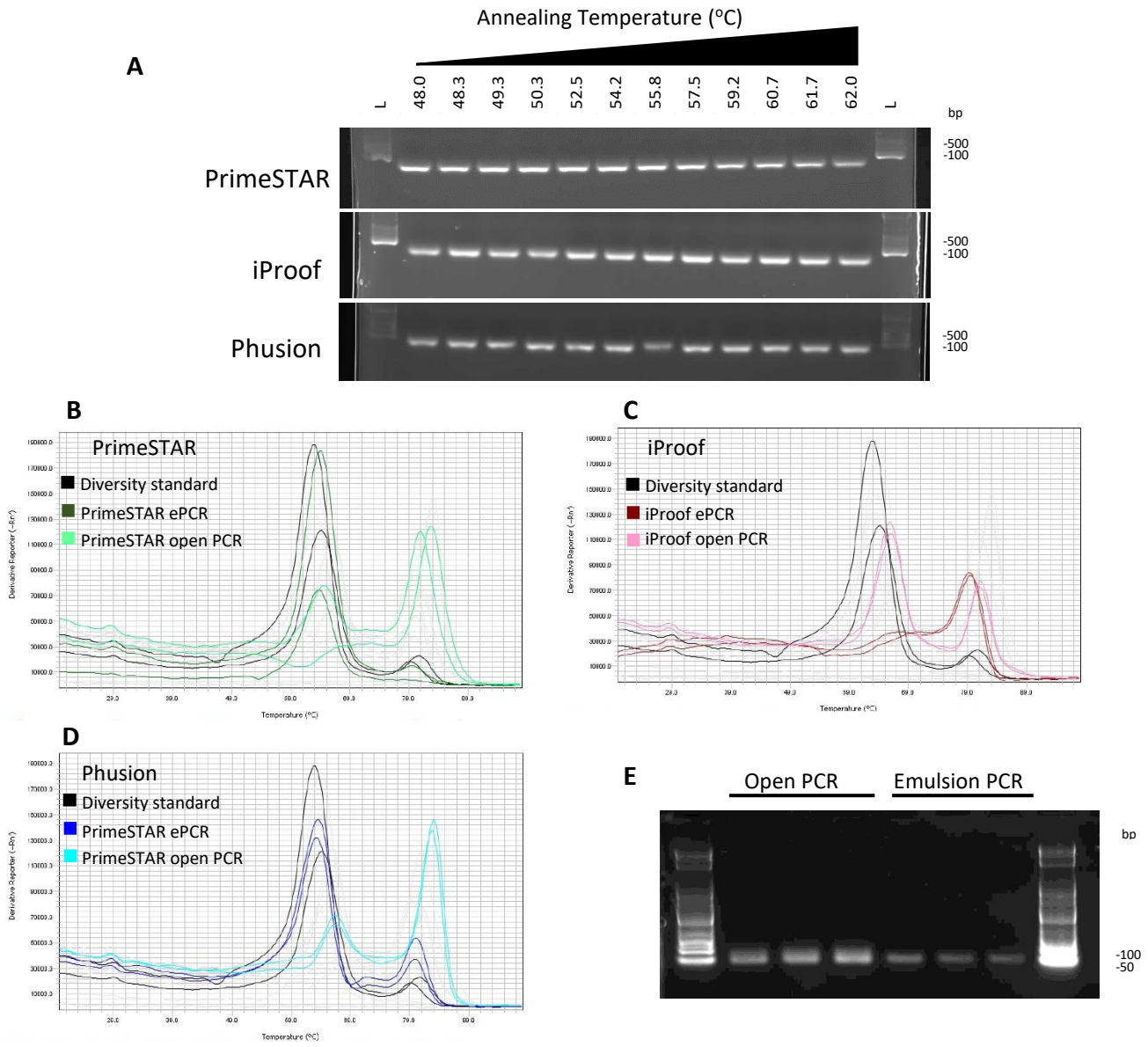


Figure 9. SELEX PCR optimization. The PrimeSTAR, iProof, and Phusion PCR kits were tested to compare the amplification efficiency and specificity. (A) Each kit was used to set up a 20 cycle gradient PCR (48-62°C) to determine the optimal primer annealing temperature. A single cycle qPCR-melt curve analysis was then set up to compare the melting temperature of PCR product through either the open PCR or ePCR approach. Melt curve of (B) PrimeSTAR, (C) iProof, and (D) Phusion PCR product was plotted along with the diversity standard (black curve), which was generated through minimum-cycling, open PCR to retain original input diversity. (E) The Open PCR and ePCR samples, amplified by the PrimeSTAR kit, were loaded in triplicates and visualized in a 2% agarose gel.

The PCR product of each of the reaction was subjected to a single cycle qPCR-melt curve analysis. The melt-curve of the PCR products were compared side-by-side with the diversity standard (Fig. 9B-D). The diversity standard had a sharp primary peak at 63^{o}C, with a small secondary peak at 80^{o}C. Highly diverse DNA samples (e.g. Bank40 library) would generate a lower qPCR-melting peak due to the abundance of non-perfectly matching hetroduplex DNA, as the mis-matching duplexes have a lower remelting temperature [191]. The secondary peak was more prominent in open PCR samples across all tested PCR kits. This could be interpreted as the loss of diversity due to preferential amplification and PCR biases, which led to the increase of homoduplex DNA. The increasing presence of homoduplex DNA would raise the remelting temperature, shifting the observed melting peak to higher temperature [191], or forming a secondary peak [279]. For ePCR samples, the PrimeSTAR polymerase was able to produce a similar melting curve pattern as the diversity standard, exhibiting a dominant primary peak at 64^{o}C (Fig. 9B). Interestingly, iProof ePCR samples had a singular melting peak at 80^{o}C, whereas its open PCR samples showed two distinctive peaks at 66^{o}C and 80^{o}C (Fig. 9C). The Phusion ePCR generated a dominant primary peak at 63^{o}C, but the secondary peak at 80^{o}C was more noticeable than the PrimeSTAR ePCR (Fig. 9D), rendered it less ideal than its counterpart. To visualize the PCR bias and the formation of byproduct in open PCR, the PCR samples were loaded onto a 2% agarose gel for comparison (Fig. 9E). PCR products from the open PCR samples formed thicker, less resolved bands than ePCR samples, which suggested over- and non-specific amplification.

4.1.2. Monitoring SELEX Selection

To select binding aptamers against SARS-CoV-2 S protein, a diverse pool of ssDNA, derived from the Bank40 library were repetitively exposed to biotin-conjugated S-RBD recombinant protein. Binding sequences were captured via magnetic streptavidin beads, isolated, and amplified by ePCR. The ePCR amplicon was then purified and denatured, generating an enriched ssDNA pool for the subsequent round of target selection. To optimize quality and quantity of the recovered binding sequence, ePCR cycling parameters were

adjusted accordingly (see Chapter Three Table 2). The quantity of the recovered ssDNA was different each round (Table 3). To select strong candidates, the selection stringency increased over time and only sequences with high specificity against S-RBD remained. As selection progressed, the sequence diversity of the retained SELEX pool decreased, and the binding sequences out-competed other weak or non-binding sequences within the population.

4.1.3. Evaluation of S-Binding Aptamer Pool

Repetitive PCR amplification is known to introduce unwanted byproduct like nucleotide inserts, deletion, primer-mismatch, and daisy chains [280]. Therefore, selecting a high-fidelity amplification approach such as ePCR reduces the incidence of incorporating unexpected PCR artifacts into the SELEX selection pool. If left unchecked, unwanted PCR byproducts might slowly dominate the selection pool due to polymerase bias, as demonstrated by the accumulation of non-specific amplicons that were generated by open PCR (Fig. 9E). The byproducts would compete with other binding aptamer sequences and potentially sabotage the selection process.

To evaluate the quality of the selection pool, ePCR samples from each selection round (1R-10R) were loaded onto the high sensitivity microfluidic chip electrophoresis DNA bioanalyzer system (Agilent) for quick visualization (Fig. 10A), along with starting Bank40 library for size reference. The 1R sample was not detected in the bioanalyzer chip possibly due to over-dilution, however the 76bp band re-appeared at the end of 2R. A faint, shorter band briefly emerged during 5R, and subsequent samples from 6R to 10R had small quantities of amplicons of various sizes, seen smudges around the 76bp band. The multiple melting peaks in intermediate rounds coincided with the observation seen in the bioanalyzer analysis (Fig. 10B).

To monitor the target affinity maturation of the aptamer pools over rounds of selection, ssDNA samples from selected SELEX rounds were tested against immobilized biotinylated SRBD on the BLI platform. The BLI platform detects molecular level target-aptamer interaction without the need of labelling the nucleic acid, which makes it a superior binding analysis approach to the traditional ELISA/ALISA method. The BLI analytical software fitted the

Table 3. Quantification of ssDNA generated from each round of SELEX cycle.

SELEX Round	Input ssDNA for target selection (ng)	Total number of ePCR cycles	1st ePCR Output yield (ng)	2nd ePCR Output yield (ng)
1	1167	30 (15+15)	773	2223
2	1111	27 (15+12)	955	9175
3	2294	15	1560	-
4	1000	15	1700	-
5	1000	15	1825	-
6	1000	13	2820	-
7	1000	11	3200	-
8	1024	20 (10+10)	813	10680
9	2670	10	1755	-
10	1018	10	4803	-

After initial ePCR amplification, the nucleic acid was purified and quantified. If there were insufficient quantity of ssDNA for the following round of SELEX (as seen in Round 1, 2, and 8), 2nd ePCR was set up to amplify the recovered ssDNA.

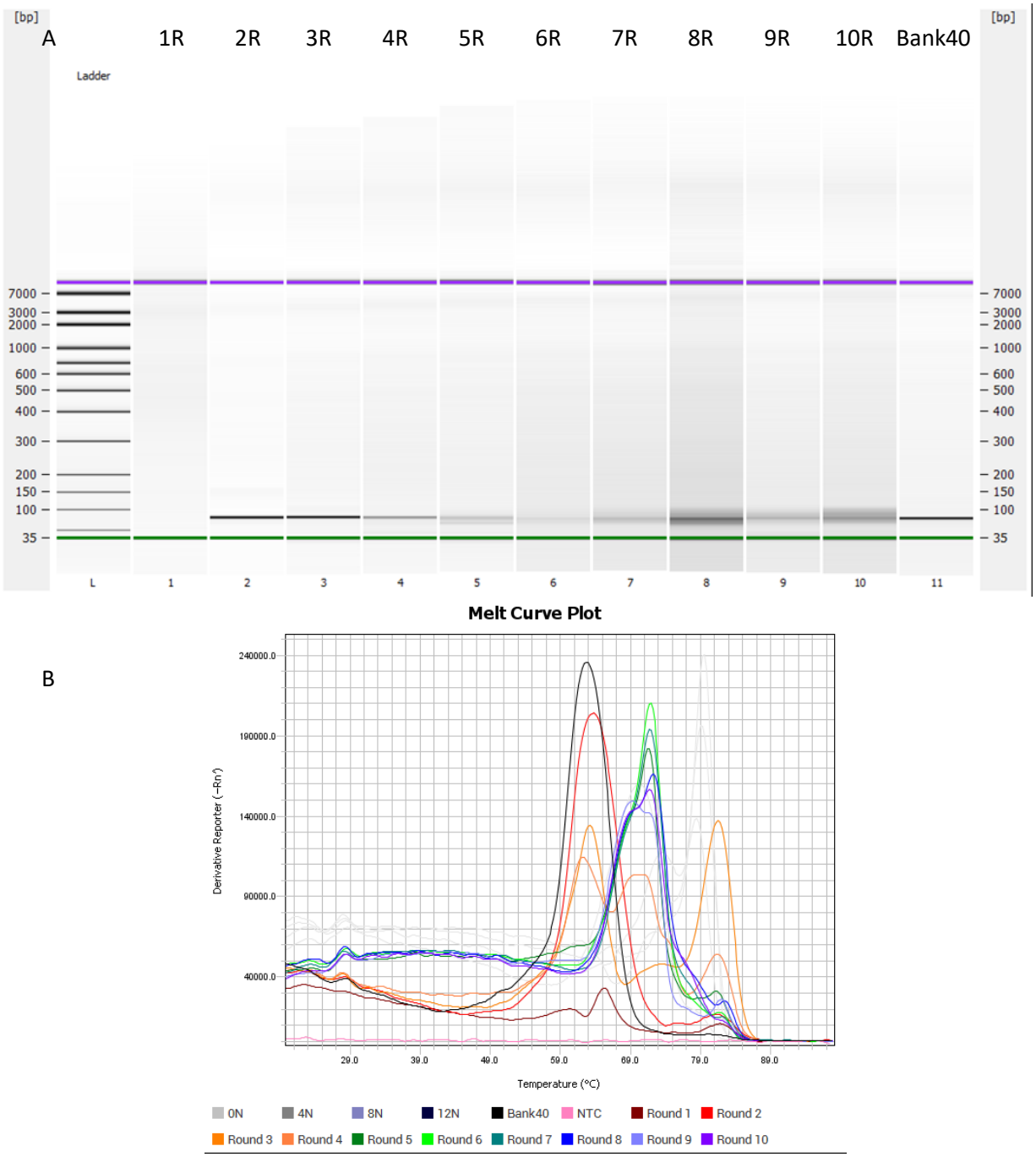


Figure 10. dsDNA characterization of 1R-10R with HS DNA bioanalyzer system (A) and qPCR melt-curve analysis (B). (A) Gel-like electropherogram of ePCR samples were collected from each round of SELEX, diluted according to manufacturer instruction, and loaded onto HS DNA bioanalyzer chip. From left to right: dsDNA ladder (L), 1R-10R (Round 1 to Round 10), Bank40 library. (B) The same ePCR samples were mixed with qPCR reagents for melt-curve analysis. NTC: no template control.

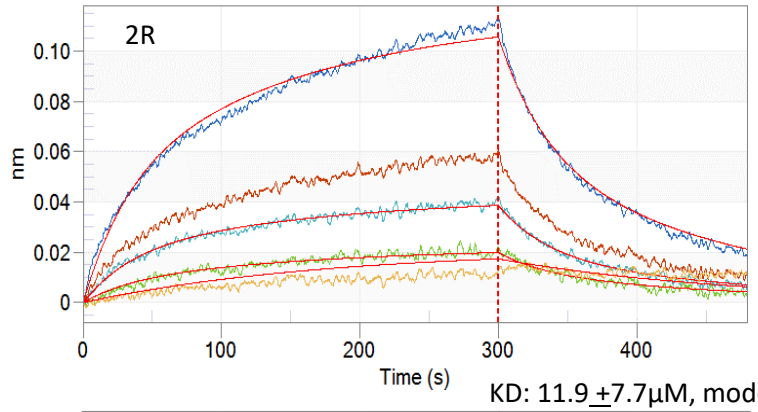
association and dissociation data against a 1:1 kinetic model (1 ligand to 1 binder) to determine the K_D value for each aptamer (Fig. 11). The aptamer pool affinity against SRBD increased from K_D: 11.9±7.7μM (2R) to 450±27nM (6R). However, the unexplained drop of affinity from 6R to 10R (K_D: 6.06±0.87μM) suggested that the final 10R pool had weaker overall binding to SRBD than the intermediate pool.

4.1.4. Identify Binding Sequence Using HTS

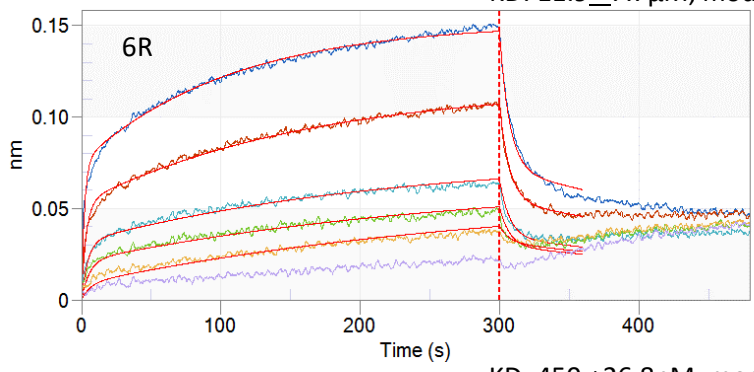
To remove unwanted short and long PCR artifacts that were presented in the 10R SELEX pool, 76nt PCR products were excised from 3% agarose gel (Fig. 12A) for sequencing preparation. For quality assurance, the gel extract was loaded onto a small RNA bioanalyzer chip along with Bank40 ssDNA starting library (Fig. 12B). Another round of gel extraction was performed after extending and amplifying 10R with NGS FWD/RVS primers. The 150bp samples were extracted from 3% agarose gel, and subjected to final index PCR (with Illumina primers, Table 1 Illumina index 1 and 2 read PCR primer), bead purification, and gel extraction to generate NGS-ready 200bp 10R samples for HTS.

The number of total raw reads was 404,608 and length of the reads ranged from 56 to 151nt. Using the Cutadapt function, only 33,806 (8.4%) and 21,001 (5.2%) forward and reverse reads, respectively, passed the 35-45nt filter after trimming the sequencing adaptors and Bank40 primers. After pairing the reads with the filterAndTrim function, most of the remaining sequences were 40bp long. The top 10 sequences were generated, as listed in Table 4.

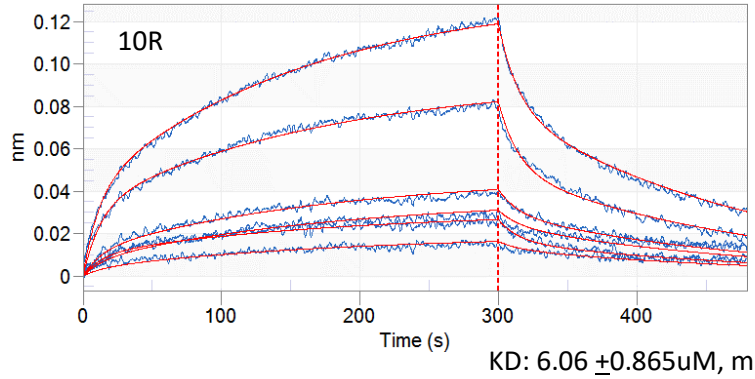
Since the final sequencing product was a dsDNA sample, the binding candidate could be either the forward or the reverse read. The top two most abundant sequences (Seq 1 and Seq 2) were picked. To cover all grounds, both the forward (-For) and reverse complement (-Rev) reads; the short 40nt randomer and the longer 76nt sequence which involved the Bank40 primer region (-B40) were sent to be synthesized for subsequent candidate characterization and binding analyses (Table 5).



KD: 11.9 ±7.7µM, model R^2: 0.99



KD: 450 ±26.8nM, model R^2: 0.99



KD: 6.06 ±0.865uM, model R^2: 0.99

Figure 11. BLI association and dissociation of 2R, 6R, 10R aptamer in serial dilution. Each selected aptamer underwent a 5-step 2-fold serial dilution, ranging from 1000-31.3nM. Biotinylated SRBD was tested against various concentration of aptamer to accurately capture the binding kinetics. The data were then fitted against a 1:1 (1 ligand : 1 binder) kinetic model and the K_D value was calculated using BioForté analytical software.

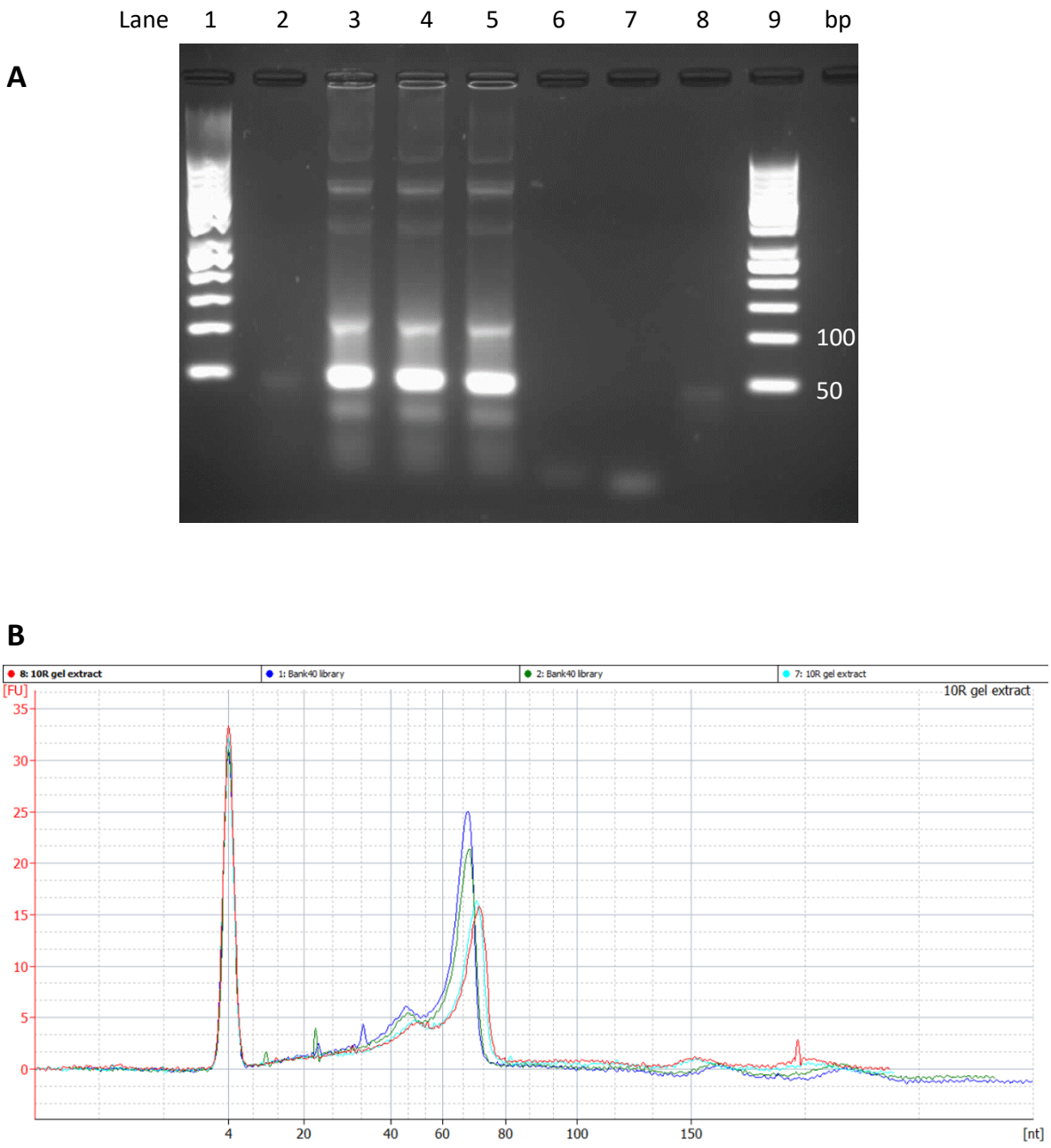


Figure 12. Gel electrophoresis of 10R aPCR amplicon and 10R gel extract visualized with small RNA bioanalyzer chip. (A) 10R aPCR was loaded onto a 3% agarose gel and imaged under UV. From left to right: Lane 1: 50bp DNA ladder; Lane 2: Bank40 ssDNA library; Lane 3-5: 10R aPCR amplicon; Lane 6: Bank40 FWD primers; Lane 7: Bank40 RVS primers; lane 8: Bank40 ssDNA library; Lane 9: 50bp DNA ladder. (B) Electropherogram of 10R gel extract (red and cyan) using small RNA bioanalyzer chip. The sample was loaded along with Bank40 ssDNA library (blue and green) as reference.

Table 4. Top ten most abundant sequences in 10R PCR pool.

Rank	Sequence	Abundance
1 (“Seq 1”)	ACCGATCGACGCGTCCGGCGCAGGACTCGATCTCAGTGTT	4661
2 (“Seq 2”)	CCAGTCAAATTGCTCCCCGACGCAGGGGTTTGATTGGACA	3295
3	ATGTCTTAAAGAAATTGCCCATCGACGCAGATGTTTCTCT	164
4	GTATCCCCGGATTGCTCCCCGACGCAGGGGTCCGGAAACAT	13
5	GTGCTGAGTTATAGCCGCATCTGGCACTAGCGGACCACCT	10
6	ACTGACGGACGCTCCCGGCGCAGGGATCCGGCTGTAGGCC	9
7	AGACGGAGCAAACAGATCTTATGATATGACCGTGCCAGCC	8
8	AGGACAATAACGCACCGATCGCAGGTTTATTTCGCCCTTA	7
9	CGTTACCACCGGGTGAGAGTCGAGGGGCATACCTCCACTT	2
10	ATGGCTCACCGGGGGCACGTATAGAACGAATGTGACAAGC	2

PCR sequences identified by Illumina iSeq platform that were presented in 10R SELEX pool. The forward and reverse reads were merged. Known streptavidin-binding motif (ACGCNNNNNNCGCA) is underlined.

Table 5. Sequences that were synthesized and tested.

Name	Size (nt)	Sequence
Seq1For	40	ACCGATCGACGCGTCCGGCGCAGGACTCGATCTCAGTGTT
Seq1ForB40	76	TGACACCGTACCTGCTCTACCGATCGACGCGTCCGGCGCAGGACTCGATCT CAGTGTTAAGCACGCCAGGGACTAT
Seq1Rev	40	AACACTGAGATCsGAGTCCTGCGCCGGACGCGTCGATCGGT
Seq1RevB40	76	ATAGTCCCTGGCGTGCTTAACACTGAGATCGAGTCCTGCGCCGGACGCGTC GATCGGTAGAGCAGGTACGGTGTCA
Seq2For	40	CCAGTCAAATTGCTCCCCGACGCAGGGGTTTGATTGGACA
Seq2ForB40	76	TGACACCGTACCTGCTCTCCAGTCAAATTGCTCCCCGACGCAGGGGTTTGAT TGGACAAAGCACGCCAGGGACTAT
Seq2Rev	40	TGTCCAATCAAACCCCTGCGTCGGGGAGCAATTTGACTGG
Seq2RevB40	76	ATAGTCCCTGGCGTGCTTTGTCCAATCAAACCCCTGCGTCGGGGAGCAATTT GACTGGAGAGCAGGTACGGTGTCA

The known streptavidin binding motif was underlined. Extended aptamers with Bank40 primer regions were highlighted in cyan (5’ primer) and yellow (3’ primer)

4.2. Aptamer Characterization

4.2.1. Seq2Rev form DNA-SRBD Complexes in Gel Electrophoresis

Each individual SELEX-derived sequence was screened using EMSA to determine if they exhibit any SRBD-binding activity. Aptamer sequences were incubated with biotinylated SRBD recombinant protein to allow ligand-binding. The mixture was then loaded onto a 6% polyacrylamide non-denaturing gel to separate aptamer-protein complexes from free unbound oligonucleotides (Fig. 13). The original Bank40 ssDNA library and the known SRBD aptamer Liu 1a [270]were tested respectively as negative and positive controls. As expected, the intensity of detected free-flowing ssDNA declined when Liu 1a was coupled with increasing concentration of SRBD (Fig. 13A). Among the 10 candidates, Seq2Rev exhibited similar reduction of band intensity when incubated with higher concentration of biotinylated SRBD (Fig. 13B). Surprisingly, its longer form, Seq2RevB40 did not show the same fading pattern (Fig. 13C). It could be that by removing the fixed Bank40 PCR primer region the truncated sequence assumes a more favourable conformation for ligand binding [162, 280].

The aptamers Seq1For (Fig. 13B), Seq1Rev (Fig. 13C) and their longer forms showed no decline in band intensity, whereas Seq2Rev (40nt) (Fig. 13E) and Liu 1a (Fig. 12A) exhibited observable intensity drop, especially at 2µM SRBD concentration. Interestingly, Seq1For (40nt) and Seq1ForB40 (76nt) contain the palindromic sequence “ACGCNNNNNNCGCA” (Table 4, Table 5, underlined), a known common streptavidin-binding motif [195]. Off-target sequences, which were bound to the streptavidin-coated beads during the SELEX selection process, could be retained and amplified. Due to their potential off-target binding, Seq1For and its derivative Seq1Rev were eliminated for further testing.

4.2.2. Weak Candidate-SRBD Binding was Detected in ALISA

To study the binding efficiency of the candidates, 1000nM of biotinylated candidates, namely the Seq2For, Seq2ForB40, Seq2Rev, Seq2RevB40, were tested against His-tagged SRBD using ALISA (Aptamer Linked-Immobilized Sorbent Assay). The biotinylated candidates were immobilized on 96 well plates via streptavidin-biotin linkage to capture free His-tagged

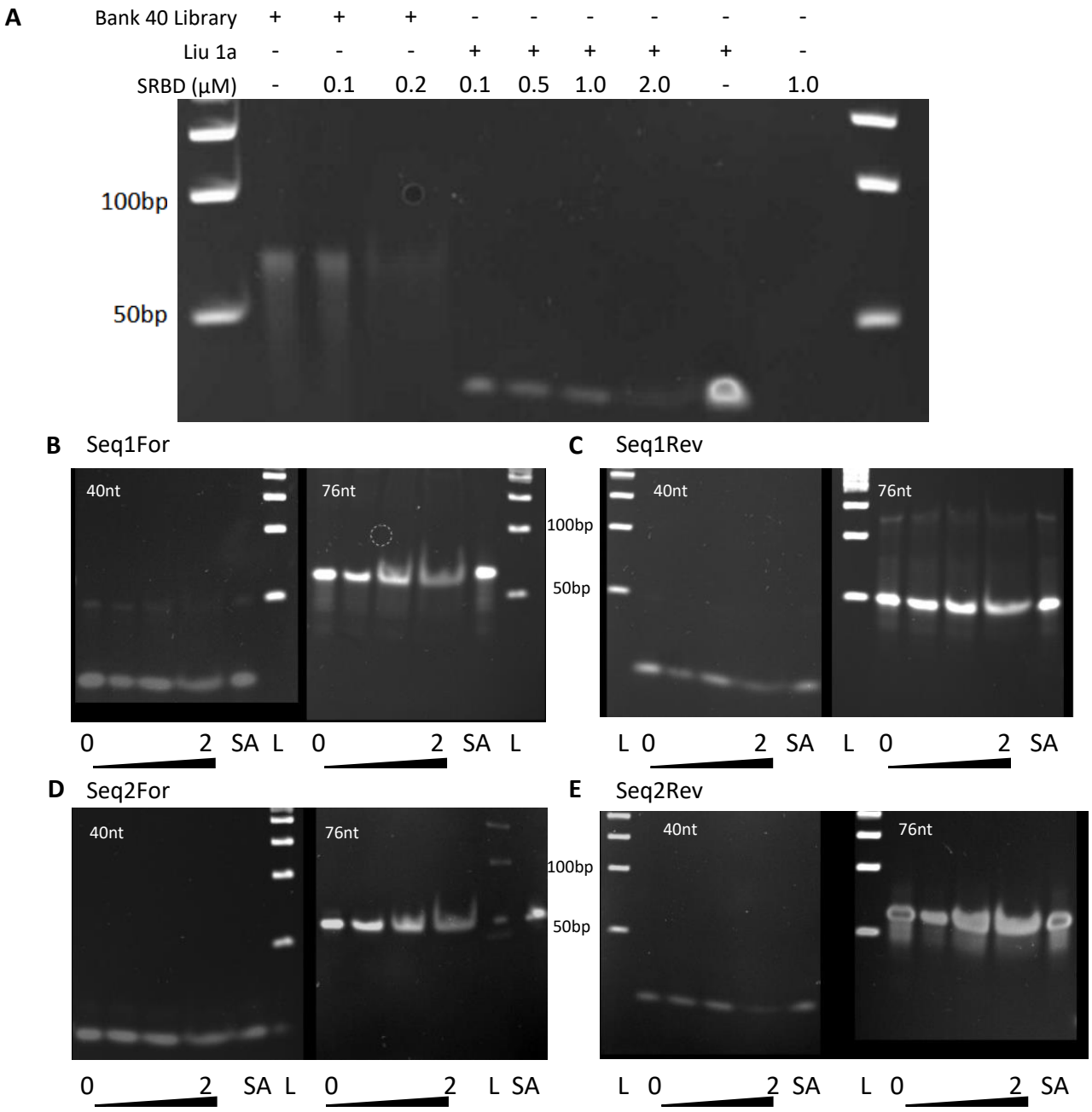


Figure 13. Gel electrophoresis of Liu 1a and SELEX aptamer candidates with SRBD. (A) One micromolar of Bank40 ssDNA library (76nt) and Liu 1a (40nt) were incubated with biotinylated SRBD protein and loaded onto DNA retardation gel. The unbound free-flowing ssDNA was stained and visualized. The diminishing intensity of the free ssDNA bands with increasing protein concentration inferred to formation of SRBD-aptamer complexes. Gel electrophoresis of Seq1For (B), Seq1Rev (C), Seq2For (D), and Seq2Rev (E) after incubation with increasing concentration of SRBD (0, 0.5, 1, 2μM) or 1 μM streptavidin as negative control. SA: Streptavidin; L: 50bp DNA ladder.

SRBD. The captured SRBD was detected using rabbit anti-SRBD and HRP-conjugated goat anti-rabbit antibodies. The positive control Liu 1a aptamer outperformed the SELEX candidates even at 1:10 dilution (100nM) (Fig. 14). All SELEX candidates except Seq2RevB40 exhibited binding activity towards SRBD was, but their activity was still significantly weaker than Liu 1a. Seq2For sequence showed higher binding affinity than its reverse counterpart. Furthermore, shorter sequences (40nt) generated higher signal than longer (76nt) sequences.

4.2.3. Seq2For, Seq2ForB40, Seq2Rev and Seq2RevB40 Showed Weak Binding Activity in BLI Analysis

To further investigate the binding activity and ligand interaction of the candidates, the BLI (Bio-layer Interferometry) assay, a highly sensitive molecule-interaction analysis platform, was used to determine the dissociation constant of the aptamers. 5'- end biotinylated sequences, namely Seq2For, Seq2For B40, Seq2Rev, and Seq2RevB40, were synthesized for the BLI analysis to couple with the streptavidin (SA) biosensors. The biosensors measure the association and dissociation of protein to immobilized biotinylated aptamers. To prevent recombinant SRBD from binding to the SA biosensors, His-tagged, instead of biotinylated, recombinant SRBD was used as the binding target. For positive control, biotinylated Liu 1a was tested along with the SELEX candidate. For each aptamer set, an aptamer-loaded biosensor was submerged in KB buffer during the association step as negative control to monitor unexpected buffer interaction. Throughout the 5-minute association stage (0-300 sec), all candidates exhibited ligand association activity but were not dissociating at the subsequent dissociation stage (300-600 sec) (Fig. 15). The association curve also had a quick initial rise and then a slower rate of binding that was unable to reach steady state, suggesting heterogeneous binding interactions [281]. Using the available data, the raw data was processed and fitted to 1:1 ligand-analyte kinetic model. The calculated dissociation constant were as follows: Seq2For K_D: 1.70$\pm$0.07µM (Fig. 15A); Seq2ForB40 K_D: 2.57$\pm$0.15µM (Fig. 15C); Seq2Rev K_D: 1.85$\pm$0.08µM (Fig. 15B); Seq2RevB40 K_D:

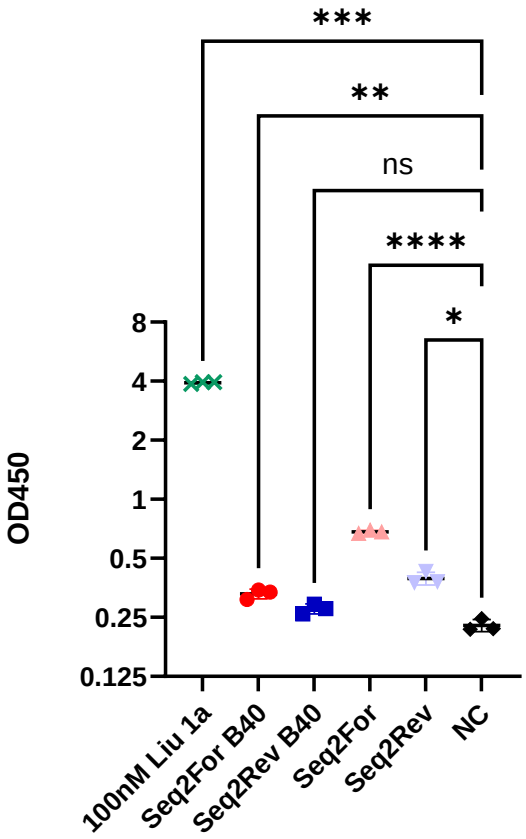


Figure 14. Capture ELISA of biotinylated aptamers. 100nM of biotinylated Liu 1a positive control aptamer and 1000nM of biotinylated SELEX aptamers were immobilized on a streptavidin-coated 96 well plate. The plate was then blocked with 5% milk PBST and incubated with 1µg/mL His-tagged SRBD. Rabbit anti-Spike mAb was added to detect binding SRBD, and secondary HRP-Goat anti-rabbit IgG was added. TMB substrate was added and incubated for 15 min and stopped with 1M sulphuric acid. OD450 was recorded with plate reader. NC: wells with no aptamer added. Error bar: standard deviation. *: $p \leq 0.05$ against NC; **: $p \leq 0.01$; ***: $p \leq 0.001$, ****: ≤ 0.0001, ns: no significance. Y axis in Log_2 scale.

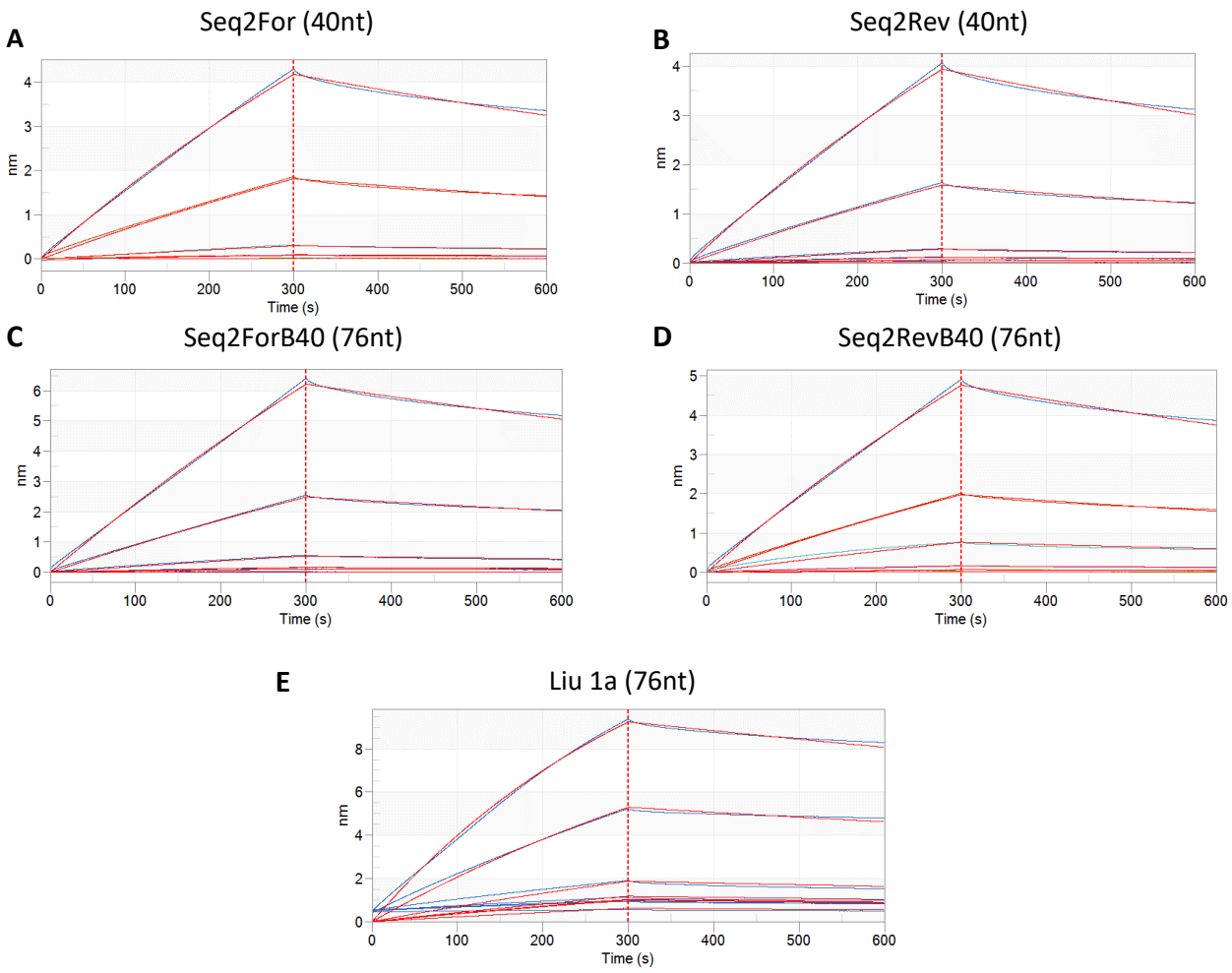


Figure 15. BLI association and dissociation sensorgram of biotinylated aptamers. Biotinylated Seq2For (A), Liu 2 ForB40 (C), Liu 2 Rev (B), Liu 2 RevB40 (D) and Liu 1a (E) biosensors were submerged in buffer containing SRBD for 300 seconds to allow protein association. The biosensors were then transferred to KB buffer for 300 seconds for protein dissociation. The association and dissociation data was recorded and processed by subtracting the baseline reading from the raw data. The processed data (blue line) was then fitted to 1:1 (one ligand to one analyte) kinetic model (red lines) to calculate dissociation constant (K_D).

1.74±0.09µM (Fig. 15D). In comparison, using the same parameters, Liu 1a's dissociation constant was calculated to be K_D: 188±6nM (Fig. 15E), which was one log lower than the tested candidates. Still, all tested candidates showed improved binding efficiency compared to its parent 10R pool (K_D: 6.06 ±0.86µM).

4.2.4 Secondary Structure Prediction of Aptamer Candidates

The secondary structure of the aptamer candidates were predicted and generated using web-based application Mfold (Fig. 16). Experimental data such as incubation temperature and ion concentration was entered and up to 10 possible conformations were generated with variable stability (presented as Gibbs free energy). The prediction with lowest Gibbs free energy was considered the most stable conformation. The Bank40 primer region of the 96nt SELEX candidates (Fig. 16 A-D) formed a complementary panhandle structure whereas their truncated derivatives (Fig. 16 E-H) had non-paired terminals.

4.2.5 Liu 1a Molecular Docking Simulation

To demonstration of 3D structure and molecular interaction modelling, the 2D structure of Liu 1a aptamer was converted into 3D structures to perform molecular docking simulation with SRBD (Fig. 17A). It took two hours to generate five 3D structure predictions for the Liu 1a sequence with 3dRNA/DNA web server, the structure with the lowest assigned 3dDNAscore (21.4772), which was based on distance- and dihedral- dependent energies, was selected for subsequent docking simulation (Fig.14B). The Liu 1a-SRBD molecular docking model was generated based on a fast Fourier transform algorithm to perform a rigid-body ligand-protein docking simulation [278]. ZDOCK web server generated and ranked 10 models based on shape complementarity, electrostatics, and statistical potential. The best model was visualized using the PyMol 2.5.2 program (Fig. 17C-D). Through PyMol, interacting molecules were identified using the polar contact function (Fig. 17D). According to the simulation, the complementary

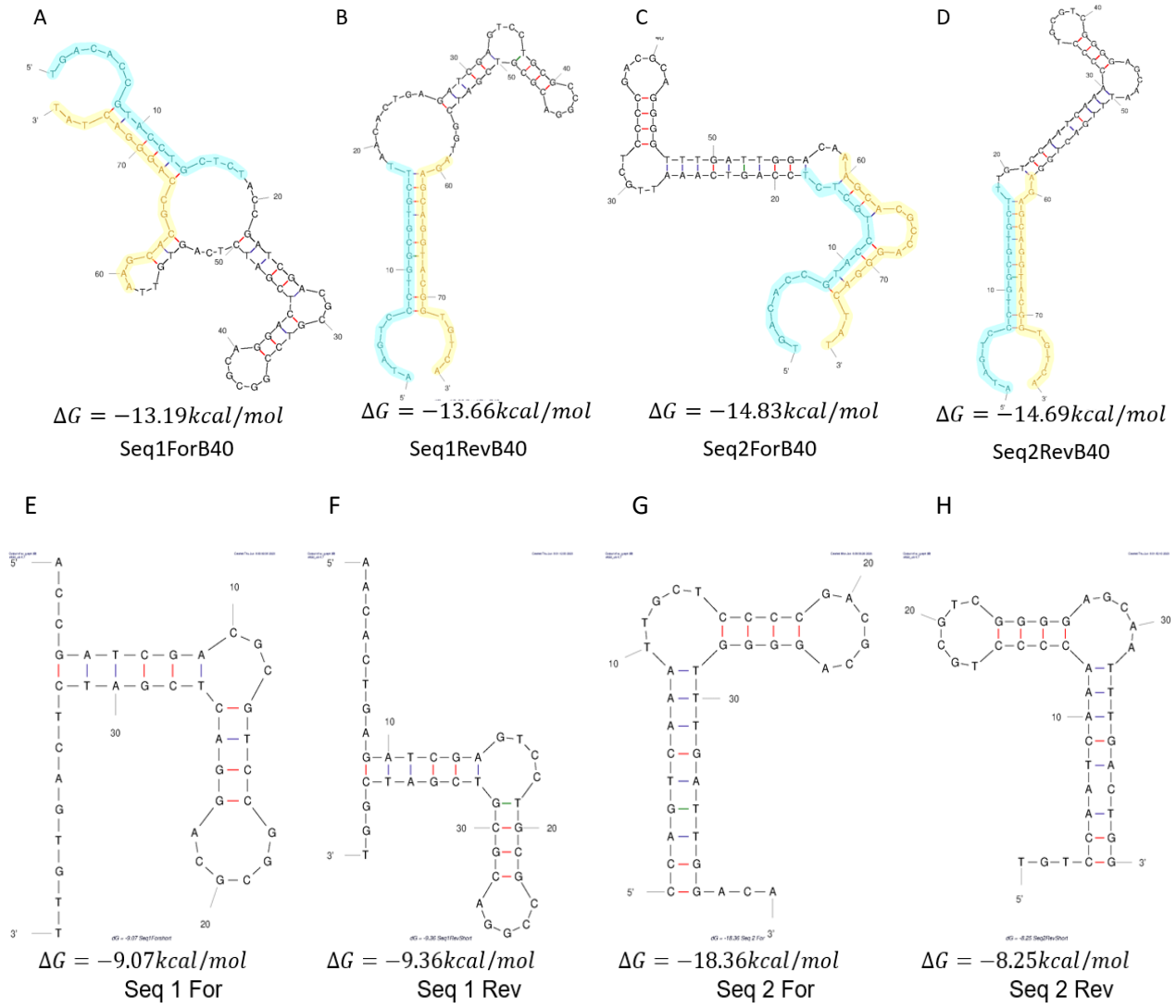


Figure 16. Predicted secondary structure of aptamer candidates. The Bank40 primer region was highlighted in cyan (5') and yellow (3').

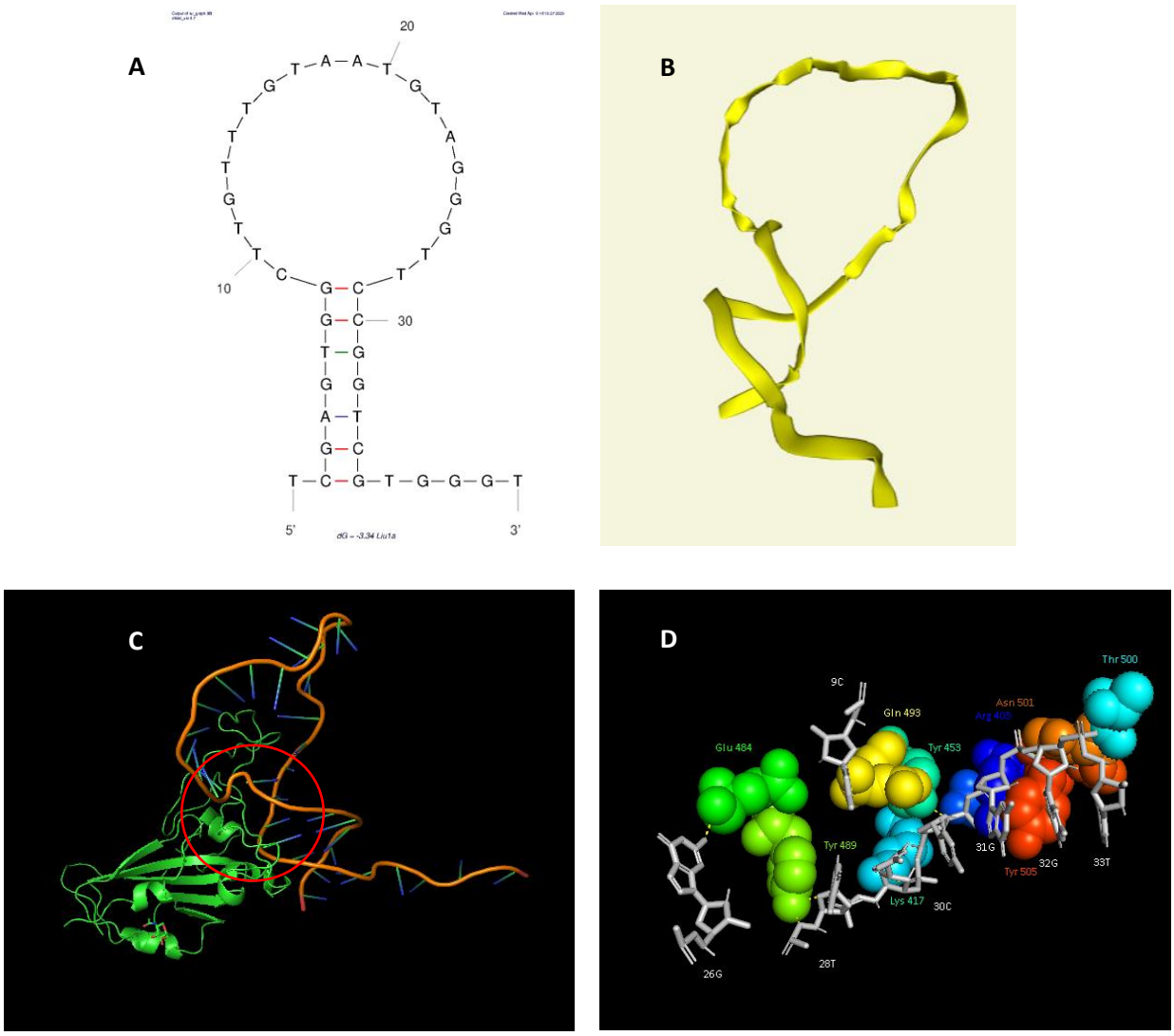


Figure 17. Liu 1a Molecular Docking Simulation. (A)2D structure prediction was generated by mFold web server. (B) The secondary structure was then used to generate 3D ssDNA model by 3dRNA/DNA web server. (C) After editing the original PDB file (PDB: 6M0J) to isolate the SRBD peptide chain, the PDB files of the Liu 1a and SRBD was uploaded to ZDOCK web server to preform molecular docking simulation. The opening of the hairpin loop structure where SRBD residues interact with the Liu 1a oligonucleotide was circled in red. (D) The top ranking docking prediction was visualized using PyMol, the polar contact (yellow dots) was identified and interacting residues were identified. Coloured text annotation of interacting nucleotides and residues was added using GNU image manipulation program (GIMP).

panhandle structure near 3' end (C30-T33) and the adjacent unpaired nucleotides at the ssDNA loop (C9, G26, and T28) interacted with the polar and charged residues, specifically residues 403 (Arg), 417 (Lys), 453 (Tyr), 484 (Glu), 489 (Tyr), 500 (Thr), 501 (Asn), and 505 (Tyr).

4.3. Biostability of Modified Aptamers in Physiological Environment

The biostability of aptamers in a physiological environment was an important factor for developing therapeutic candidates. Unmodified DNA aptamers are susceptible to environmental degradation such as UV, heat, and endogenous nuclease digestion. Phosphorothioate-modified aptamer candidates were synthesized and tested to determine their biostability under physiological conditions.

After 48 hours of incubation at 37^{o}C in 5% FBS DMEM cell media, the modified aptamers were loaded onto agarose gel to assess its integrity (Fig. 18). Although the fetal bovine serum (FBS) that was added to culture media was heat inactivated (56^{o}C for 30 minutes), the media should still contain serum nucleases that could potentially degrade unmodified nucleases [282]. In retrospect, the assay should include an unmodified aptamer sequence to verify the presence of nucleases and to compare the progress of nucleic acid degradation between the modified aptamer and unprotected ssDNA. The result showed the band intensity of the modified sample had gradually decrease over the course of 48 hours, the mean grey value dropped from 40.51 (0hr), to 34.98 (24hr), and ended at 24.51 by 48 hours, which suggested gradual nucleic acid degradation. The modified aptamer appeared to have remained intact, as there was no detectable smear after 24 and 48 hours of media incubation.

4.4. *In vitro* Microneutralization of Pseudotype Virus with Aptamers

Since it was unclear if the pseudotype lentivirus microneutralization assay would be applicable for an aptamer-based neutralization assay, the positive control aptamer Liu 1a (known SRBD binding aptamer) was used to explore and optimize experimental parameters for testing subsequent SELEX aptamer candidates. Biotinylated Liu 1a aptamer was incubated with SARS-CoV-2 Spike presenting pseudotype lentivirus. The incubation buffer (DPBS) was prepared

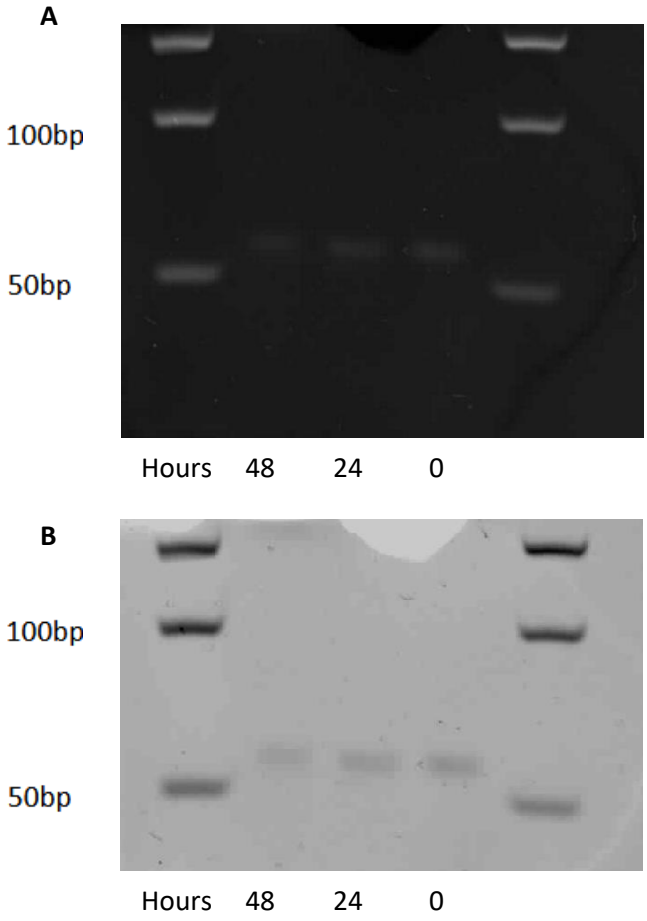


Figure 18. Gel electrophoresis of phosphorothioate-modified Seq2RevB40 at 0, 24, 48 hours DMEM incubation. (A) Original image and (B) colour-inverted image of the stained gel. 1000nM of modified aptamer (76nt) was diluted with 5% FBS DMEM and incubated in a 96-well plate at 37°C. Samples were collected at 0, 24, and 48 hour time points and analyzed through gel electrophoresis. From left to right: DNA 50bp ladder, 48 hr, 24hr, and 0hr time point, 50bp ladder.

with additional magnesium ions to stabilize and support the functional ssDNA folded structure so that the aptamer can bind to SRBD as described in literature [270].

Typically, to increase the infection efficiency of pseudotype lentivirus, cationic reagents such as polybrene are added to the assay media to encourage virion attachment [252, 273]. However, the conformation of an aptamer is sensitive to charged molecules, therefore alternative transduction-enhancing measures were considered. Instead of neutralizing the negative charge of the cell surface and the virion, low centrifugal force was applied to the inoculation plate to mechanically promote cell-virion contact, in a process called spinoculation [283, 284]. Authors of the Liu 1a study also utilized the spinoculation approach to bypass the need of adding cationic reagents (supplementary documentation of original paper [270]). Two other control groups (uninfected cells and infected-untreated cells) were set up along with the same centrifugation treatment to monitor the effect of centrifugal force on cellular stress and efficiency of transduction.

The assay was set up so that the Spike-presenting pseudotype lentivirus was treated with biotinylated Liu 1a; or an unmodified 60nt NGS sequencing primer as negative control; or rabbit anti-SRBD antibody as positive control to see if the neutralization effect was comparable. The pilot study was not successful as there were no statistical difference between Liu 1a and negative control group, whereas the positive control anti-Spike rabbit antibody group exhibited viral inhibition (Fig. 19A). Liu 1a is a known Spike blocker which is described to block SRBD-ACE2 interaction and neutralize viral infection *in vitro* [270]. To investigate the failure to replicate the result described by the authors of the original study, a separate experiment was set up with phosporotioate-modified Liu 1a and a phosporotioate-modified 60nt negative control PhosThio PhiX (see Table 1 for full sequence, originated from a random region of the enterobactoria phage PhiX174 genome) to minimize potential nucleotide degradation. The subsequent experiment also failed as phosphorothioate-modified Liu 1a and other SELEX candidates (Seq2Rev and Seq2RevB40) were not able to show detectable viral inhibition (Fig. 19B). Although the spinoculation groups showed improved infection efficiency compared to the passive adsorption group, they also showed signs of cellular stress and abnormal cell morphology after 48 hours of incubation than the group without spinning step (Fig. 20B).

Alternative approaches such as switching to phosphorothioate-modified aptamers or using lower passage cells were ineffective. The inability to establish working experimental parameters for modified Liu 1a to neutralize Spike-presenting pseudovirus is an obstacle to be overcome and should be followed up in future studies.

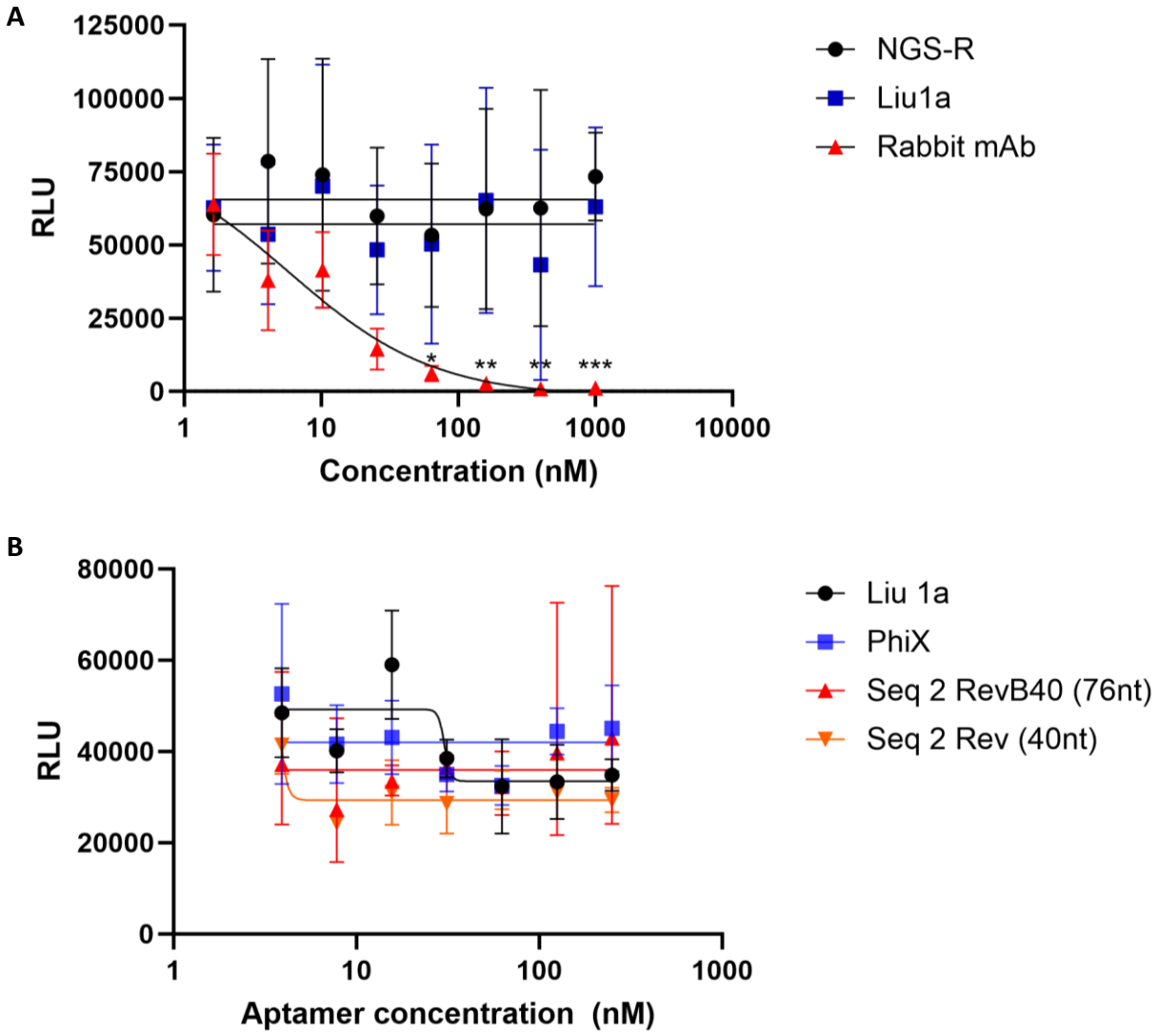


Figure 19. Luciferase signal of LV pseudovirus infected cells after mAb or aptamer treatment. (A) Luciferace-LV pseudovirus was treated with biotinylated SRBD aptamer Liu 1a, NGS-R, a 60nt NGS sequencing primer as negative control, or Rabbit mAB: anti-Spike rabbit monoclonal antibody (Sino Biological) as additional positive control. Error bar: standard deviation. *: $p \leq 0.05$ against NGS-R; **: $p \leq 0.01$; ***: $p \leq 0.001$. The relative luminescence unit (RLU) of the infected cells was recorded after 48 hours of incubation. (B) in a separate microneutralization experiment with same inoculation parameter, LV pseudovirus was treated with phosphorothioate-modified Liu 1a as positive control, PhiX oligonucleotide library as negative control, or Seq2Rev candidates (40nt and 76nt).

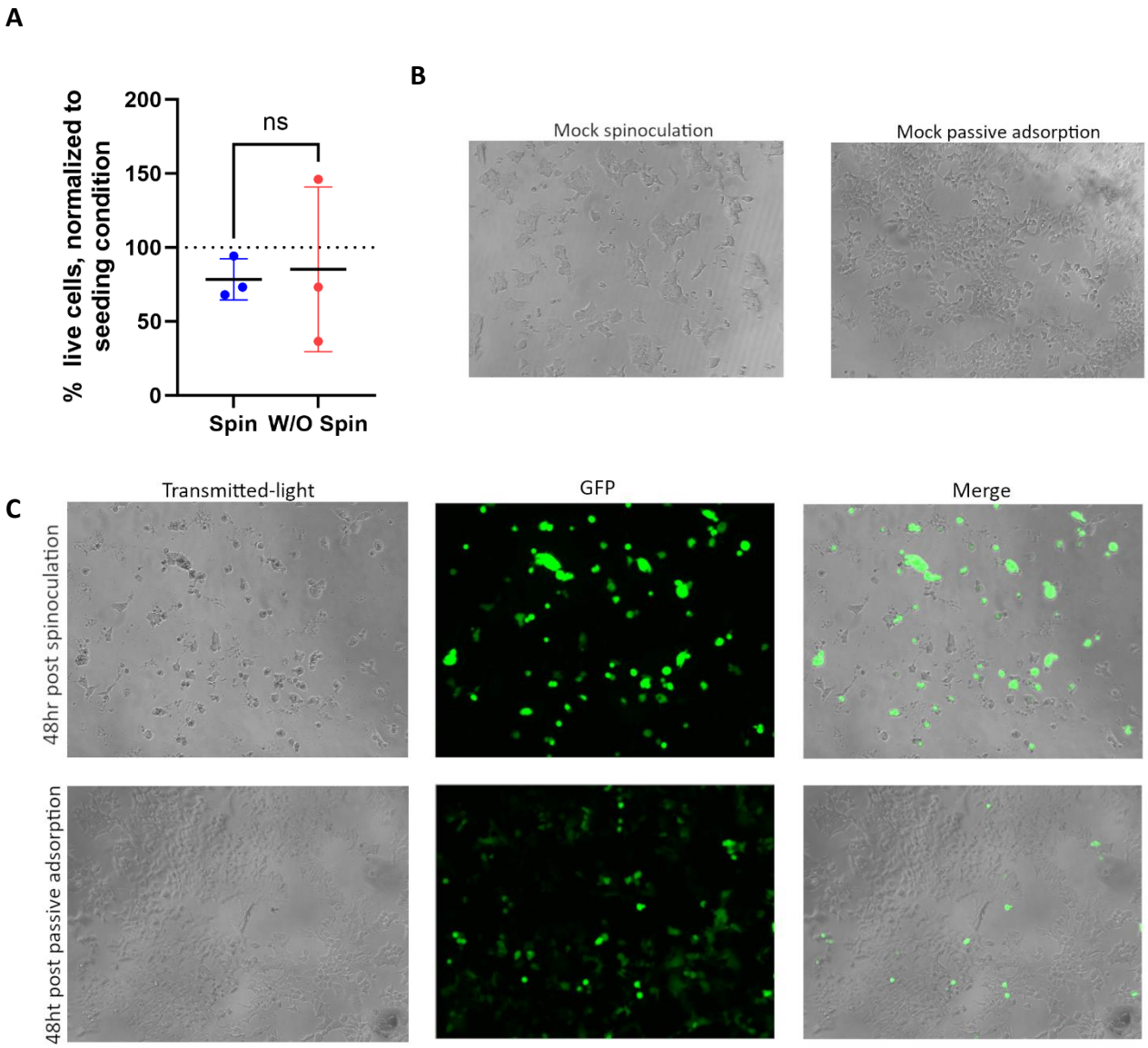


Figure 20. Effects of spinoculation on HEK293T-ACE2/TMPRSS2 cell morphology and pseudotype lentivirus transduction efficiency. (A) Live cell count of mock inoculation groups with (spin) and without (W/O spin) spinning step after 40 hours of incubation. (B) Cell morphology change 48 hours after different mock inoculation methods. Left: spinoculation; right: passive adsorption. (C) Transduction efficiency of different inoculation method, 48 hours after Spike-GFP pseudotype lentivirus inoculation. Upper: spinoculation; lower: passive adsorption.

Chapter Five: Discussion

5.1. SELEX and Aptamer Selection

The goal of the thesis was to generate aptamer candidates that can identify and bind to the SARS-CoV-2 Spike receptor binding domain. The selection process was achieved through the process of SELEX, in which a commercial SELEX ssDNA library, Bank40, was exposed to the target biotinylated recombinant SRBD protein. SELEX is the gold standard for aptamer selection and discovery, as it is intended to be straightforward, convenient, and cost effective. Yet, each step of the process requires careful fine-tuning and quality evaluation to maximize the chance of generating a successful binding candidate. Studies have speculated that the success rate of traditional SELEX approach regarding selecting of a strong binding aptamer might be lower than 30% [176, 285].

In my study, the advantage of using commercial aptamer discovery kit was that it included a ready-to-use ssDNA library (bank40) and a suggested workflow template which guided the user to develop and optimize their own protocol to suit their needs. The Bank40 library had a fixed PCR primer region to complement the suggested PCR-SELEX protocol. Yet, the suggested protocol did not account for potential PCR bias and PCR artifacts which had become a prominent issue throughout the optimization phase. During the PCR amplification stage, each ssDNA generated an extra complementary DNA strand. Theoretically, the PCR step doubled the sequence diversity just before each round of selection, and the complementary strand could be a new candidate itself. In other studies, complementary strands were removed or avoided to retain starting ssDNA sequences through various treatments, such as asymmetric PCR amplification, or tagging the ssDNA with a biotin-labelled primer for streptavidin column separation to recover only ssDNA [162, 286, 287]. Alternatively, by amplifying the sense strand with a chemically-modified primer to 5’-phosphorylarte the wanted strand, the unprotected complementary antisense strand could be removed by an additional T7 gene 6 exonuclease digestion step post-PCR; on the other hand, for the Lambda exonuclease approach, the 5’-phosphorelayed antisense strand would be digested instead [162, 183].

One of the main concerns with PCR-SELEX is the retention of unwanted PCR byproducts. The presence of PCR artifacts could affect the selection efficiency as they can act as binding

competitors that block binders from the target. The presence of long PCR by-products also hindered the PCR efficiency, and further generated more by-products [186]. Self-annealing (secondary structures) sequences, GC-rich or other difficult sequences could also cause amplification bias [162, 183]. To address this, a series of PCR optimizations were set up to determine the optimal PCR approach for amplifying Bank40 and subsequent aptamer pool (Fig. 9). Between emulsion PCR (ePCR) and conventional "open" PCR, ePCR had the optimal balance between amplification efficiency, fidelity, and yield. The difference between open PCR and ePCR could be easily observed on an agarose gel electrophoresis analysis, as the ePCR sample produced a more resolved, sharp band than the open PCR sample (Fig. 9E). After weighing the tradeoff of fidelity and amplification yield, I decided to choose ePCR as it provided the best fidelity among the tested methods to generate binding candidates. The PrimeSTAR polymerase kit was not designed to perform ePCR with the specified amplification parameters as stated in the XELEX kit user handbook. The prolonged annealing (60 sec) and extension (180 sec) time could cause spurious priming and non-specific amplification; yet, I decided to go with the original protocol as there was no apparent sign of by-product formation during the early ePCR optimization stage (Fig. 9E). The number of PCR cycles and concentration of input template was adjusted accordingly for subsequent SELEX cycles to minimize PCR by-products and avoid over-amplification [162, 176, 183, 186]. In my SRBD study, the Bioanalyzer platform detected PCR artifacts that were present in 5R to 10R samples, visualized as extra smear adjacent to the 76bp band (Fig. 10A). It was unclear whether the detected PCR artifacts had affected the downstream aptamer-target selection or not. A follow-up BLI aptamer pool target-binding assessment indicated that there were binding sequences in 10R (Fig. 11), therefore I proceed to prepare the 10R pool for the sequencing step. To avoid further complications, the final 10R sample was treated with a series of purification steps, including high-density agarose gel extraction and SPRI bead clean-ups before HTS in hopes of generating data with less noise.

In retrospect, adding intermediate sequencing steps in-between rounds of SELEX would help monitor population changes and emergence of dominant sequences. The real-time PCR melting-curve result (Fig. 10B) showed that there was a sharp single melting point peak at the 5^{th} round of selection at 72^{o}C, unlike 3^{rd} and 4^{th} round where there were two peaks at 63 ^{o}C and

82°C. The peak remained in the selection pool until the 10th round but it gradually became broader, spreading from 69-72°C, and less prominent as the selection progressed. This suggested that a homogenous, dominating sequence with single melting temperature (T_m) emerged and dominated the aptamer population by round 5, but the subsequent selection procedures introduced unexpected sequences with a variety of T_m that interfered with the SELEX pool. Additionally, the aptamer pool BLI assay also showed that the average binding affinity of pool 6R was higher than pool 10R (Fig. 11). This further supported the implication that strong binders were dominating the pool by 6R. Monitoring the evolution of the pool by setting up checkpoints such as the melt peak [288], BLI assays [289, 290], or HTS [176, 197] in between selection round would provide more data to track binder emergence and on-going binder maturation, which potentially reduces the resources needed and shortens the selection process for a more dynamic, flexible SELEX. By ensuring that the selection process was working as intended, additional quality control steps could potentially lower the number of SELEX rounds needed to achieve sequence enrichment, and minimize the total number of PCR cycles [197]. In hindsight, only after completing 10 rounds of selection, I realized the lack of checkpoints and functional tests in between rounds of selection was a great oversight in my experimental design. An experimental consideration that prevented me from actively monitoring the progression of SELEX at each cycle, was the ePCR amplification was kept to a minimum to avoid introducing more PCR bias. Therefore, one of the challenges of implementing inter-step functional tests was the availability of recovered aptamer after ssDNA regeneration (Table 3). The amount of aptamer needed to perform target-aptamer functional test such as EMSA, BLI, and ALISA far exceeded the material needed for nucleic acid-based tests such as the bioanalyzer chip and single-cycle melt curve analysis. More than half of the recovered ssDNA from certain SELEX rounds (namely Round 3, 4, 5, and 9 that had <2000ng recovered ssDNA) were re-introduced into the following rounds of selection, which made setting up inter-step analysis challenging. A workaround solution is to collect an aptamer pool sample after the SELEX PCR step (Fig. 5, step 6) from each round for further SELEX-independent amplification, just to generate sufficient working material for quality assessment and functional tests. That way, the SELEX aptamer pool would remain unaffected whereas the testing aptamer

pool could be amplified for downstream manipulation. Although this would not be a perfect solution, but it could at least provide some feedback regarding the state of selection.

When processing the HTS data to isolate and identify individual aptamer sequences, the filter and trimming program (Cutadapt) detected and removed 57-64% of reads with intact adaptors (Illumina adaptor and SELEX primer) that were shorter than the defined 35nt cutoff length (see Appendix for Cutadapt summary). The Cutadapt function filtered and removed a collection of sequences with various lengths (ranging from 3bp to 140bp) with no apparent pattern. This could be an indication that short PCR artifacts were accumulating throughout the SELEX cycles and were retained after the series of purification treatments [186]. There were multiple purification and clean-up steps during and after the SELEX selection, the persistence of these short oligonucleotides indicated underlying experiment design flaws. The microfluidic gel electropherogram of 10R (Fig. 12B) showed a considerable amount of sequences were smaller than the 76nt mark before the SPRI bead clean-up, therefore the spin-column based DNA purification kits were insufficient for removing short fragments. The magnetic bead washing also failed to remove short oligonucleotides after the target-aptamer binding step despite multiple washes. This could be due excess binding between nonspecific nucleic acid and highly charged amino acids that was present in the RBD [291], which made the elimination of small weak binders difficult.

The HTS result showed that the 10R pool also contained a high abundance of sequences with a streptavidin-binding motif (i.e. sequence number 1, 6, 8,Table 4). This indicated the negative selection setup was insufficient to remove many of the off-target binders. Although target-magnetic bead immobilization is widely considered as the most popular and straightforward method for positive selection, the aptamer can bind against the coupling linkage or uncoupled bead coatings instead of the intended target [162, 176, 183]. My results suggested that there was insufficient negative selection to remove all streptavidin-binders, which could contribute to the poor selection outcome. Studies have proposed workarounds such as flooding the pool with free streptavidin to “flush out” the off-target binders, in order to curb the emergence of streptavidin-binding sequences throughout the selection process [183, 290]. Another suggestion is to alternate coupling linkages (biotinylated, His-tagged, Fc-tagged

etc.) in between rounds of SELEX instead of relying on one singular immobilization method entirely [178, 179, 203]. An alternative, label-free approach is capillary electrophoresis SELEX, which circumvents the limitation of target immobilization by separating the target-aptamer complexes and the free-flowing non-binders based on charge and weight in a gel matrix [178, 203, 292].

5.2. Aptamer Characterization

After sequencing, the top 10 most abundant sequences were identified. Before realizing the streptavidin-binding motif that was present in Seq 1, the top two sequences and their derivatives (Seq 1, Seq 2) were sent to be synthesized. Since the 10R pool showed SRBD-binding activity, the expectation was that strong binders were retained and populated the final pool. The synthesized sequences were then screened via gel electrophoresis or EMSA. Even though it was an inexpensive and quick approach to screen through multiple candidate simultaneously, the band distortion and poor band resolution clouded the result interpretation (Fig. 13). To visualize the differential rate of migration between target-aptamer complexes and free-flowing oligonucleotides, I explored different types of gel matrixes and staining strategies, such as high-density agarose gel, blue native PAGE, Coomassie Blue and Silver protein staining protocols. Using Liu 1a, the known SRBD aptamer published by Liu *et al*. [270] as positive control, one of the SELEX candidates, Seq2Rev (40nt), showed signs of complex-formation which lead to a decrease of free flowing aptamer (Fig. 13E). Interestingly, band warping was observed when the aptamers were incubated with higher concentration of SRBD recombinant protein, which suggested the gel wells were overloaded. In the context of the experiment, the goal of using a higher protein concentration was to induce detectable migration rate differences between aptamer-protein complexes and the unbound oligonucleotides due to the poor stain sensitivity. Unfortunately, the increased protein concentration was unable to generate detectable migration retardation, perhaps due to weak aptamer binder or poor stain performance. The sensitivity of EMSA could be improved by switching to fluorescent dye-tagged aptamer or radiolabeled nucleotides, which circumvent the limitation of post-electrophoresis staining [293].

To validate gel electrophoresis results, I turned to other analytical systems with higher sensitivity. Conventional methods such as direct ALISA and FLAA were explored but met with little success, possibly due to low sensitivity. These methods were based on detection of target-bound oligonucleotides and relied on fluorescent ssDNA dye such as GelRed (Biotinum) and Oligreen (Invitrogen). To overcome the difficulty of detecting target-bound aptamer in solution, I set up a capture ALISA with immobilized biotinylated aptamer to capture free His-tagged SRBD, which was reported to have similar or higher sensitivity compared to conventional mAb ELISA [199]. Biotinylated Liu 1a (positive control) was diluted to reliably generate quantifiable colorimetric signal without overloading the plate reader (Fig. 14). Interestingly, contradictory to the EMSA finding**,** the capture ALISA data suggested that the Seq2For sequence - instead of Seq2Rev – exhibited highest binding activity to SRBD among the four remaining SELEX candidates. The contradicting result was concerning due to fact that the chance of both forward and reverse strands of the same sequence exhibiting target-binding activity was very slim. In retrospect, an unrelated biotinylated DNA sequence, such as the PhiX sequence, should be implemented in both EMSA and ALISA experiments. A biotinylated short oligonucleotide could have been a better negative control for measuring background binding, and to subtract the baseline signal from the raw data, so that the candidates could be properly assessed. Still, considering the positive control Liu 1a-SRBD dwarfed the signal of Seq 2 SELEX candidates, it showed that all SELEX candidates were significantly weaker SRBD binders than Liu 1a.

Although Seq 1 (and its derivatives) was not tested to determine its affinity towards streptavidin, considering that the known streptavidin-binding motif was found on Seq 1 (Table 4), I still removed Seq 1 from the group of potential aptamer candidates to save resources. As discussed above, the off-target streptavidin-affinity that was unintentionally introduced throughout the selection process might explain the failure of generating stronger SRBD binder. Combining the data that was shown in the aptamer pool BLI (Fig. 11) and the aptamer pool qPCR-melt curve (Fig. 10B) analyses, it was likely that the aptamer pool started to divert at round 6 (6R), gradually losing the optimum binding sequences over subsequent SELEX rounds, and ended up with a pool of weaker binders by round 10. In future follow-up studies, other than implementing better optimized selection procedures (e.g. saturating the ssDNA pool with

free streptavidin during positive selection, adding functional checkpoints in-between rounds, switching target protein for positive control), perhaps it might be worthwhile to sequence and investigate the individual aptamers in the 6R pool. Furthermore, there are reports that suggest the sequence enrichment rate, the rate that a binding sequence expands over rounds of selection, is a better indication of strong binder than prevalence alone [183, 294]. In this project, the top two most abundant sequences in 10^{th} round pool (10R), Seq 1 and Seq 2, were chosen for downstream analysis based on of the assumption that they were the strongest SRBD binders. The tracking of sequence enrichment could be achieved by implementing round-by-round HTS and bioinformatics analysis, to monitor the emergence of rare but high-affinity sequences.

To investigate the target-aptamer interaction on a molecular level, BLI is one of the most sensitive platforms for evaluating the binding dynamics and quantifying binding affinity between the aptamer and the target. Similar to the capture ALISA approach, the aptamer was bound to the biosensor before dipping into an increasing concentration of His-SRBD. Several other proteins (SRBD, S1 subunit, and full Spike), in-house His tagged Ebolavirus glycoprotein and His tagged prion protein) and alternative functional linkages (mFc and His) were tested (data not shown) during the optimization phase. Interestingly, the same problem that was present in conventional ALISA was also observed here, where it was difficult to establish a working immobilized protein-aptamer association system. To address this, biotinylated aptamers were instead immobilized on the streptavidin-coated biosensor instead of the protein ligand (Fig. 15A-D). Unlike capture ALISA, the capture BLI system was sensitive enough to generate sensorgram data that shed some light on the nature of binding between target protein and immobilized aptamer. At the association phase, the association between Seq 2 and SRBD was unable to reach equilibrium state (R_{eq}), which might be an indication of non-ideal heterogeneous binding, or presence of aggregation or impurities in the reaction wells [281]. It was possible that the SELEX candidates were unexpectedly great binders, so that the actual dissociation would then be masked by target re-association [295]. However, the same phenomenon was also observed when the positive control Liu 1a aptamer was tested (Fig. 15E), which was not reported in the original aptamer study [270]. Considering that Liu 1a (K_D: 88nM)

outperformed the best SELEX candidate (Seq2For, K_D: 1700nM) by a log, the more plausible explanation would be sub-optimal experiment setup. The sequence-target association might be interfered by impurities or additives, such as blocking protein (BSA), biotin, and ionic molecules. Ideally, to better optimize the aptamer-BLI parameters, additional experiments should be set up to measure the non-specific electrostatic interaction of SELEX candidates with other non-target proteins. The performance of the aptamers might vary when the association condition of the SELEX binding step and the BLI assays were not exactly the same, especially when they used different buffers (SELEX buffer verses KB buffer) and assay temperature (25^{o}C room temperature verses 30^{o}C BLI instrument temperature). Perhaps it would shed some insights onto the underlying problem of non-specific amino acid-nucleotide attraction.

In silico characterization and 2D structure prediction of the SELEX candidates are the next steps in studying the aptamers' binding motifs. The terminals of the SELEX candidates with fixed primer regions (highlighted in yellow and cyan) were expected to form complementary pairs and panhandle secondary structure (Fig. 16 A-D), whereas the terminals of the primer-free SELEX candidates (Fig. 16 E-H) were left unpaired. The formation of secondary structures at the primer region could potentially interfere with target binding, but perhaps it is intentionally designed to form a panhandle structure so that would not interact with randomized region of the aptamer, which is crucial for its functionality [159, 162]. Furthermore, terminal hairpin-loop could be part of the protein-aptamer interacting structure. A hairpin-loop is a quintessential structure that can found in many protein-binding aptamers. An *in silico* study of an anti-SRBD aptamer suggested that the exposed negatively charged phosphate dsDNA backbone of a hairpin loop could interact with the positively charged RBD, and the unpaired loop could provide greater flexibility and structural variability for the double-stranded helix [296, 297]. This was further supported with the molecular docking simulation with Liu 1a aptamer and SRBD (Fig. 17). Rigid-body molecular docking simulation suggested that the positively charged RBD residues, such as the R403 and K493, were attracted to the complementary DNA duplexes, possibly due to the negatively charged dsDNA backbone (Fig. 17D). Other polar and negatively charged residues fit into the Liu 1a hairpin-loop pocket where the nucleotide bases were more exposed, but yet somewhat stabilized by the adjacent complementary helix structure. The

docking model predicted that Liu 1a aptamer would interact with Q493, T500, N501, and Y505 residues, which were crucial ACE2 binding residues [298]. The molecular docking simulation predicts molecular interaction and generates a snapshot of the predicted conformation between target molecule and aptamer. The ZDOCK web server was user-friendly and reported to have high protein-protein prediction accuracy (>70%) [278], which lowers the technical barrier for performing computationally-heavy analysis. To validate the docking result, to determine the conformational stability of the 3D structures, and to examine the intermolecular forces between the target and the aptamer, the next logical step is to perform a molecular dynamic simulation which measures and records the conformational changes and atomic distances over a given time period (usually nanoseconds to microseconds) [187]. However, *in silico* simulations like molecular docking and molecular dynamics require high computational power and extensive technical knowledge, therefore they are beyond the scope of this investigation. One of the limitations of computer-assisted aptamer modelling is that it relies on experimental data based on existing solved structures in databases, which might be inadequate for deriving accurate models for novel candidates [299, 300]. There is a growing library of experimentally solved protein-aptamer structures [301], which would improve the accuracy of aptamer-specific molecular structural and interaction modelling. By comparing aptamer pool samples that are collected in between rounds of selection, analytical software can also track the emergence and maturation of binding motifs [195, 196, 302]. As the artificial intelligence technology matures, there is an emerging trend toward pairing experimental data and machine learning approaches to simulate atomic-level aptamer-target molecular interactions and 3D structures [207, 303]. Another aptamer discovery approach is to map the structure of the binding site of the target protein *in silico* and design aptamer sequences with nucleotides binding to specific amino acids [304–306].

Studies have suggested creative workarounds to address PCR related limitations in the aptamer selection process. For example, aptamers can be selected through alternative SELEX (non-SELEX) systems that skip the PCR amplification step, which effectible eliminates any PCR biases. For example, capillary electrophoresis to separate protein-aptamer complexes with increasingly more stringent parameters [307]; or exposing increasing concentration of starting

library to alternating positive and negative target to promote competitive binding selection [181]; or using negative selection target-coated magnetic nanoparticles to remove off-target sequences from selection pool repetitively have been successfully used [308]. Another study has proposed to add complementary short primer oligonucleotides that would hybridize with the primer regions of the aptamer so to limit the interaction between the fixed primer region and the target molecule [309]. Another approach is to set up a target-binding selection step with a primer-independent randomized library, in which the primer region can be added-on or removed after and before the selection process through ligation [310]. These methods claim to generate aptamers with higher specificity and stronger target-affinity, but compared to the simplicity and straightforwardness of conventional SELEX, most alternatives raise new challenges such as introducing more uncertainties, lower efficiencies, unexpected off-target binding, technologically demanding, and labour intensive steps.

5.3. *In vitro* Microneutralization of Pseudovirus by Aptamers

Seq2For (40nt) was the most promising aptamer among the eight SELEX candidates, albeit a relatively weaker SRBD binder in comparison to positive control aptamer Liu 1a. A follow-up *in vitro* experiment where its antiviral potential was evaluated by measuring the aptamer's neutralizing capability was performed. Seq2For was unable to elicit any detectable neutralizing effect in the lentivirus (LV) pseudotype virus infection model. To further investigate the underlying issue, the experiment was repeated using known positive control Liu 1a. Unfortunately, the experiment was unable replicate the reported result that demonstrated its ability to efficiently neutralize virus [266].

I explored other virus neutralization platforms before I chose to settle on the aforementioned LV pseudotype virus protocol. A microneutralization assay using authentic virus in biosafety level 3 setting was also considered initially, but the plan was ultimately discontinued given the poor performance of SELEX candidates in previous experiments. The LV pseudotype virus platform was an accessible and popular model to assess the neutralizing effect of small molecules such as novel drugs and monoclonal antibodies (mAb) [261, 269]. It is

also biosafety level 2 compatible, and relatively forgiving to protocol changes, which is crucial for designing a working microneutralization approach to accommodate aptamer-specific treatment.

One of the biggest challenges in physiological application of aptamers is nuclease digestion and denaturation, as the typical half-life of non-modified ssDNA aptamers in serum reported to be 60 minutes [311]. While trying to develop the working protocol for the project, the pseudotype LV were treated with non-chemically-modified aptamers, which showed no detectable neutralization effect. The non modified-aptamers were then replaced with terminally biotinylated aptamers, and in subsequently experiments, aptamers with phosphorothioate-modification. The chemically modified aptamers, although showing signs of slow degradation by 48 hours (decrease band intensity), were resistant against ambient nuclease that was presented in cell media with serum, even in elevated temperature (37^{o}C) for prolonged incubation period (up to 48 hours), as shown in the aptamer biostability assay (Fig. 18). Although the FBS that was added in DMEM was heat inactivated (56^{o}C for 30 minutes), studies have suggested that the heat treatment might not be sufficient to inactivate nuclease activity [282]. Still, the presence of active nuclease could not be verified without the inclusion of an unmodified nucleic acid control, and repeating the assay with a larger sample size would have provided more confidence in the analysis of the assay outcome. In retrospect, although the sequence remained intact after prolonged incubation, the functionality of the recovered aptamer could be investigated through ALISA or BLI, to assess its target binding property. To further minimize potential effects due to nuclease digestion, the LV pseudovirus was treated with modified aptamer in DPBS, and transferred to HEK293T cells for two hours before replacing the inoculation with cell media. If the chemically modified Liu1a was still structurally intact, it should bind to SRBD and block the pseudovirus infection, yet it did not exhibit detectable neutralization effect (Fig. 19B).

The inability to reproduce the viral neutralization result with the aptamer positive control Liu 1a was unexpected. To investigate the cause of the failure, the design of the microneutralization assay was scrutinized. The assay protocol was based on the Liu *et al.* study [270] and the LV pseudovirus surrogate neutralization study [256]. The purpose of the

spinoculation centrifugation step is to overcome the charge repulsion between the membrane proteins of the cells and the LV particles. Despite the adjustment of centrifugation force (changing from 4000xg for 30 minutes, the force that was described in the Liu *et al.* neutralization protocol, to 2570xg for 30 minutes, the maximum force our plate spinner could handle), the spinoculation was successful as the luciferase assays showed increased luciferase expression after 48 hours post inoculation compared to controls that were infected without spinoculation (Fig. 20C). However, as mentioned in the previous chapter (Chapter 4.4), there were observable morphological changes between the spinoculated cells and the passive adsorption group (Fig. 20B). Although spinoculation increased the sensitivity of the platform by increasing transduction efficiency, the negative effects of the extra mechanical stress were not fully understood [312–314]. Furthermore, it was unclear how HEK293T-ACE2/TMPRSS2 cells, the cell line that was used in the current protocol, would react to the mechanical treatment. A follow-up mock-infection cell viability analysis suggested that the mechanical strain might contribute to cell morphological changes (Fig. 20B). Despite this, the fact that the anti-SARS-CoV-2 Spike mAb was able to elicit neutralizing effect in the pseudotype LV model (Fig. 19A) but not the aptamer positive control suggested that the spinoculation might not be the root cause of the failed Liu 1a inhibition.

One possible cause of the failed *in vitro* aptamer inhibition might be related to the cell line that was used in the microneutralization assay. TMPRSS2, a membrane bound protease that is crucial to Spike cleavage to facilitate SARS-CoV-2 entry [61], was not significantly expressed in ACE2-HEK293T [61] and Vero E6 [315] cell lines, which were used to develop Liu 1a in its original 2021 study [270]. Although Liu 1a aptamer was reported to block ACE2-SRBD interaction, perhaps it was unable to inhibit other RBD-independent route of entry [316, 317] due to its relatively small size (6-30kDa) compared to anti-SRBD antibody (50-180kDa) [247]. Perhaps the stable expression of TMPRSS2 in the HEK293T-ACE2/TMPRSS2 cell line that was used in my microneutralization assay provided an alternative viral entry route that bypassed the ACE2-aptamer-RBD blockage, which could be validated by a follow-up neutralization experiment to compare the inhibition effect of Liu 1a between cell lines with and without TMPRSS2 expression. However, without further investigation, it was not clear if the cause of Liu

1a's failure was the presence of TMPRSS2, due to the fact that the anti-SRBD mAb targeted the same Spike viral component and was able to neutralize the LV pseudovirus with the same susceptible cell line (Fig. 19A). Without repeating the experiment with the same ACE2-HEK293T cell line (the one that was used in Liu *et al.* study), it would be difficult to pinpoint the cause of the failed inhibition. Another option was to validate the microneutralization assay with other known, published SRBD-blocking aptamer sequences. Valero *et al.* has developed a RBD-binding 2' fluoro-pyrimidine-modified 36nt RNA aptamer that is able to neutralize Spike-presenting viral-like particle in ACE2/TMPRSS2-HEK293T cells [204], which suggests that despite the small molecular size, aptamer-based inhibitor still has the potential to block ACE2-TMPRSS2 mediated cell entry. It would be interesting to select RBD-binding aptamer candidates that could also inhibit RBD-independent viral entry routes in future studies.

5.4. Aptamer Applications and Their Role in COVID-19 Diagnostics and Therapeutics

Due to its role in cell attachment, immunogenicity, and spatial accessibility, Spike protein of SARS-CoV-2 was a popular target for both antiviral and diagnostics research. Vaccine and mAbs that targeted S protein were able to provide protection against viral infection. However, the development of mAbs or synthetic molecules that targeted SARS-CoV-2 Spike were also challenged by the emergence of antigenic drift and immune escape throughout the pandemic. Since 2020 April, multiple groups have developed and published aptamer sequences that recognize the viral S protein, and some of them even exhibit cross-reactivity against variant of concern (VOC) Spike proteins [179, 201, 270, 272, 292, 318–325]. Some studies claimed to have achieved picomolar viral protein concentration sensitivity, which outperformed many anti-Spike mAb counterparts [205, 231]. As the pandemic progressed, individual SARS-CoV-2 protein structures became more readily available, including viral antigens from emerging strains. Submission of high-resolution Spike 3D models in protein databases were used to predict binding sites of newly developed anti-Spike aptamers [218, 326]. Previous SARS-CoV studies have proposed to design evolution-resistant aptamers that target viral antigens that are under lower selective pressure, such as the those against the nucleocapsid (NP) and membrane protein [327, 328]. In the context of SARS-CoV-2 response, novel diagnostic platforms were

developed based on NP [201, 329]. The scope of SARS-CoV-2 aptamer research has expanded to include other common coronavirus species, and has even lead to the discovery of pan-human coronavirus aptamers [326].

Some studies have explored the potential of generating therapeutic aptamers that target host elements, independent of SARS-CoV-2, which potentially bypass the viral antigenic drift and strain mutations. For example, a study proposed that hACE2 binders could block the attachment of SARS-CoV-2 to host receptor, thus effectively inhibiting viral infection [330]. Alternatively, aptamers that targeted cellular inflammatory factors and pathways involved in COVID-19 pathogenesis were shown to mitigate cell inflammation *in vitro* [331].

The greatest hurdle that the aptamer-based technology faced was the innate vulnerability of its nucleic acid biochemistry. Aptamers with natural nucleotides are subject to ambient nuclease digestion, and can be easily unfolded by suboptimal heat, pH, and ionic conditions. As mentioned in previous chapters, the current trend of aptamer research is to include post-SELEX modifications that could enhance the stability and resistance of the sequence for both POC testing and physiological application. The SARS-CoV-2 pandemic provided an opportunity for exploring novel aptamer approaches. For example, a study generated an anti-Spike aptamer with nuclease-resistant synthetic nucleotides (xeno-nucleotides) that had higher binding affinity than aptamers with naturally-occurring nucleotides [332]. Modifications such as colourmetric tags and fluorescent nucleic acids were able to generate versatile biosensors and reporters for *in vitro* SARS-CoV-2 detection [333]. There was also rising interest in exploring the synergy of combining aptamer and nanoparticle technologies, which resulted in improved drug delivery and diagnostic efficiency [224, 225, 231, 334, 335]. Aptamer-based diagnostic tools are as capable as their antibody protein counterpart, and arguably more convenient than non-deployable laboratory diagnostic approaches such as PCR and ELISA due to its simplicity and versatile platform (e.g. lateral flow strip, dot blot) integration [211]. Another advantage of aptamer over antibody is that the production of aptamers is highly scalable and does not require growing and maintaining mammalian cell cultures, making it more economical and accessible [336]. In the context of pandemic response, aptamer-based diagnostics could be easily deployed and utilized in the field, POC testing,

healthcare, and laboratory settings [211, 213]. The modified oligonucleotide has high stability and low production cost, making them desirable diagnostic tools for remote and developing regions [211, 212]. On top of that, unlike mAbs, aptamers could target non-protein molecules, such as pathogen-associated lipid and toxin, further expanding its diagnostic potential beyond the limits of human, bacterial, and viral proteins [211].

Similar to conventional drug discovery, the aptamer discovery pipeline also involves screening and analyzing a library of candidates. However, its antibody-like ability to "mature" and "evolve" over the course of selection, while capable of targeting a wider range of targets than antibodies, makes it a powerful molecular tool. Aptamer development also comes with its own challenges such as high failure rate [288] and low reproducibility [337]. I have developed and analyzed a set of unique SRBD binders that were not previously reported by other groups, despite using the same SARS-CoV-2 Spike RBD target. Although the sequences that I've developed were weak SRBD binders, I have explored various aptamer discovery, sequencing, and analytical approaches, and assessed the shortcomings and limitation of the experimental designs. Specifically, the aptamers were evaluated through: bench top experimental molecular interaction assays, computational 3D modelling characterization, and *in vitro* antiviral assessment with SARS-CoV-2 Spike presenting LV pseudovirus. The comprehensive analyses were crucial to evaluate the diagnostic and therapeutic potential of a binding aptamer, bridging the gap between aptamer development and aptamer application. The effort and time that was put into the process, from developing and optimizing SELEX, all the way to evaluating the antiviral potential of the candidates with pseudoviruses was considerable, especially when working without prior experience. However, since the late 1980s when the idea of aptamers was first invented, there are newer approaches and tools that aim to improve aptamer functionality, specificity, degradation resistance, and ease of development, as mentioned above. Researchers with the appropriate experimental background could greatly streamline the development process, shortening the timeline from years to weeks [162, 214].

Throughout the pandemic, there were many published literature exploring the therapeutic potential SARS-CoV-2-targeting aptamers. However, the marketability of aptamer-based therapeutics was overshadowed by the established competing technologies (e.g. mAb

and conventional antivirals), and the controversial past of aptamer technology itself. Notably, in clinical trials for Pegnivacogin (a PEGylated RNA aptamer that binds and inhibits factor IXa), human volunteers had experienced severe allergic reactions after therapeutic aptamer injection, which led to immediate termination of associated clinical trials, and greatly stunted interests and investment in therapeutic aptamer research for many years [248, 338]. Due to past criticisms, there is more interest in aptamer-based diagnostics than therapeutic aptamers. Fortunately, the pandemic provided an opportunity for researcher to experiment and improve aptamer modifications and delivery formulation for *in vivo* administration, which showed promising results and minimal side effects in mouse models [339, 340]. Interestingly, the SARS-CoV-2 pandemic also gave rise to the popularity of nucleic-acid nanoparticle-based vaccines [341–343], which brought new technologies and insights to both nucleic acid-vaccine and aptamer-based therapeutic research. Perhaps the advancements that were made during the COVID-19 pandemic could bring new blood into the field, and potentially make aptamers a recognizable powerhouse for future outbreak and pandemic response.

Chapter Six: Concluding Remarks and Future Direction

For my thesis project, I have developed and characterized DNA aptamers that targeted SARS-CoV-2 SRBD. Through the process of SELEX selection, SRBD-binding aptamers were isolated and identified. Despite multiple rounds of negative selection, off-target streptavidin-binding motifs were retained due to the use of streptavidin-coated magnetic beads during the target immobilization step. The screening of the SELEX candidates revealed that Seq2For, a 40nt aptamer, had the highest binding affinity among the 8 oligonucleotides derived from the top two identified sequences. Interestingly, the data suggested that the elimination of the fixed primer region that was used in the SELELX PCR amplification step improved the target binding affinity. Molecular docking data predicted that the positively charged residues on SRBD were more likely to interact with negatively charged oligonucleotide backbone presented on hybridized complementary region. Nonetheless, the process of designing and optimizing SELEX provided valuable insights on potential selection biases and blind spots that were often overlooked, such as choosing an appropriate target immobilization approach to minimize off-target binding. It also emphasized the importance of establishing inter-step quality control and functional checkpoints to monitor the progress of the "evolving" sequence. The study would have also benefited from implementing multiple sequencing steps throughout the selection process to track the emergence of strong binders. The current study is a starting point for generating aptamers that recognize wild-type Wuhan SARS-CoV-2 SRBD. Ideally, with the help of powerful computational simulations, the molecular interaction between the predicted structure of the developed aptamer and SARS-CoV-2 Spike protein can be validated and studied in the future. I hope that the project will be a stepping stone for developing strong binding aptamers that target other SARS-CoV-2 viral subunits, and potentially tested against different VOCs.

The project also shed light on challenges of developing therapeutic aptamers, as demonstrated in the attempt to modify an established pseudotype LV microneutralization assay to test the antiviral capability of the aptamers. This could be due to alternative viral entry routes that the aptamer was unable to overcome. For future studies, other major SARS-CoV-2 co-receptors and alternative viral entry routes should also be considered and tested to

maximize the antiviral effect of novel SARS-CoV-2 neutralizing aptamer. This highlighted the difficulties of developing aptamer-specific *in vitro* assays and functional delivery system for aptamer-based therapeutics. Modification and delivery options including nanoparticle technologies and substituted artificial nucleotides should be explored in future projects to further stabilize the integrity of the aptamer and enhance its specificity and binding affinity. With newfound understanding and improvement to the technology, promising aptamer candidates should be tested on different diagnostic platforms to evaluate their diagnostic potential. The lessons that we learnt from this project should be applied in future aptamer discovery for rapid outbreak and pandemic response.

Chapter Seven: References

1. Guo YR, Cao QD, Hong ZS, et al (2020) The origin, transmission and clinical therapies on coronavirus disease 2019 (COVID-19) outbreak- A n update on the status. Mil Med Res 7

2. Zhou P, Yang X Lou, Wang XG, et al (2020) A pneumonia outbreak associated with a new coronavirus of probable bat origin. Nature 579:270–273. https://doi.org/10.1038/s41586-020-2012-7

3. Lu R, Zhao X, Li J, et al (2020) Genomic characterisation and epidemiology of 2019 novel coronavirus: implications for virus origins and receptor binding. The Lancet 395:565–574. https://doi.org/10.1016/S0140-6736(20)30251-8

4. Temmam S, Vongphayloth K, Baquero E, et al (2022) Bat coronaviruses related to SARS-CoV-2 and infectious for human cells. Nature 604:330–336. https://doi.org/10.1038/s41586-022-04532-4

5. Roberts DL, Rossman JS, Jarić I (2021) Dating first cases of COVID-19. PLoS Pathog 17:e1009620. https://doi.org/10.1371/journal.ppat.1009620

6. David J. Sencer CDC Museum (2023) CDC Museum COVID-19 Timeline. In: Centers for Disease Control and Prevention. https://www.cdc.gov/museum/timeline/covid19.html. Accessed 27 Nov 2023

7. Rauf A, Jin Z, Roshi EE, et al COVID-19 outbreak: Impact on global economy

8. World Health Organization Emergency Comittee (2020) Statement on the second meeting of the International Health Regulations (2005) Emergency Committee regarding the outbreak of novel coronavirus (2019-nCoV). In: WHO. https://www.who.int/news-room/detail/30-01-2020-statement-on-the-second-meeting-of-the-international-health-regulations-(2005)-emergency-committee-regarding-the-outbreak-of-novel-coronavirus-(2019-ncov). Accessed 27 Nov 2023

9. (2020) Naming the coronavirus disease (COVID-19) and the virus that causes it. In: World Health Organization. https://www.who.int/emergencies/diseases/novel-coronavirus-2019/technical-guidance/naming-the-coronavirus-disease-(covid-2019)-and-the-virus-that-causes-it. Accessed 27 Nov 2023

10. Ball P (2021) The lightning-fast quest for COVID vaccines — and what it means for other diseases. Nature 589:16–18. https://doi.org/10.1038/d41586-020-03626-1

11. Medicines and Healthcare products Regulatory Agency (2020) Press release: UK medicines regulator gives approval for first UK COVID-19 vaccine . In: Medicines and Healthcare products Regulatory Agency . https://www.gov.uk/government/news/uk-medicines-regulator-gives-approval-for-first-uk-covid-19-vaccine. Accessed 27 Nov 2023

12. Davies NG, Abbott S, Barnard RC, et al (2021) Estimated transmissibility and impact of SARS-CoV-2 lineage B.1.1.7 in England. Science (1979) 372:. https://doi.org/10.1126/science.abg3055

13. Koelle K, Martin MA, Antia R, et al (2022) The changing epidemiology of SARS-CoV-2. Science (1979) 375:1116–1121. https://doi.org/10.1126/science.abm4915

14. Volz E, Mishra S, Chand M, et al (2021) Assessing transmissibility of SARS-CoV-2 lineage B.1.1.7 in England. Nature 593:266–269. https://doi.org/10.1038/s41586-021-03470-x

15. McCrone JT, Hill V, Bajaj S, et al (2022) Context-specific emergence and growth of the SARS-CoV-2 Delta variant. Nature 610:154–160. https://doi.org/10.1038/s41586-022-05200-3

16. Mlcochova P, Kemp SA, Dhar MS, et al (2021) SARS-CoV-2 B.1.617.2 Delta variant replication and immune evasion. Nature 599:114–119. https://doi.org/10.1038/s41586-021-03944-y

17. Chavda V, Bezbaruah R, Deka K, et al (2022) The delta and omicron variants of SARS-CoV-2: what we know so far. Vaccines (Basel) 10:1926. https://doi.org/10.3390/vaccines10111926

18. World Health Organization (2021) Classification of Omicron (B.1.1.529): SARS-CoV-2 variant of concern. In: World Health Organization. https://www.who.int/news/item/26-11-2021-classi%EF%AC%81cation-of-omicron-(b.1.1.529)-sars-cov-2-variant-of-concern. Accessed 27 Nov 2023

19. Grewal R, Nguyen L, Buchan SA, et al (2023) Effectiveness of mRNA COVID-19 vaccine booster doses against Omicron severe outcomes. Nat Commun 14:. https://doi.org/10.1038/s41467-023-36566-1

20. Mannar D, Saville JW, Zhu X, et al (2022) SARS-CoV-2 omicron variant: antibody evasion and cryo-EM structure of spike protein–ACE2 complex. Science (1979) 375:760–764. https://doi.org/10.1126/science.abn7760

21. Sah R, Rais MA, Mohanty A, et al (2023) Omicron (B.1.1.529) variant and its subvariants and lineages may lead to another COVID-19 wave in the world? -An overview of current evidence and counteracting strategies. International Journal of Surgery Open 55:100625. https://doi.org/10.1016/j.ijso.2023.100625

22. WHO Director-General (2023) WHO Director-General's opening remarks at the media briefing – 5 May 2023. In: World Health Organization. https://www.who.int/director-general/speeches/detail/who-director-general-s-opening-remarks-at-the-media-briefing---5-may-2023. Accessed 3 Sep 2024

23. World Health Organization (2025) WHO Coronavirus (COVID-19) Dashboard. In: World Health Organization. https://covid19.who.int/?mapFilter=deaths. Accessed 30 Jan 2025

24. Santarpia JL, Rivera DN, Herrera VL, et al (2020) Aerosol and surface contamination of SARS-CoV-2 observed in quarantine and isolation care. Sci Rep 10:12732. https://doi.org/10.1038/s41598-020-69286-3

25. Meyerowitz EA, Richterman A, Gandhi RT, Sax PE (2021) Transmission of SARS-CoV-2: A review of viral, host, and environmental factors. Ann Intern Med 174:69–79. https://doi.org/10.7326/M20-5008

26. Kohanski MA, Lo LJ, Waring MS (2020) Review of indoor aerosol generation, transport, and control in the context of COVID-19. Int Forum Allergy Rhinol 10:1173–1179. https://doi.org/10.1002/alr.22661

27. Asadi S, Bouvier N, Wexler AS, Ristenpart WD (2020) The coronavirus pandemic and aerosols: Does COVID-19 transmit via expiratory particles? Aerosol Science and Technology 54:635–638. https://doi.org/10.1080/02786826.2020.1749229

28. Chen B, Jia P, Han J (2021) Role of indoor aerosols for COVID-19 viral transmission: a review. Environ Chem Lett 19:1953–1970. https://doi.org/10.1007/s10311-020-01174-8

29. Pickering B, Lung O, Maguire F, et al (2022) Divergent SARS-CoV-2 variant emerges in white-tailed deer with deer-to-human transmission. Nat Microbiol 7:2011–2024. https://doi.org/10.1038/s41564-022-01268-9

30. Garigliany M, Van Laere A-S, Clercx C, et al (2020) SARS-CoV-2 natural transmission from human to cat, Belgium, March 2020. Emerg Infect Dis 26:3069–3071. https://doi.org/10.3201/eid2612.202223

31. Oude Munnink BB, Sikkema RS, Nieuwenhuijse DF, et al (2021) Transmission of SARS-CoV-2 on mink farms between humans and mink and back to humans. Science (1979) 371:172–177. https://doi.org/10.1126/science.abe5901

32. Dusseldorp F, Bruins-van-Sonsbeek LGR, Buskermolen M, et al (2023) SARS-CoV-2 in lions, gorillas and zookeepers in the Rotterdam Zoo, the Netherlands, a One Health investigation, November 2021. Eurosurveillance 28:. https://doi.org/10.2807/1560-7917.ES.2023.28.28.2200741

33. Wu Y, Kang L, Guo Z, et al (2022) Incubation period of COVID-19 xaused by unique SARS-CoV-2 atrains. JAMA Netw Open 5:e2228008. https://doi.org/10.1001/jamanetworkopen.2022.28008

34. Alene M, Yismaw L, Assemie MA, et al (2021) Serial interval and incubation period of COVID-19: a systematic review and meta-analysis. BMC Infect Dis 21:. https://doi.org/10.1186/s12879-021-05950-x

35. Tanaka H, Ogata T, Shibata T, et al (2022) Shorter incubation period among COVID-19 cases with the BA.1 omicron variant. Int J Environ Res Public Health 19:6330. https://doi.org/10.3390/ijerph19106330

36. Nishiura H, Kobayashi T, Miyama T, et al (2020) Estimation of the asymptomatic ratio of novel coronavirus infections (COVID-19). International Journal of Infectious Diseases 94:154–155. https://doi.org/10.1016/j.ijid.2020.03.020

37. Yu W, Guo Y, Zhang S, et al (2022) Proportion of asymptomatic infection and nonsevere disease caused by SARS-CoV-2 Omicron variant: A systematic review and analysis. J Med Virol 94:5790–5801. https://doi.org/10.1002/jmv.28066

38. Menni C, Valdes AM, Freidin MB, et al (2020) Real-time tracking of self-reported symptoms to predict potential COVID-19. Nat Med 26:1037–1040. https://doi.org/10.1038/s41591-020-0916-2

39. Siordia JA (2020) Epidemiology and clinical features of COVID-19: A review of current literature. Journal of Clinical Virology 127:104357. https://doi.org/10.1016/j.jcv.2020.104357

40. Huang C, Wang Y, Li X, et al (2020) Clinical features of patients infected with 2019 novel coronavirus in Wuhan, China. The Lancet 395:497–506. https://doi.org/10.1016/S0140-6736(20)30183-5

41. Parasher A (2021) COVID-19: current understanding of its pathophysiology, clinical presentation and treatment. Postgrad Med J 97:312–320. https://doi.org/10.1136/postgradmedj-2020-138577

42. Ragab D, Salah Eldin H, Taeimah M, et al (2020) The COVID-19 cytokine storm; what we know so far. Front Immunol 11:. https://doi.org/10.3389/fimmu.2020.01446

43. Selickman J, Vrettou CS, Mentzelopoulos SD, Marini JJ (2022) COVID-19-related ARDS: Key mechanistic features and treatments. J Clin Med 11:4896. https://doi.org/10.3390/jcm11164896

44. Tsai P-H, Lai W-Y, Lin Y-Y, et al (2021) Clinical manifestation and disease progression in COVID-19 infection. Journal of the Chinese Medical Association 84:3–8. https://doi.org/10.1097/JCMA.0000000000000463

45. Tian S, Xiong Y, Liu H, et al (2020) Pathological study of the 2019 novel coronavirus disease (COVID-19) through postmortem core biopsies. Modern Pathology 33:1007–1014. https://doi.org/10.1038/s41379-020-0536-x

46. Tabatabai M, Juarez PD, Matthews-Juarez P, et al (2023) An analysis of COVID-19 mortality during the dominancy of Alpha, Delta, and Omicron in the USA. J Prim Care Community Health 14:215013192311701. https://doi.org/10.1177/21501319231170164

47. Ejaz H, Alsrhani A, Zafar A, et al (2020) COVID-19 and comorbidities: deleterious impact on infected patients. J Infect Public Health 13:1833–1839. https://doi.org/10.1016/j.jiph.2020.07.014

48. Chang D, Chang X, He Y, Tan KJK (2022) The determinants of COVID-19 morbidity and mortality across countries. Sci Rep 12:5888. https://doi.org/10.1038/s41598-022-09783-9

49. Davis HE, McCorkell L, Vogel JM, Topol EJ (2023) Long COVID: major findings, mechanisms and recommendations. Nat Rev Microbiol 21:133–146. https://doi.org/10.1038/s41579-022-00846-2

50. Xie Y, Xu E, Bowe B, Al-Aly Z (2022) Long-term cardiovascular outcomes of COVID-19. Nat Med 28:583–590. https://doi.org/10.1038/s41591-022-01689-3

51. Ballering A V, van Zon SKR, olde Hartman TC, Rosmalen JGM (2022) Persistence of somatic symptoms after COVID-19 in the Netherlands: an observational cohort study. The Lancet 400:452–461. https://doi.org/10.1016/S0140-6736(22)01214-4

52. Chen B, Julg B, Mohandas S, Bradfute SB (2023) Viral persistence, reactivation, and mechanisms of long COVID. Elife 12:. https://doi.org/10.7554/eLife.86015

53. Klein J, Wood J, Jaycox JR, et al (2023) Distinguishing features of long COVID identified through immune profiling. Nature 623:139–148. https://doi.org/10.1038/s41586-023-06651-y

54. Yin Y, Wunderink RG (2018) MERS, SARS and other coronaviruses as causes of pneumonia. Respirology 23:130–137

55. Perlman S, Masters PS (2021) Coronaviridae: the viruses and their replication. In: Howley PM, Knipe DM (eds) Fields virology: emerging viruses, 7th ed. Wolters Kluwer, Philadelphia, pp 410–448

56. Wang M-Y, Zhao R, Gao L-J, et al (2020) SARS-CoV-2: structure, biology, and structure-based therapeutics development. Front Cell Infect Microbiol 10:. https://doi.org/10.3389/fcimb.2020.587269

57. Huang Y, Yang C, Xu X, et al (2020) Structural and functional properties of SARS-CoV-2 spike protein: potential antivirus drug development for COVID-19. Acta Pharmacol Sin 41:1141–1149. https://doi.org/10.1038/s41401-020-0485-4

58. Lan J, Ge J, Yu J, et al (2020) Structure of the SARS-CoV-2 spike receptor-binding domain bound to the ACE2 receptor. Nature 581:215–220. https://doi.org/10.1038/s41586-020-2180-5

59. Wrapp D, Wang N, Corbett KS, et al (2020) Cryo-EM structure of the 2019-nCoV spike in the prefusion conformation. Science (1979) 367:1260–1263. https://doi.org/10.1126/science.abb2507

60. Benton DJ, Wrobel AG, Xu P, et al (2020) Receptor binding and priming of the spike protein of SARS-CoV-2 for membrane fusion. Nature 588:327–330. https://doi.org/10.1038/s41586-020-2772-0

61. Hoffmann M, Kleine-Weber H, Schroeder S, et al (2020) SARS-CoV-2 cell entry depends on ACE2 and TMPRSS2 and Is blocked by a clinically proven protease inhibitor. Cell 181:271-280.e8. https://doi.org/10.1016/j.cell.2020.02.052

62. Jackson CB, Farzan M, Chen B, Choe H (2022) Mechanisms of SARS-CoV-2 entry into cells. Nat Rev Mol Cell Biol 23:3–20. https://doi.org/10.1038/s41580-021-00418-x

63. Cai Y, Zhang J, Xiao T, et al (2020) Distinct conformational states of SARS-CoV-2 spike protein. Science (1979) 369:1586–1592. https://doi.org/10.1126/science.abd4251

64. V'kovski P, Kratzel A, Steiner S, et al (2021) Coronavirus biology and replication: implications for SARS-CoV-2. Nat Rev Microbiol 19:155–170. https://doi.org/10.1038/s41579-020-00468-6

65. Sola I, Almazán F, Zúñiga S, Enjuanes L (2015) Continuous and discontinuous RNA synthesis in coronaviruses. Annu Rev Virol 2:265–288. https://doi.org/10.1146/annurev-virology-100114-055218

66. de Haan CAM, Rottier PJM (2005) Molecular interactions in the assembly of coronaviruses. pp 165–230

67. Tian D, Sun Y, Xu H, Ye Q (2022) The emergence and epidemic characteristics of the highly mutated SARS-CoV-2 Omicron variant. J Med Virol 94:2376–2383. https://doi.org/10.1002/jmv.27643

68. Zhang L, Jackson CB, Mou H, et al (2020) SARS-CoV-2 spike-protein D614G mutation increases virion spike density and infectivity. Nat Commun 11:6013. https://doi.org/10.1038/s41467-020-19808-4

69. Korber B, Fischer WM, Gnanakaran S, et al (2020) Tracking changes in SARS-CoV-2 spike: evidence that D614G increases infectivity of the COVID-19 virus. Cell 182:812-827.e19. https://doi.org/10.1016/j.cell.2020.06.043

70. McCallum M, Czudnochowski N, Rosen LE, et al (2022) Structural basis of SARS-CoV-2 Omicron immune evasion and receptor engagement. Science (1979) 375:864–868. https://doi.org/10.1126/science.abn8652

71. Shah M, Ahmad B, Choi S, Woo HG (2020) Mutations in the SARS-CoV-2 spike RBD are responsible for stronger ACE2 binding and poor anti-SARS-CoV mAbs cross-neutralization. Comput Struct Biotechnol J 18:3402–3414. https://doi.org/10.1016/j.csbj.2020.11.002

72. Böger B, Fachi MM, Vilhena RO, et al (2021) Systematic review with meta-analysis of the accuracy of diagnostic tests for COVID-19. Am J Infect Control 49:21–29. https://doi.org/10.1016/j.ajic.2020.07.011

73. Shafie MH, Antony Dass M, Ahmad Shaberi HS, Zafarina Z (2023) Screening and confirmation tests for SARS-CoV-2: benefits and drawbacks. Beni Suef Univ J Basic Appl Sci 12:6. https://doi.org/10.1186/s43088-023-00342-3

74. Núñez I, Belaunzarán-Zamudio PF, Caro-Vega Y (2022) Result turnaround time of RT-PCR for SARS-CoV-2 is the main cause of COVID-19 diagnostic delay: a country-wide observational study of Mexico and Colombia. Revista De Investigacion Clinica 74:. https://doi.org/10.24875/RIC.21000542

75. Larremore DB, Wilder B, Lester E, et al (2021) Test sensitivity is secondary to frequency and turnaround time for COVID-19 screening. Sci Adv 7:. https://doi.org/10.1126/sciadv.abd5393

76. Huang WE, Lim B, Hsu C, et al (2020) RT-LAMP for rapid diagnosis of coronavirus SARS-CoV-2. Microb Biotechnol 13:950–961. https://doi.org/10.1111/1751-7915.13586

77. Amaral C, Antunes W, Moe E, et al (2021) A molecular test based on RT-LAMP for rapid, sensitive and inexpensive colorimetric detection of SARS-CoV-2 in clinical samples. Sci Rep 11:16430. https://doi.org/10.1038/s41598-021-95799-6

78. Tang W-F, Tran A-T, Wang L-Y, Horng J-T (2023) SARS-CoV-2 pandemics: An update of CRISPR in diagnosis and host–virus interaction studies. Biomed J 46:100587. https://doi.org/10.1016/j.bj.2023.02.007

79. Rahimi H, Salehiabar M, Barsbay M, et al (2021) CRISPR systems for COVID-19 diagnosis. ACS Sens 6:1430–1445. https://doi.org/10.1021/acssensors.0c02312

80. Fang L, Yang L, Han M, et al (2023) CRISPR-cas technology: A key approach for SARS-CoV-2 detection. Front Bioeng Biotechnol 11:. https://doi.org/10.3389/fbioe.2023.1158672

81. Budd J, Miller BS, Weckman NE, et al (2023) Lateral flow test engineering and lessons learned from COVID-19. Nature Reviews Bioengineering 1:13–31. https://doi.org/10.1038/s44222-022-00007-3

82. Frew E, Roberts D, Barry S, et al (2021) A SARS-CoV-2 antigen rapid diagnostic test for resource limited settings. Sci Rep 11:23009. https://doi.org/10.1038/s41598-021-02128-y

83. Bai Z, Cao Y, Liu W, Li J (2021) The SARS-CoV-2 Nucleocapsid protein and Its role in viral structure, biological functions, and a potential target for drug or vaccine mitigation. Viruses 13:1115. https://doi.org/10.3390/v13061115

84. Dinnes J, Sharma P, Berhane S, et al (2022) Rapid, point-of-care antigen tests for diagnosis of SARS-CoV-2 infection. Cochrane Database of Systematic Reviews 2022:. https://doi.org/10.1002/14651858.CD013705.pub3

85. Mercer TR, Salit M (2021) Testing at scale during the COVID-19 pandemic. Nat Rev Genet 22:415–426. https://doi.org/10.1038/s41576-021-00360-w

86. Arevalo-Rodriguez I, Buitrago-Garcia D, Simancas-Racines D, et al (2020) False-negative results of initial RT-PCR assays for COVID-19: A systematic review. PLoS One 15:e0242958. https://doi.org/10.1371/journal.pone.0242958

87. Schuit E, Veldhuijzen IK, Venekamp RP, et al (2021) Diagnostic accuracy of rapid antigen tests in asymptomatic and presymptomatic close contacts of individuals with confirmed SARS-CoV-2 infection: cross sectional study. BMJ n1676. https://doi.org/10.1136/bmj.n1676

88. Ong DSY, Fragkou PC, Schweitzer VA, et al (2021) How to interpret and use COVID-19 serology and immunology tests. Clinical Microbiology and Infection 27:981–986. https://doi.org/10.1016/j.cmi.2021.05.001

89. Li G, Hilgenfeld R, Whitley R, De Clercq E (2023) Therapeutic strategies for COVID-19: progress and lessons learned. Nat Rev Drug Discov 22:449–475

90. Taylor PC, Adams AC, Hufford MM, et al (2021) Neutralizing monoclonal antibodies for treatment of COVID-19. Nat Rev Immunol 21:382–393. https://doi.org/10.1038/s41577-021-00542-x

91. Chen Y, Zhao X, Zhou H, et al (2023) Broadly neutralizing antibodies to SARS-CoV-2 and other human coronaviruses. Nat Rev Immunol 23:189–199. https://doi.org/10.1038/s41577-022-00784-3

92. Xu J, Xu K, Jung S, et al (2021) Nanobodies from camelid mice and llamas neutralize SARS-CoV-2 variants. Nature 595:278–282. https://doi.org/10.1038/s41586-021-03676-z

93. Modhiran N, Lauer SM, Amarilla AA, et al (2023) A nanobody recognizes a unique conserved epitope and potently neutralizes SARS-CoV-2 omicron variants. iScience 26:107085. https://doi.org/10.1016/j.isci.2023.107085

94. Focosi D, McConnell S, Casadevall A, et al (2022) Monoclonal antibody therapies against SARS-CoV-2. Lancet Infect Dis 22:e311–e326. https://doi.org/10.1016/S1473-3099(22)00311-5

95. Owen C, Robinson S, Christofides A, Sehn LH (2022) A Canadian perspective: Monoclonal antibodies for pre- and post-exposure protection from COVID-19 in vulnerable patients with hematological malignancies. Current Oncology 29:3940–3949. https://doi.org/10.3390/curroncol29060315

96. Govender K, Chuturgoon A (2022) An overview of repurposed drugs for potential COVID-19 treatment. Antibiotics 11:1678. https://doi.org/10.3390/antibiotics11121678

97. Chakraborty C, Sharma AR, Bhattacharya M, et al (2021) The Drug repurposing for COVID-19 clinical trials provide cery effective therapeutic combinations: Lessons learned from major clinical studies. Front Pharmacol 12:. https://doi.org/10.3389/fphar.2021.704205

98. Wong CKH, Lau JJ, Au ICH, et al (2023) Optimal timing of nirmatrelvir/ritonavir treatment after COVID-19 symptom onset or diagnosis: target trial emulation. Nat Commun 14:8377. https://doi.org/10.1038/s41467-023-43706-0

99. Gonçalves A, Bertrand J, Ke R, et al (2020) Timing of antiviral treatment initiation is critical to reduce SARS-CoV-2 viral load. CPT Pharmacometrics Syst Pharmacol 9:509–514. https://doi.org/10.1002/psp4.12543

100. Investigators WC for the R-C (2023) Effect of angiotensin-converting enzyme inhibitor and angiotensin receptor blocker initiation on organ support–free days in patients hospitalized with COVID-19: A randomized clinical trial. JAMA 329:1183–1196. https://doi.org/10.1001/jama.2023.4480

101. Zhang H, Lv P, Jiang J, et al (2023) Advances in developing ACE2 derivatives against SARS-CoV-2. Lancet Microbe 4:e369–e378. https://doi.org/10.1016/S2666-5247(23)00011-3

102. Centers for Disease Control and Prevention (2024) COVID-19 treatments and medications. In: Centers for Disease Control and Prevention. https://www.cdc.gov/coronavirus/2019-ncov/your-health/treatments-for-severe-illness.html. Accessed 15 Jul 2024

103. Bartoszko JJ, Siemieniuk RA, Kum E, et al (2021) Prophylaxis against covid-19: living systematic review and network meta-analysis. BMJ n949. https://doi.org/10.1136/bmj.n949

104. World Health Organization (2023) Drugs to prevent COVID-19: Living guideline. Geneva

105. Public Health Agency of Canada (2021) Clinical management of patients with COVID-19: Second interim guidance. In: Public Health Agency of Canada. https://www.canada.ca/en/public-health/services/diseases/2019-novel-coronavirus-infection/clinical-management-covid-19.2020#a10. Accessed 15 Jul 2024

106. van de Veerdonk FL, Giamarellos-Bourboulis E, Pickkers P, et al (2022) A guide to immunotherapy for COVID-19. Nat Med 28:39–50. https://doi.org/10.1038/s41591-021-01643-9

107. Kalinke U, Barouch DH, Rizzi R, et al (2022) Clinical development and approval of COVID-19 vaccines. Expert Rev Vaccines 21:609–619. https://doi.org/10.1080/14760584.2022.2042257

108. Chaudhary N, Weissman D, Whitehead KA (2021) mRNA vaccines for infectious diseases: principles, delivery and clinical translation. Nat Rev Drug Discov 20:817–838. https://doi.org/10.1038/s41573-021-00283-5

109. Health Canada (2024) Drug and vaccine authorizations for COVID-19: List of authorized drugs, vaccines and expanded indications. In: Health Canada. https://www.canada.ca/en/transport-canada/news/2021/10/mandatory-covid-19-vaccination-requirements-for-federally-regulated-transportation-employees-and-travellers.html. Accessed 3 Sep 2024

110. Polack FP, Thomas SJ, Kitchin N, et al (2020) Safety and efficacy of the BNT162b2 mRNA Covid-19 vaccine. New England Journal of Medicine 383:2603–2615. https://doi.org/10.1056/NEJMoa2034577

111. Jackson LA, Anderson EJ, Rouphael NG, et al (2020) An mRNA vaccine against SARS-CoV-2 — Preliminary report. New England Journal of Medicine 383:1920–1931. https://doi.org/10.1056/NEJMoa2022483

112. Eygeris Y, Patel S, Jozic A, Sahay G (2020) Deconvoluting lipid nanoparticle structure for messenger RNA Delivery. Nano Lett 20:4543–4549. https://doi.org/10.1021/acs.nanolett.0c01386

113. Verbeke R, Hogan MJ, Loré K, Pardi N (2022) Innate immune mechanisms of mRNA vaccines. Immunity 55:1993–2005. https://doi.org/10.1016/j.immuni.2022.10.014

114. Lederer K, Castaño D, Gómez Atria D, et al (2020) SARS-CoV-2 mRNA vaccines foster potent antigen-specific germinal center responses associated with neutralizing antibody generation. Immunity 53:1281-1295.e5. https://doi.org/10.1016/j.immuni.2020.11.009

115. Mendonça SA, Lorincz R, Boucher P, Curiel DT (2021) Adenoviral vector vaccine platforms in the SARS-CoV-2 pandemic. NPJ Vaccines 6:97. https://doi.org/10.1038/s41541-021-00356-x

116. Mendonça SA, Lorincz R, Boucher P, Curiel DT (2021) Adenoviral vector vaccine platforms in the SARS-CoV-2 pandemic. NPJ Vaccines 6:97. https://doi.org/10.1038/s41541-021-00356-x

117. Dicks MDJ, Spencer AJ, Edwards NJ, et al (2012) A novel chimpanzee adenovirus vector with low human seroprevalence: Improved systems for vector derivation and comparative Immunogenicity. PLoS One 7:e40385. https://doi.org/10.1371/journal.pone.0040385

118. Ward BJ, Gobeil P, Séguin A, et al (2021) Phase 1 randomized trial of a plant-derived virus-like particle vaccine for COVID-19. Nat Med 27:1071–1078. https://doi.org/10.1038/s41591-021-01370-1

119. Hemmati F, Hemmati-Dinarvand M, Karimzade M, et al (2022) Plant-derived VLP: a worthy platform to produce vaccine against SARS-CoV-2. Biotechnol Lett 44:45–57. https://doi.org/10.1007/s10529-021-03211-0

120. Keech C, Albert G, Cho I, et al (2020) Phase 1–2 trial of a SARS-CoV-2 recombinant spike protein nanoparticle vaccine. New England Journal of Medicine 383:2320–2332. https://doi.org/10.1056/NEJMoa2026920

121. Gao Q, Bao L, Mao H, et al (2020) Development of an inactivated vaccine candidate for SARS-CoV-2. Science (1979) 369:77–81. https://doi.org/10.1126/science.abc1932

122. Zhang Y, Zeng G, Pan H, et al (2021) Safety, tolerability, and immunogenicity of an inactivated SARS-CoV-2 vaccine in healthy adults aged 18–59 years: a randomised, double-blind, placebo-controlled, phase 1/2 clinical trial. Lancet Infect Dis 21:181–192. https://doi.org/10.1016/S1473-3099(20)30843-4

123. Gupta D, Parthasarathy H, Sah V, et al (2021) Inactivation of SARS-CoV-2 by β-propiolactone causes aggregation of viral particles and loss of antigenic potential. Virus Res 305:198555. https://doi.org/10.1016/j.virusres.2021.198555

124. Tanriover MD, Doğanay HL, Akova M, et al (2021) Efficacy and safety of an inactivated whole-virion SARS-CoV-2 vaccine (CoronaVac): interim results of a double-blind, randomised, placebo-controlled, phase 3 trial in Turkey. The Lancet 398:213–222. https://doi.org/10.1016/S0140-6736(21)01429-X

125. Shao W, Chen X, Zheng C, et al (2022) Effectiveness of COVID-19 vaccines against SARS-CoV-2 variants of concern in real-world: a literature review and meta-analysis. Emerg Microbes Infect 11:2383–2392. https://doi.org/10.1080/22221751.2022.2122582

126. Chenchula S, Karunakaran P, Sharma S, Chavan M (2022) Current evidence on efficacy of COVID-19 booster dose vaccination against the Omicron variant: A systematic review. J Med Virol 94:2969–2976. https://doi.org/10.1002/jmv.27697

127. Canada Border Services Agency (2021) Timeline – CBSA Border Measures. In: Public Safety Canada. https://www.publicsafety.gc.ca/cnt/trnsprnc/brfng-mtrls/prlmntry-bndrs/20210907/05-en.aspx. Accessed 3 Sep 2024

128. Transport Canada (2020) Government of Canada and partners improve process to notify air travellers potentially exposed to COVID-19 on domestic flights. In: Government of Canada. https://www.canada.ca/en/transport-canada/news/2020/09/government-of-canada-and-partners-improve-process-to-notify-air-travellers-potentially-exposed-to-covid-19-on-domestic-flights.html. Accessed 3 Sep 2024

129. Health Canada (2021) Pan-Canadian COVID-19 Testing and Screening Guidance: Technical guidance and implementation plan. In: Health Canada. https://www.canada.ca/en/health-canada/services/drugs-health-products/covid19-industry/medical-devices/testing/pan-canadian-guidance.html. Accessed 3 Sep 2024

130. Baik Y, Cilloni L, Kendall E, et al (2022) Symptom-based vs asymptomatic testing for controlling SARS-CoV-2 transmission in low- and middle-income countries: A modelling analysis. Epidemics 41:100631. https://doi.org/10.1016/j.epidem.2022.100631

131. Barathidasan R, Sharmila FM, Raj RV, et al (2022) Pooled sample testing for COVID-19 diagnosis: Evaluation of bi-directional matrix pooling strategies. J Virol Methods 304:114524. https://doi.org/10.1016/j.jviromet.2022.114524

132. Hrudey SE, Bischel HN, Charrois J, et al (2022) Wastewater surveillance for SARS-CoV-2 RNA in Canada. FACETS 7:1493–1597. https://doi.org/10.1139/facets-2022-0148

133. Li X, Liu H, Gao L, et al (2023) Wastewater-based epidemiology predicts COVID-19-induced weekly new hospital admissions in over 150 USA counties. Nat Commun 14:4548. https://doi.org/10.1038/s41467-023-40305-x

134. Masri NZ, Card KG, Caws EA, et al (2022) Testing specificity and sensitivity of wastewater-based epidemiology for detecting SARS-CoV-2 in four communities on Vancouver Island, Canada. Environmental Advances 9:100310. https://doi.org/10.1016/j.envadv.2022.100310

135. Hewitt J, Trowsdale S, Armstrong BA, et al (2022) Sensitivity of wastewater-based epidemiology for detection of SARS-CoV-2 RNA in a low prevalence setting. Water Res 211:118032. https://doi.org/10.1016/j.watres.2021.118032

136. Amman F, Markt R, Endler L, et al (2022) Viral variant-resolved wastewater surveillance of SARS-CoV-2 at national scale. Nat Biotechnol 40:1814–1822. https://doi.org/10.1038/s41587-022-01387-y

137. Chadwick FJ, Clark J, Chowdhury S, et al (2022) Combining rapid antigen testing and syndromic surveillance improves community-based COVID-19 detection in a low-income country. Nat Commun 13:2877. https://doi.org/10.1038/s41467-022-30640-w

138. Smith E, Pigeau C, Ahmadian-Yazdi J, et al (2023) Utility of the Peterborough Public Health COVID-19 rapid antigen test self-report tool: Implications for COVID-19 surveillance. Can Commun Dis Rep 49:44–49

139. Public Health Agency of Canada (2023) Testing for COVID-19: Roles and responsibilities across Canada. In: Testing for COVID-19: Roles and responsibilities across Canada. https://www.canada.ca/en/public-health/services/diseases/2019-novel-coronavirus-infection/symptoms/testing/roles-responsibilities.html. Accessed 3 Sep 2024

140. Lewis HC, Ware H, Whelan M, et al (2022) SARS-CoV-2 infection in Africa: a systematic review and meta-analysis of standardised seroprevalence studies, from January 2020 to December 2021. BMJ Glob Health 7:e008793. https://doi.org/10.1136/bmjgh-2022-008793

141. Charlton CL, Nguyen LT, Bailey A, et al (2021) Pre-Vaccine Positivity of SARS-CoV-2 antibodies in Alberta, Canada during the first two waves of the COVID-19 pandemic. Microbiol Spectr 9:. https://doi.org/10.1128/Spectrum.00291-21

142. Congrave-Wilson Z, Cheng WA, Lee Y, et al (2022) Twelve-month longitudinal serology in SARS-CoV-2 naïve and experienced vaccine recipients and unvaccinated COVID-19-infected individuals. Vaccines (Basel) 10:813. https://doi.org/10.3390/vaccines10050813

143. Olmstead AD, Nikiforuk AM, Schwartz S, et al (2022) Characterizing longitudinal antibody responses in recovered individuals following COVID-19 infection and single-dose vaccination: a prospective cohort study. Viruses 14:2416. https://doi.org/10.3390/v14112416

144. Amirthalingam G, Bernal JL, Andrews NJ, et al (2021) Serological responses and vaccine effectiveness for extended COVID-19 vaccine schedules in England. Nat Commun 12:7217. https://doi.org/10.1038/s41467-021-27410-5

145. Bergeri I, Whelan MG, Ware H, et al (2022) Global SARS-CoV-2 seroprevalence from January 2020 to April 2022: A systematic review and meta-analysis of standardized population-based studies. PLoS Med 19:e1004107. https://doi.org/10.1371/journal.pmed.1004107

146. Hertz T, Levy S, Ostrovsky D, et al (2023) Correlates of protection for booster doses of the SARS-CoV-2 vaccine BNT162b2. Nat Commun 14:4575. https://doi.org/10.1038/s41467-023-39816-4

147. Stojanovic MN, Landry DW (2002) Aptamer-based colorimetric probe for cocaine. J Am Chem Soc 124:9678–9679. https://doi.org/10.1021/ja0259483

148. Mao K, Zhang H, Pan Y, et al (2020) Nanomaterial-based aptamer sensors for analysis of illicit drugs and evaluation of drugs consumption for wastewater-based epidemiology. TrAC - Trends in Analytical Chemistry 130

149. Zhang G, Li T, Zhang J, Chen A (2018) A simple FRET-based turn-on fluorescent aptasensor for 17B-estradiol determination in environmental water, urine and milk samples. Sens Actuators B Chem 273:1648–1653. https://doi.org/10.1016/j.snb.2018.07.066

150. Wang B, Zhao C, Wang Z, et al (2022) Wearable aptamer-field-effect transistor sensing system for noninvasive cortisol monitoring. Sci Adv 8:. https://doi.org/10.1126/sciadv.abk0967

151. Guo W, Zhang C, Ma T, et al (2021) Advances in aptamer screening and aptasensors' detection of heavy metal ions. J Nanobiotechnology 19

152. Yamamoto R, Kumar PKR (2000) Molecular beacon aptamer fluoresces in the presence of Tat protein of HIV-1. Genes to Cells 5:. https://doi.org/10.1046/j.1365-2443.2000.00331.x

153. Tesmer VM, Lennarz S, Mayer G, Tesmer JJG (2012) Molecular Mechanism for Inhibition of G Protein-Coupled Receptor Kinase 2 by a Selective RNA Aptamer. Structure 20:1300–1309. https://doi.org/10.1016/j.str.2012.05.002

154. Zou X, Wu J, Gu J, et al (2019) Application of aptamers in virus detection and antiviral therapy. Front Microbiol 10:. https://doi.org/10.3389/fmicb.2019.01462

155. Zeng Z, Zhang P, Zhao N, et al (2010) Using oligonucleotide aptamer probes for immunostaining of formalin-fixed and paraffin-embedded tissues. Modern Pathology 23:1553–1558. https://doi.org/10.1038/modpathol.2010.151

156. Meng HM, Fu T, Zhang XB, Tan W (2015) Cell-SELEX-based aptamer-conjugated nanomaterials for cancer diagnosis and therapy. Natl Sci Rev 2:71–84

157. Bunka DHJ, Stockley PG (2006) Aptamers come of age – at last. Nat Rev Microbiol 4:588–596. https://doi.org/10.1038/nrmicro1458

158. Gilbert W (1986) Origin of life: The RNA world. Nature 319:618–618. https://doi.org/10.1038/319618a0

159. Vorobyeva MA, Davydova AS, Vorobjev PE, et al (2018) Key aspects of nucleic acid library design for in vitro selection. Int J Mol Sci 19

160. Amero P, Lokesh GLR, Chaudhari RR, et al (2021) Conversion of RNA aptamer into modified DNA aptamers provides for prolonged stability and enhanced antitumor activity. J Am Chem Soc 143:7655–7670. https://doi.org/10.1021/jacs.9b10460

161. Ni S, Yao H, Wang L, et al (2017) Chemical modifications of nucleic acid aptamers for therapeutic purposes. Int J Mol Sci 18

162. Wang T, Chen C, Larcher LM, et al (2019) Three decades of nucleic acid aptamer technologies: Lessons learned, progress and opportunities on aptamer development. Biotechnol Adv 37:28–50

163. Wolter O, Mayer G (2017) Aptamers as Valuable Molecular Tools in Neurosciences. The Journal of Neuroscience 37:2517–2523. https://doi.org/10.1523/JNEUROSCI.1969-16.2017

164. O. Tucker W, T. Shum K, A. Tanner J (2012) G-quadruplex DNA aptamers and their ligands: structure, function and application. Curr Pharm Des 18:2014–2026. https://doi.org/10.2174/138161212799958477

165. Zuker M, Sankoff D (1984) RNA secondary structures and their prediction. Bull Math Biol 46:591–621. https://doi.org/10.1007/BF02459506

166. Ruigrok VJB, Levisson M, Hekelaar J, et al (2012) Characterization of aptamer-protein complexes by x-ray crystallography and alternative approaches. Int J Mol Sci 13:10537–10552

167. Long SB, Long MB, White RR, Sullenger BA (2008) Crystal structure of an RNA aptamer bound to thrombin. RNA 14:2504–2512. https://doi.org/10.1261/rna.1239308

168. Someya T, Baba S, Fujimoto M, et al (2012) Crystal structure of Hfq from Bacillus subtilis in complex with SELEX-derived RNA aptamer: insight into RNA-binding properties of bacterial Hfq. Nucleic Acids Res 40:1856–1867. https://doi.org/10.1093/nar/gkr892

169. Gong S, Wang Y, Wang Z, Zhang W (2017) Computational methods for modeling aptamers and designing riboswitches. Int J Mol Sci 18:2442. https://doi.org/10.3390/ijms18112442

170. Emami N, Pakchin PS, Ferdousi R (2020) Computational predictive approaches for interaction and structure of aptamers. J Theor Biol 497

171. Navien TN, Thevendran R, Hamdani HY, et al (2021) In silico molecular docking in DNA aptamer development. Biochimie 180:54–67

172. Laing C, Schlick T (2011) Computational approaches to RNA structure prediction, analysis, and design. Curr Opin Struct Biol 21:306–318. https://doi.org/10.1016/j.sbi.2011.03.015

173. Tuerk C, Gold L (1990) Systematic Evolution of Ligands by Exponential Enrichment: RNA ligands to bacteriophage T4 DNA polymerase. Science (1979) 249:505–510. https://doi.org/10.1126/science.2200121

174. Hall B, Micheletti JM, Satya P, et al (2009) Design, synthesis, and amplification of DNA pools for In vitro selection. Curr Protoc Mol Biol 88:. https://doi.org/10.1002/0471142727.mb2402s88

175. Ohuchi S (2012) Cell-SELEX technology. Biores Open Access 1:265–272. https://doi.org/10.1089/biores.2012.0253

176. Kohlberger M, Gadermaier G (2022) SELEX: Critical factors and optimization strategies for successful aptamer selection. Biotechnol Appl Biochem 69:1771–1792. https://doi.org/10.1002/bab.2244

177. Goto S, Tsukakoshi K, Ikebukuro K (2017) Development of aptamers against unpurified proteins. Biotechnol Bioeng 114:2706–2716. https://doi.org/10.1002/bit.26389

178. Mosing RK, Bowser MT (2009) Isolating aptamers using Capillary Electrophoresis–SELEX (CE–SELEX). pp 33–43

179. Kacherovsky N, Yang LF, Dang H V., et al (2021) Discovery and characterization of spike N-terminal domain-binding aptamers for rapid SARS-CoV-2 detection. Angewandte Chemie International Edition 60:21211–21215. https://doi.org/10.1002/anie.202107730

180. Kolm C, Cervenka I, Aschl UJ, et al (2020) DNA aptamers against bacterial cells can be efficiently selected by a SELEX process using state-of-the art qPCR and ultra-deep sequencing. Sci Rep 10:20917. https://doi.org/10.1038/s41598-020-77221-9

181. Kushwaha A, Takamura Y, Nishigaki K, Biyani M (2019) Competitive non-SELEX for the selective and rapid enrichment of DNA aptamers and its use in electrochemical aptasensor. Sci Rep 9:6642. https://doi.org/10.1038/s41598-019-43187-6

182. Liu R, Zhang F, Shi M, et al (2022) In vitro selection and optimization of high-affinity aptamer for milk allergen α-lactalbumin and its application in dual-mode detection. Front Nutr 9:. https://doi.org/10.3389/fnut.2022.1005230

183. Komarova N, Kuznetsov A (2019) Inside the black box: what makes SELEX better? Molecules 24:3598. https://doi.org/10.3390/molecules24193598

184. Bittker JA, Le B V., Liu DR (2002) Nucleic acid evolution and minimization by nonhomologous random recombination. Nat Biotechnol 20:1024–1029. https://doi.org/10.1038/nbt736

185. Pressman A, Moretti JE, Campbell GW, et al (2017) Analysis of in vitro evolution reveals the underlying distribution of catalytic activity among random sequences. Nucleic Acids Res 45:8167–8179. https://doi.org/10.1093/nar/gkx540

186. Tolle F, Wilke J, Wengel J, Mayer G (2014) By-product formation in repetitive PCR amplification of DNA libraries during SELEX. PLoS One 9:e114693. https://doi.org/10.1371/journal.pone.0114693

187. Buglak AA, Samokhvalov A V., Zherdev A V., Dzantiev BB (2020) Methods and applications of in silico aptamer design and modeling. Int J Mol Sci 21:8420. https://doi.org/10.3390/ijms21228420

188. Hamada M (2018) In silico approaches to RNA aptamer design. Biochimie 145:8–14. https://doi.org/10.1016/j.biochi.2017.10.005

189. Ahirwar R, Nahar S, Aggarwal S, et al (2016) In silico selection of an aptamer to estrogen receptor alpha using computational docking employing estrogen response elements as aptamer-alike molecules. Sci Rep 6:21285. https://doi.org/10.1038/srep21285

190. Vakser IA (2020) Challenges in protein docking. Curr Opin Struct Biol 64:160–165. https://doi.org/10.1016/j.sbi.2020.07.001

191. Schütze T, Arndt PF, Menger M, et al (2009) A calibrated diversity assay for nucleic acid libraries using DiStRO-a Diversity Standard of Random Oligonucleotides. Nucleic Acids Res 38:. https://doi.org/10.1093/nar/gkp1108

192. Blind M, Blank M (2015) Aptamer selection technology and recent advances. Mol Ther Nucleic Acids 4:e223. https://doi.org/10.1038/mtna.2014.74

193. Ozer A, Pagano JM, Lis JT (2014) New technologies provide quantum changes in the scale, speed, and success of SELEX methods and aptamer characterization. Mol Ther Nucleic Acids 3:e183. https://doi.org/10.1038/mtna.2014.34

194. Civit L, Taghdisi SM, Jonczyk A, et al (2018) Systematic evaluation of cell-SELEX enriched aptamers binding to breast cancer cells. Biochimie 145:53–62. https://doi.org/10.1016/j.biochi.2017.10.007

195. Schütze T, Wilhelm B, Greiner N, et al (2011) Probing the SELEX process with next-generation sequencing. PLoS One 6:. https://doi.org/10.1371/journal.pone.0029604

196. Kramer ST, Gruenke PR, Alam KK, et al (2022) FASTAptameR 2.0: A web tool for combinatorial sequence selections. Mol Ther Nucleic Acids 29:862–870. https://doi.org/10.1016/j.omtn.2022.08.030

197. Komarova N, Barkova D, Kuznetsov A (2020) Implementation of high-throughput sequencing (Hts) in aptamer selection technology. Int J Mol Sci 21:1–22. https://doi.org/10.3390/ijms21228774

198. Wochner A, Glökler J (2007) Nonradioactive fluorescence microtiter plate assay monitoring aptamer selections. Biotechniques 42:578–582. https://doi.org/10.2144/000112472

199. Toh SY, Citartan M, Gopinath SCB, Tang T-H (2015) Aptamers as a replacement for antibodies in enzyme-linked immunosorbent assay. Biosens Bioelectron 64:392–403. https://doi.org/10.1016/j.bios.2014.09.026

200. Seo H Bin, Gu MB (2017) Aptamer-based sandwich-type biosensors. J Biol Eng 11:11. https://doi.org/10.1186/s13036-017-0054-7

201. Zhang L, Fang X, Liu X, et al (2020) Discovery of sandwich type COVID-19 nucleocapsid protein DNA aptamers. Chemical Communications 56:10235–10238. https://doi.org/10.1039/d0cc03993d

202. Vargas-Montes M, Cardona N, Moncada DM, et al (2019) Enzyme-Linked Aptamer Assay (ELAA) for detection of Toxoplasma ROP18 protein in human serum. Front Cell Infect Microbiol 9:. https://doi.org/10.3389/fcimb.2019.00386

203. Ruff P, Pai RB, Storici F (2012) Real-Time PCR-coupled CE-SELEX for DNA aptamer selection. ISRN Mol Biol 2012:1–9. https://doi.org/10.5402/2012/939083

204. An Valero J, Civit L, Dupont DM, et al A serum-stable RNA aptamer specific for SARS-CoV-2 neutralizes viral entry. https://doi.org/10.1073/pnas.2112942118/-/DCSupplemental

205. Stanborough T, Given FM, Koch B, et al (2021) Optical detection of CoV-SARS-2 viral proteins to sub-picomolar concentrations. ACS Omega 6:6404–6413. https://doi.org/10.1021/acsomega.1c00008

206. Mukherjee M, Appaiah P, Sistla S, et al (2022) Bio-Layer Interferometry-Based SELEX and Label-Free Detection of Patulin Using Generated Aptamer. J Agric Food Chem 70:6239–6246. https://doi.org/10.1021/acs.jafc.2c01591

207. Jeddi I, Saiz L (2017) Three-dimensional modeling of single stranded DNA hairpins for aptamer-based biosensors. Sci Rep 7:. https://doi.org/10.1038/s41598-017-01348-5

208. Nosrati M, Roushani M (2023) Three-dimensional modeling of streptomycin binding single-stranded DNA for aptamer-based biosensors, a molecular dynamics simulation approach. J Biomol Struct Dyn 41:3430–3439. https://doi.org/10.1080/07391102.2022.2050945

209. Navien TN, Thevendran R, Hamdani HY, et al (2021) In silico molecular docking in DNA aptamer development. Biochimie 180:54–67

210. Zuker M (2003) Mfold web server for nucleic acid folding and hybridization prediction. Nucleic Acids Res 31:3406–3415. https://doi.org/10.1093/nar/gkg595

211. Kulabhusan PK, Hussain B, Yüce M (2020) Current perspectives on aptamers as diagnostic tools and therapeutic agents. Pharmaceutics 12:1–23

212. Kaur H, Bruno JG, Kumar A, Sharma TK (2018) Aptamers in the therapeutics and diagnostics pipelines. Theranostics 8:4016–4032. https://doi.org/10.7150/thno.25958

213. Dhiman A, Kalra P, Bansal V, et al (2017) Aptamer-based point-of-care diagnostic platforms. Sens Actuators B Chem 246:535–553

214. Ni S, Zhuo Z, Pan Y, et al (2021) Recent Progress in Aptamer Discoveries and Modifications for Therapeutic Applications. ACS Appl Mater Interfaces 13:9500–9519. https://doi.org/10.1021/acsami.0c05750

215. Odeh F, Nsairat H, Alshaer W, et al (2019) Aptamers chemistry: Chemical modifications and conjugation strategies. Molecules 25:3. https://doi.org/10.3390/molecules25010003

216. Volk D, Lokesh G (2017) Development of phosphorothioate DNA and DNA thioaptamers. Biomedicines 5:41. https://doi.org/10.3390/biomedicines5030041

217. Zhang Y, Zhang H, Chan DWH, et al (2022) Strategies for developing long-lasting therapeutic nucleic acid aptamer targeting circulating protein: The present and the future. Front Cell Dev Biol 10:. https://doi.org/10.3389/fcell.2022.1048148

218. Song Y, Song J, Wei X, et al (2020) Discovery of aptamers targeting the receptor-binding domain of the SARS-CoV-2 spike glycoprotein. Anal Chem 92:9895–9900. https://doi.org/10.1021/acs.analchem.0c01394

219. Jiang Y, Pan X, Chang J, et al (2018) Supramolecularly engineered circular bivalent aptamer for enhanced functional protein delivery. J Am Chem Soc 140:6780–6784. https://doi.org/10.1021/jacs.8b03442

220. Paige JS, Wu KY, Jaffrey SR (2011) RNA mimics of green fluorescent protein. Science (1979) 333:642–646. https://doi.org/10.1126/science.1207339

221. Autour A, C. Y. Jeng S, D. Cawte A, et al (2018) Fluorogenic RNA Mango aptamers for imaging small non-coding RNAs in mammalian cells. Nat Commun 9:656. https://doi.org/10.1038/s41467-018-02993-8

222. Kelly L, Maier KE, Yan A, Levy M (2021) A comparative analysis of cell surface targeting aptamers. Nat Commun 12:6275. https://doi.org/10.1038/s41467-021-26463-w

223. Shangguan D, Li Y, Tang Z, et al (2006) Aptamers evolved from live cells as effective molecular probes for cancer study. Proceedings of the National Academy of Sciences 103:11838–11843. https://doi.org/10.1073/pnas.0602615103

224. Smith JE, Griffin DK, Leny JK, et al (2014) Colorimetric detection with aptamer-gold nanoparticle conjugates coupled to an android-based color analysis application for use in the field. Talanta 121:247–255. https://doi.org/10.1016/j.talanta.2013.12.062

225. Zhang F, Liu J (2021) Label-Free colorimetric biosensors based on aptamers and gold banoparticles: A critical review. Analysis & Sensing 1:30–43. https://doi.org/10.1002/anse.202000023

226. Chang C-C (2021) Recent advancements in aptamer-based surface plasmon resonance biosensing strategies. Biosensors (Basel) 11:233. https://doi.org/10.3390/bios11070233

227. Aslan Y, Atabay M, Chowdhury HK, et al (2023) Aptamer-based point-of-care devices: Emerging technologies and integration of computational methods. Biosensors (Basel) 13:569. https://doi.org/10.3390/bios13050569

228. Kawano R, Osaki T, Sasaki H, et al (2011) Rapid detection of a cocaine-binding aptamer using biological nanopores on a chip. J Am Chem Soc 133:8474–8477. https://doi.org/10.1021/ja2026085

229. Canoura J, Alkhamis O, Venzke M, et al (2024) Developing aptamer-based colorimetric opioid tests. JACS Au 4:1059–1072. https://doi.org/10.1021/jacsau.3c00801

230. Dolai S, Tabib-Azar M (2020) Whole virus detection using aptamers and paper-based sensor potentiometry. Med Devices Sens 3:. https://doi.org/10.1002/mds3.10112

231. Yang LF, Kacherovsky N, Panpradist N, et al (2022) Aptamer sandwich lateral flow assay (AptaFlow) for antibody-Free SARS-CoV-2 detection. Anal Chem 94:7278–7285. https://doi.org/10.1021/acs.analchem.2c00554

232. Li H-Y, Jia W-N, Li X-Y, et al (2020) Advances in detection of infectious agents by aptamer-based technologies. Emerg Microbes Infect 9:1671–1681. https://doi.org/10.1080/22221751.2020.1792352

233. Ruiz Ciancio D, Vargas MR, Thiel WH, et al (2018) Aptamers as diagnostic tools in cancer. Pharmaceuticals 11:86. https://doi.org/10.3390/ph11030086

234. Kraemer S, Vaught JD, Bock C, et al (2011) From SOMAmer-vased viomarker discovery to diagnostic and clinical applications: A SOMAmer-based, streamlined multiplex proteomic assay. PLoS One 6:e26332. https://doi.org/10.1371/journal.pone.0026332

235. Rohloff JC, Gelinas AD, Jarvis TC, et al (2014) Nucleic acid ligands with protein-like side chains: Modified aptamers and their use as diagnostic and therapeutic agents. Mol Ther Nucleic Acids 3:e201

236. Candia J, Daya GN, Tanaka T, et al (2022) Assessment of variability in the plasma 7k SomaScan proteomics assay. Sci Rep 12:17147. https://doi.org/10.1038/s41598-022-22116-0

237. Chen M, Yu Y, Jiang F, et al (2016) Development of cell-SELEX technology and Its application in cancer diagnosis and therapy. Int J Mol Sci 17:2079. https://doi.org/10.3390/ijms17122079

238. Shigdar S, Agnello L, Fedele M, et al (2021) Profiling cancer cells by cell-SELEX: Use of aptamers for discovery of actionable biomarkers and therapeutic applications thereof. Pharmaceutics 14:28. https://doi.org/10.3390/pharmaceutics14010028

239. Go G, Lee C-S, Yoon YM, et al (2021) PrPC aptamer conjugated–gold nanoparticles for targeted delivery of doxorubicin to colorectal cancer cells. Int J Mol Sci 22:1976. https://doi.org/10.3390/ijms22041976

240. Kadkhoda J, Aghanejad A, Safari B, et al (2022) Aptamer-conjugated gold nanoparticles for targeted paclitaxel delivery and photothermal therapy in breast cancer. J Drug Deliv Sci Technol 67:102954. https://doi.org/10.1016/j.jddst.2021.102954

241. Kim D-M, Kim M, Park H-B, et al (2019) Anti-MUC1/CD44 dual-aptamer-conjugated liposomes for cotargeting breast cancer cells and cancer stem cells. ACS Appl Bio Mater 2:4622–4633. https://doi.org/10.1021/acsabm.9b00705

242. Hashemitabar S, Yazdian-Robati R, Hashemi M, et al (2019) ABCG2 aptamer selectively delivers doxorubicin to drug-resistant breast cancer cells. J Biosci 44:39. https://doi.org/10.1007/s12038-019-9854-x

243. Porciani D, Cardwell LN, Tawiah KD, et al (2018) Modular cell-internalizing aptamer nanostructure enables targeted delivery of large functional RNAs in cancer cell lines. Nat Commun 9:2283. https://doi.org/10.1038/s41467-018-04691-x

244. Quirico L, Orso F, Esposito CL, et al (2020) Axl-148b chimeric aptamers inhibit breast cancer and melanoma progression. Int J Biol Sci 16:1238–1251. https://doi.org/10.7150/ijbs.39768

245. Ng EWM, Shima DT, Calias P, et al (2006) Pegaptanib, a targeted anti-VEGF aptamer for ocular vascular disease. Nat Rev Drug Discov 5:123–132. https://doi.org/10.1038/nrd1955

246. Kovacevic KD, Gilbert JC, Jilma B (2018) Pharmacokinetics, pharmacodynamics and safety of aptamers. Adv Drug Deliv Rev 134:36–50. https://doi.org/10.1016/j.addr.2018.10.008

247. Keefe AD, Pai S, Ellington A (2010) Aptamers as therapeutics. Nat Rev Drug Discov 9:537–550. https://doi.org/10.1038/nrd3141

248. Moreno A, Pitoc GA, Ganson NJ, et al (2019) Anti-PEG antibodies inhibit the anticoagulant activity of PEGylated aptamers. Cell Chem Biol 26:634-644.e3. https://doi.org/10.1016/j.chembiol.2019.02.001

249. Case JB, Bailey AL, Kim AS, et al (2020) Growth, detection, quantification, and inactivation of SARS-CoV-2. Virology 548:39–48. https://doi.org/10.1016/j.virol.2020.05.015

250. Kumar S, Sarma P, Kaur H, et al (2021) Clinically relevant cell culture models and their significance in isolation, pathogenesis, vaccine development, repurposing and screening of new drugs for SARS-CoV-2: a systematic review. Tissue Cell 70:101497. https://doi.org/10.1016/j.tice.2021.101497

251. Mulay A, Konda B, Garcia G, et al (2021) SARS-CoV-2 infection of primary human lung epithelium for COVID-19 modeling and drug discovery. Cell Rep 35:109055. https://doi.org/10.1016/j.celrep.2021.109055

252. Youk J, Kim T, Evans K V., et al (2020) Three-dimensional human alveolar stem cell culture models reveal infection response to SARS-CoV-2. Cell Stem Cell 27:905-919.e10. https://doi.org/10.1016/j.stem.2020.10.004

253. Huang J, Hume AJ, Abo KM, et al (2020) SARS-CoV-2 infection of pluripotent stem cell-derived human lung alveolar type 2 cells elicits a rapid epithelial-intrinsic inflammatory response. Cell Stem Cell 27:962-973.e7. https://doi.org/10.1016/j.stem.2020.09.013

254. Wang Y, Zhou Z, Wu X, et al (2023) Pseudotyped Virus. In: Wang Y (ed) Advances in Experimental Medicine and Biology. Springer Nature Singapore Pte Ltd, Singapore, pp 1–27

255. Chen M, Zhang X-E (2021) Construction and applications of SARS-CoV-2 pseudoviruses: a mini review. Int J Biol Sci 17:1574–1580. https://doi.org/10.7150/ijbs.59184

256. Nie J, Li Q, Wu J, et al (2020) Establishment and validation of a pseudovirus neutralization assay for SARS-CoV-2. Emerg Microbes Infect 9:680–686. https://doi.org/10.1080/22221751.2020.1743767

257. Beitari S, Agbayani G, Hewitt M, et al (2023) Effectiveness of VSV vectored SARS-CoV-2 spike when administered through intranasal, intramuscular or a combination of both. Sci Rep 13:21390. https://doi.org/10.1038/s41598-023-48397-7

258. Dieterle ME, Haslwanter D, Bortz RH, et al (2020) A replication-competent vesicular stomatitis virus for studies of SARS-CoV-2 spike-mediated cell entry and Its inhibition. Cell Host Microbe 28:486-496.e6. https://doi.org/10.1016/j.chom.2020.06.020

259. Neerukonda SN, Vassell R, Herrup R, et al (2021) Establishment of a well-characterized SARS-CoV-2 lentiviral pseudovirus neutralization assay using 293T cells with stable expression of ACE2 and TMPRSS2. PLoS One 16:e0248348. https://doi.org/10.1371/journal.pone.0248348

260. Crawford KHD, Eguia R, Dingens AS, et al (2020) Protocol and reagents for pseudotyping lentiviral particles with SARS-CoV-2 spike protein for neutralization assays. Viruses 12:513. https://doi.org/10.3390/v12050513

261. Merluza J, Ung J, Makowski K, et al (2023) Validation and establishment of the SARS-CoV-2 lentivirus surrogate neutralization assay as a prescreening tool for the plaque reduction neutralization test. Microbiol Spectr 11:. https://doi.org/10.1128/spectrum.03789-22

262. Zheng Y, Larragoite ET, Williams ESCP, et al (2021) Neutralization assay with SARS-CoV-1 and SARS-CoV-2 spike pseudotyped murine leukemia virions. Virol J 18:1. https://doi.org/10.1186/s12985-020-01472-1

263. Moser MJ, Hill-Batorski L, Bowen RA, et al (2023) Intranasal single-replication influenza vector induces cross-reactive serum and mucosal antibodies against SARS-CoV-2 variants. Vaccines (Basel) 11:1063. https://doi.org/10.3390/vaccines11061063

264. Hörner C, Schürmann C, Auste A, et al (2020) A highly immunogenic and effective measles virus-based Th1-biased COVID-19 vaccine. Proceedings of the National Academy of Sciences 117:32657–32666. https://doi.org/10.1073/pnas.2014468117

265. Mercado NB, Zahn R, Wegmann F, et al (2020) Single-shot Ad26 vaccine protects against SARS-CoV-2 in rhesus macaques. Nature 586:583–588. https://doi.org/10.1038/s41586-020-2607-z

266. van Doremalen N, Lambe T, Spencer A, et al (2020) ChAdOx1 nCoV-19 vaccine prevents SARS-CoV-2 pneumonia in rhesus macaques. Nature 586:578–582. https://doi.org/10.1038/s41586-020-2608-y

267. Zhu F-C, Li Y-H, Guan X-H, et al (2020) Safety, tolerability, and immunogenicity of a recombinant adenovirus type-5 vectored COVID-19 vaccine: a dose-escalation, open-label, non-randomised, first-in-human trial. The Lancet 395:1845–1854. https://doi.org/10.1016/S0140-6736(20)31208-3

268. Xiang Q, Li L, Wu J, et al (2022) Application of pseudovirus system in the development of vaccine, antiviral-drugs, and neutralizing antibodies. Microbiol Res 258:126993. https://doi.org/10.1016/j.micres.2022.126993

269. Cantoni D, Mayora-Neto M, Temperton N (2021) The role of pseudotype neutralization assays in understanding SARS CoV-2. Oxf Open Immunol 2:. https://doi.org/10.1093/oxfimm/iqab005

270. Liu X, Wang Y, Wu J, et al (2021) Neutralizing aptamers block S/RBD-ACE2 interactions and prevent host cell infection. Angewandte Chemie International Edition 60:10273–10278. https://doi.org/10.1002/anie.202100345

271. Tabarzad M, Kazemi B, Vahidi H, et al (2014) Challenges to design and develop of DNA aptamers for protein targets. I. Optimization of asymmetric PCR for generation of a single stranded DNA library . Iran J Pharm Res 13(Suppl):133–141

272. Martínez-Roque MA, Franco-Urquijo PA, García-Velásquez VM, et al (2022) DNA aptamer selection for SARS-CoV-2 spike glycoprotein detection. Anal Biochem 645:114633. https://doi.org/10.1016/j.ab.2022.114633

273. Fu Y, Wu P-H, Beane T, et al (2018) Elimination of PCR duplicates in RNA-seq and small RNA-seq using unique molecular identifiers. BMC Genomics 19:531. https://doi.org/10.1186/s12864-018-4933-1

274. Callahan BJ, McMurdie PJ, Rosen MJ, et al (2016) DADA2: High-resolution sample inference from Illumina amplicon data. Nat Methods 13:581–583. https://doi.org/10.1038/nmeth.3869

275. Lan J, Ge J, Yu J, et al (2020) Structure of the SARS-CoV-2 spike receptor-binding domain bound to the ACE2 receptor. Nature 581:215–220. https://doi.org/10.1038/s41586-020-2180-5

276. Zhang Y, Xiong Y, Xiao Y (2022) 3dDNA: A computational method of building DNA 3D structures. Molecules 27:5936. https://doi.org/10.3390/molecules27185936

277. Wang J, Zhao Y, Zhu C, Xiao Y (2015) 3dRNAscore: a distance and torsion angle dependent evaluation function of 3D RNA structures. Nucleic Acids Res 43:e63–e63. https://doi.org/10.1093/nar/gkv141

278. Pierce BG, Wiehe K, Hwang H, et al (2014) ZDOCK server: interactive docking prediction of protein–protein complexes and symmetric multimers. Bioinformatics 30:1771–1773. https://doi.org/10.1093/bioinformatics/btu097

279. Luo Z, He L, Wang J, et al (2017) Developing a combined strategy for monitoring the progress of aptamer selection. Analyst 142:3136–3139. https://doi.org/10.1039/c7an01131h

280. Pan W, Clawson GA (2009) The shorter the better: reducing fixed primer regions of oligonucleotide libraries for aptamer selection. Molecules 14:1353–69. https://doi.org/10.3390/molecules14041353

281. Sultana A, Lee JE (2015) Measuring protein-protein and protein-nucleic acid interactions by biolayer interferometry. Curr Protoc Protein Sci 79:. https://doi.org/10.1002/0471140864.ps1925s79

282. von Köckritz-Blickwede M, Chow OA, Nizet V (2009) Fetal calf serum contains heat-stable nucleases that degrade neutrophil extracellular traps. Blood 114:5245–5246. https://doi.org/10.1182/blood-2009-08-240713

283. O'Doherty U, Swiggard WJ, Malim MH (2000) Human Immunodeficiency Virus type 1 spinoculation enhances infection through virus binding. J Virol 74:10074–10080. https://doi.org/10.1128/JVI.74.21.10074-10080.2000

284. Denning W, Das S, Guo S, et al (2013) Optimization of the transductional efficiency of lentiviral vectors: effect of sera and polycations. Mol Biotechnol 53:308–314. https://doi.org/10.1007/s12033-012-9528-5

285. Famulok M, Mayer G (2014) Aptamers and SELEX in chemistry and biology. Chem Biol 21:1055–1058. https://doi.org/10.1016/j.chembiol.2014.08.003

286. Pagratis N (1996) Rapid preparation of single stranded DNA from PCR products by streptavidin induced electrophoretic mobility shift. Nucleic Acids Res 24:3645–3646. https://doi.org/10.1093/nar/24.18.3645

287. Espelund M, Stacy RAP, Jakobsen KS (1990) A simple method for generating single-stranded DNA probes labeled to high activities. Nucleic Acids Res 18:6157–6158. https://doi.org/10.1093/nar/18.20.6157

288. Kissmann A-K, Bolotnikov G, Li R, et al (2024) IMPATIENT-qPCR: monitoring SELEX success during in vitro aptamer evolution. Appl Microbiol Biotechnol 108:284. https://doi.org/10.1007/s00253-024-13085-7

289. Mukherjee M, Appaiah P, Sistla S, et al (2022) Bio-Layer interferometry-based SELEX and label-free detection of patulin using generated aptamer. J Agric Food Chem 70:6239–6246. https://doi.org/10.1021/acs.jafc.2c01591

290. Kaur H, Shorie M, Sabherwal P (2020) Biolayer interferometry-SELEX for Shiga toxin antigenic-peptide aptamers & detection via chitosan-WSe2 aptasensor. Biosens Bioelectron 167:112498. https://doi.org/10.1016/j.bios.2020.112498

291. Nguyen HL, Lan PD, Thai NQ, et al (2020) Does SARS-CoV-2 bind to human ACE2 more strongly than does SARS-CoV? J Phys Chem B 124:7336–7347. https://doi.org/10.1021/acs.jpcb.0c04511

292. Yang G, Li Z, Mohammed I, et al (2021) Identification of SARS-CoV-2-against aptamer with high neutralization activity by blocking the RBD domain of spike protein 1. Signal Transduct Target Ther 6:. https://doi.org/10.1038/s41392-021-00649-6

293. Hellman LM, Fried MG (2007) Electrophoretic mobility shift assay (EMSA) for detecting protein–nucleic acid interactions. Nat Protoc 2:1849–1861. https://doi.org/10.1038/nprot.2007.249

294. Levay A, Brenneman R, Hoinka J, et al (2015) Identifying high-affinity aptamer ligands with defined cross-reactivity using high-throughput guided systematic evolution of ligands by exponential enrichment. Nucleic Acids Res 43:e82–e82. https://doi.org/10.1093/nar/gkv534

295. Shah NB, Duncan TM (2014) Bio-layer interferometry for measuring Kinetics of protein-protein interactions and allosteric ligand effects. Journal of Visualized Experiments. https://doi.org/10.3791/51383

296. Gelinas AD, Davies DR, Janjic N (2016) Embracing proteins: structural themes in aptamer–protein complexes. Curr Opin Struct Biol 36:122–132. https://doi.org/10.1016/j.sbi.2016.01.009

297. Mironov V, Shchugoreva IA, Artyushenko P V., et al (2022) Structure- and Interaction-Based Design of Anti-SARS-CoV-2 Aptamers. Chemistry - A European Journal 28:. https://doi.org/10.1002/chem.202104481

298. Borkotoky S, Dey D, Hazarika Z (2023) Interactions of angiotensin-converting enzyme-2 (ACE2) and SARS-CoV-2 spike receptor-binding domain (RBD): a structural perspective. Mol Biol Rep 50:2713–2721. https://doi.org/10.1007/s11033-022-08193-4

299. Fasogbon IV, Ondari EN, Tusubira D, et al (2025) Recent focus in non-SELEX-computational approach for de novo aptamer design: A mini review. Anal Biochem 699:115756. https://doi.org/10.1016/j.ab.2024.115756

300. Sun D, Sun M, Zhang J, et al (2022) Computational tools for aptamer identification and optimization. TrAC Trends in Analytical Chemistry 157:116767. https://doi.org/10.1016/j.trac.2022.116767

301. Troisi R, Balasco N, Autiero I, et al (2023) Structural insights into protein–aptamer recognitions emerged from experimental and computational studies. Int J Mol Sci 24:16318. https://doi.org/10.3390/ijms242216318

302. Alam KK, Chang JL, Burke DH (2015) FASTAptamer: A bioinformatic toolkit for high-throughput sequence analysis of combinatorial selections. Mol Ther Nucleic Acids 4:e230. https://doi.org/10.1038/mtna.2015.4

303. Bashir A, Yang Q, Wang J, et al (2021) Machine learning guided aptamer refinement and discovery. Nat Commun 12:2366. https://doi.org/10.1038/s41467-021-22555-9

304. Song J, Zheng Y, Huang M, et al (2020) A sequential multidimensional analysis algorithm for aptamer identification based on structure analysis and machine learning. Anal Chem 92:3307–3314. https://doi.org/10.1021/acs.analchem.9b05203

305. Zulkeflee Sabri M, Azzar Abdul Hamid A, Mariam Sayed Hitam S, Zulkhairi Abdul Rahim Mohd (2019) In-silico selection of aptamer: a review on the revolutionary approach to understand the aptamer design and interaction through computational chemistry. Mater Today Proc 19:1572–1581. https://doi.org/10.1016/j.matpr.2019.11.185

306. Chen Z, Hu L, Zhang B-T, et al (2021) Artificial intelligence in aptamer–target binding prediction. Int J Mol Sci 22:3605. https://doi.org/10.3390/ijms22073605

307. Berezovski M, Musheev M, Drabovich A, Krylov SN (2006) Non-SELEX selection of aptamers. J Am Chem Soc 128:1410–1411. https://doi.org/10.1021/ja056943j

308. Tsao S-M, Lai J-C, Horng H-E, et al (2017) Generation of aptamers from a primer-free randomized ssDNA library using magnetic-assisted rapid aptamer selection. Sci Rep 7:45478. https://doi.org/10.1038/srep45478

309. Ouellet E, Lagally ET, Cheung KC, Haynes CA (2014) A simple method for eliminating fixed-region interference of aptamer binding during SELEX. Biotechnol Bioeng 111:2265–2279. https://doi.org/10.1002/bit.25294

310. Pan W, Xin P, Clawson GA (2008) Minimal primer and primer-free SELEX protocols for selection of aptamers from random DNA libraries. Biotechniques 44:351–360. https://doi.org/10.2144/000112689

311. Kratschmer C, Levy M (2017) Effect of chemical modifications on aptamer stability in serum. Nucleic Acid Ther 27:335–344. https://doi.org/10.1089/nat.2017.0680

312. Oefinger PE, Shawar RM, Loo SH, et al (1990) Enhanced recovery of cytomegalovirus in conventional tube cultures with a spin-amplified adsorption. J Clin Microbiol 28:965–969. https://doi.org/10.1128/jcm.28.5.965-969.1990

313. Oefinger PE, Loo SH, Gander RM (1988) Modified spin-amplified adsorption procedure with conventional tissue culture tubes for rapid detection and increased recovery of herpes simplex virus from clinical specimens. J Clin Microbiol 26:2195–2199. https://doi.org/10.1128/jcm.26.10.2195-2199.1988

314. Guo J, Wang W, Yu D, Wu Y (2011) Spinoculation triggers dynamic actin and cofilin activity that facilitates HIV-1 infection of transformed and resting CD4 T cells. J Virol 85:9824–9833. https://doi.org/10.1128/JVI.05170-11

315. Matsuyama S, Nao N, Shirato K, et al (2020) Enhanced isolation of SARS-CoV-2 by TMPRSS2-expressing cells. Proceedings of the National Academy of Sciences 117:7001–7003. https://doi.org/10.1073/pnas.2002589117

316. Shen X-R, Geng R, Li Q, et al (2022) ACE2-independent infection of T lymphocytes by SARS-CoV-2. Signal Transduct Target Ther 7:83. https://doi.org/10.1038/s41392-022-00919-x

317. Lim S, Zhang M, Chang TL (2022) ACE2-independent alternative receptors for SARS-CoV-2. Viruses 14:2535. https://doi.org/10.3390/v14112535

318. Chen Y, Yang X, Liu J, et al (2023) In vitro selection of a single-strand DNA aptamer targeting the receptor-binding domain of SARS-CoV-2 spike protein. Nucleosides Nucleotides Nucleic Acids 42:105–118. https://doi.org/10.1080/15257770.2022.2109170

319. Li J, Zhang Z, Gu J, et al (2021) Diverse high-affinity DNA aptamers for wild-type and B.1.1.7 SARS-CoV-2 spike proteins from a pre-structured DNA library. Nucleic Acids Res 49:7267–7279. https://doi.org/10.1093/nar/gkab574

320. Schmitz A, Weber A, Bayin M, et al (2021) A SARS-CoV-2 spike binding DNA aptamer that inhibits pseudovirus infection by an RBD-independent mechanism. Angewandte Chemie International Edition 60:10279–10285. https://doi.org/10.1002/anie.202100316

321. Liang C, Guo B, Wu H, et al (2015) Aptamer-functionalized lipid nanoparticles targeting osteoblasts as a novel RNA interference–based bone anabolic strategy. Nat Med 21:288–294. https://doi.org/10.1038/nm.3791

322. Silwal AP, Thennakoon SKS, Arya SP, et al (2022) DNA aptamers inhibit SARS-CoV-2 spike-protein binding to hACE2 by an RBD- independent or dependent approach. Theranostics 12:5522–5536. https://doi.org/10.7150/thno.74428

323. Silwal AP, Jahan R, Thennakoon SKS, et al (2022) A universal DNA aptamer as an efficient inhibitor against spike-protein/hACE2 interactions. Chemical Communications 58:8049–8052. https://doi.org/10.1039/D2CC02647C

324. Sun M, Liu S, Wei X, et al (2021) Aptamer blocking strategy inhibits SARS-CoV-2 virus infection. Angewandte Chemie - International Edition 60:10266–10272. https://doi.org/10.1002/anie.202100225

325. Zhang Z, Li J, Gu J, et al (2022) A universal DNA aptamer that recognizes spike proteins of diverse SARS-CoV-2 Variants of Concern. Chemistry - A European Journal 28:. https://doi.org/10.1002/chem.202200078

326. Yang M, Li C, Ye G, et al (2024) Aptamers targeting SARS-CoV-2 nucleocapsid protein exhibit potential anti pan-coronavirus activity. Signal Transduct Target Ther 9:40. https://doi.org/10.1038/s41392-024-01748-w

327. Das D, Suresh MR (2006) Copious production of SARS-CoV nucleocapsid protein employing codon optimized synthetic gene. J Virol Methods 137:343–346. https://doi.org/10.1016/j.jviromet.2006.06.029

328. Roh C, Jo SK (2011) Quantitative and sensitive detection of SARS coronavirus nucleocapsid protein using quantum dots-conjugated RNA aptamer on chip. Journal of Chemical Technology & Biotechnology 86:. https://doi.org/10.1002/jctb.2721

329. Chen Z, Wu Q, Chen J, et al (2020) A DNA aptamer based method for detection of SARS-CoV-2 nucleocapsid protein. Virol Sin 35:351–354. https://doi.org/10.1007/s12250-020-00236-z

330. Villa A, Brunialti E, Dellavedova J, et al (2022) DNA aptamers masking angiotensin converting enzyme 2 as an innovative way to treat SARS-CoV-2 pandemic. Pharmacol Res 175:105982. https://doi.org/10.1016/j.phrs.2021.105982

331. Yang G, Zhang S, Wang Y, et al (2022) Aptamer blocking S-TLR4 interaction selectively inhibits SARS-CoV-2 induced inflammation. Signal Transduct Target Ther 7:4–6. https://doi.org/10.1038/s41392-022-00968-2

332. Ferreira-Bravo IA, Destefano JJ (2021) Xeno-nucleic acid (Xna) 2'-fluoro-arabino nucleic acid (fana) aptamers to the receptor-binding domain of sars-cov-2 s protein block ace2 binding. Viruses 13:. https://doi.org/10.3390/v13101983

333. VarnBuhler BS, Moon J, Dey SK, et al (2022) Detection of SARS-CoV-2 RNA using a DNA aptamer mimic of green fluorescent protein. ACS Chem Biol 17:840–853. https://doi.org/10.1021/acschembio.1c00893

334. Smith JE, Chávez JL, Hagen JA, Kelley-Loughnane N (2016) Design and development of aptamer-gold nanoparticle based colorimetric assays for in-the-field applications. Journal of Visualized Experiments. https://doi.org/10.3791/54063

335. Shi L, Wang L, Ma X, et al (2021) Aptamer-functionalized nanochannels for one-step detection of SARS-CoV-2 in samples from COVID-19 patients. Anal Chem 93:16646–16654. https://doi.org/10.1021/acs.analchem.1c04156

336. Song K-M, Lee S, Ban C (2012) Aptamers and their biological applications. Sensors 12:612–631. https://doi.org/10.3390/s120100612

337. Meehan C, Hamilton EL, Mansour CG, et al (2025) A new method for the reproducible development of aptamers (Neomers). PLoS One 20:e0311497. https://doi.org/10.1371/journal.pone.0311497

338. Povsic TJ, Lawrence MG, Lincoff AM, et al (2016) Pre-existing anti-PEG antibodies are associated with severe immediate allergic reactions to pegnivacogin, a PEGylated aptamer. Journal of Allergy and Clinical Immunology 138:1712–1715. https://doi.org/10.1016/j.jaci.2016.04.058

339. Ayass MA, Tripathi T, Griko N, et al (2022) Highly efficacious and safe neutralizing DNA aptamer of SARS-CoV-2 as an emerging therapy for COVID-19 disease. Virol J 19:227. https://doi.org/10.1186/s12985-022-01943-7

340. D'Agostino MR, Li J, Zhang Z, et al (2024) Respiratory mucosal administration of DNA aptamer nanomaterials protects against antigenically diverse SARS-CoV-2 variants

341. Ho W, Gao M, Li F, et al (2021) Next-generation vaccines: nanoparticle-mediated DNA and mRNA delivery. Adv Healthc Mater 10:. https://doi.org/10.1002/adhm.202001812

342. Schoenmaker L, Witzigmann D, Kulkarni JA, et al (2021) mRNA-lipid nanoparticle COVID-19 vaccines: Structure and stability. Int J Pharm 601:120586. https://doi.org/10.1016/j.ijpharm.2021.120586

343. Kumar US, Afjei R, Ferrara K, et al (2021) Gold-nanostar-chitosan-mediated delivery of SARS-CoV-2 DNA vaccine for respiratory mucosal immunization: development and proof-of-principle. ACS Nano 15:17582–17601. https://doi.org/10.1021/acsnano.1c05002

Chapter Eight: Appendix

8.1. R codes for NGS data quality assessment and processing

```
## Preparation: Installing required packages ##
install.packages("readr")
if (!require("BiocManager", quietly = TRUE))
  install.packages("BiocManager")
BiocManager::install("ShortRead")
install("ggplot2")
library(ggplot2)

# Check if properly installed
library("ShortRead")
library("ggplot2")
library("tidyr")

## Part 1: Reads fastq file and store it as data
FwdRead_1 <- readFastq("SELEX10R_S1_L001_R1_001.fastq")


## Part 2: Gives you a general overlook of the file
countFastq("SELEX10R_S1_L001_R1_001.fastq")
summary(FwdRead_1)
head(FwdRead_1)
head(sread(FwdRead_1),3)


# Plotting a histogram of the sequence lengths
reads <- sread(FwdRead_1)
widths <- as.data.frame(reads@ranges@width)
ggplot(widths) +
  geom_histogram(aes(x=reads@ranges@width))


# Check quality of reads
quals <- quality(FwdRead_1)
head(quals)

# Visualize read quality by converting the ASCII language score into
# numerical scores
numqScores <- as(quals, "matrix")
avgScore <- rowMeans(numqScores, na.rm=TRUE)
avgScore <- as.data.frame(avgScore)
ggplot(avgScore) +
  geom_histogram(aes(x=avgScore))


## Part 3: check if paired reads are really paired.
Raw1fq <- readFastq("SELEX10R_S1_L001_R1_001.fastq")
Raw2fq <- readFastq("SELEX10R_S1_L001_R2_001.fastq")
```

```
readFwdid <- Raw1fq@id
readRvsid <- Raw2fq@id

# Count how many of them is true
countTrue <- substr(readRvsid, 1, 44) == substr(readFwdid, 1, 44)
length(countTrue[countTrue==FALSE])
length(countTrue[countTrue==TRUE])
  # Check if every id matches.


## Part 4: Using the filterAndTrim, filter all the low quality reads
  # the function allocates all the low quality reads to a separate
  # file, so only high quality reads are retained.
  # Low quality reads = sequence with ambiguous calls (e.g.N nucleotides)

fnFs.filtN <- file.path("./", "filtNPaired",
basename("SELEX10R_S1_L001_R1_001.fastq"))
fnRs.filtN <- file.path("./", "filtNPaired",
basename("SELEX10R_S1_L001_R2_001.fastq"))
filterAndTrim("SELEX10R_S1_L001_R1_001.fastq", fnFs.filtN,
              "SELEX10R_S1_L001_R2_001.fastq", fnRs.filtN,
              maxN = 0, matchIDs = TRUE, multithread = FALSE)


## Part 5: Post-filter quality assessment (ShortRead workflow)
setwd("~/R/FASTQ_dada2_processing/10R_sequencing_10Mar23/filtNPaired")
fls <- dir("./", "*fastq$", full=TRUE )
qaSummary <- qa(fls, type="fastq")
browseURL(report(qaSummary))
  # A webpage summary will pop-out.


## Part 6: Removing primers
Bank40Fwd <- "TGACACCGTACCTGCTCT"
Bank40Rvs <- "ATAGTCCCTGGCGTGCTT"

# Make sure that every orientation of primer is covered
allOrients <- function(primer) {
  require(Biostrings)
  dna <- DNAString(primer)
  orients <- c(Foward = dna, Complement = complement(dna),
               Reverse = reverse(dna), RevComp = reverseComplement(dna))
  return(sapply(orients, toString))
}
FWD.orients <- allOrients(Bank40Fwd)
REV.orients <- allOrients(Bank40Rvs)
primerHits <- function(primer, fn) {
  nhits <- vcountPattern(primer, sread(readFastq(fn)), fixed=FALSE)
  return(sum(nhits>0))
}
  # summary of primers in different orientation within sequencing data
```

```
rbind(FWD.ForwardReads = sapply(FWD.orients, primerHits, fn =
fnFs.filtN[[1]]),
      FWD.ReverseReads = sapply(FWD.orients, primerHits, fn =
fnRs.filtN[[1]]),
      REV.ForwardReads = sapply(REV.orients, primerHits, fn =
fnFs.filtN[[1]]),
      REV.ReverseReads = sapply(REV.orients, primerHits, fn =
fnRs.filtN[[1]]))

# Open WSL (Windows Subsystem for Linux), cut primers
cutadapt <- "-i -c 'conda activate cutadaptenv; cutadapt --version'"
# using version 4.2 of cutadapt
FWD.RC <- dada2:::rc(Bank40Fwd)
REV.RC <- dada2:::rc(Bank40Rvs)
  # For forward reads, select the correct primer orientation, also removing
  # sequences that are too short/long (more than 5nt shorter/longer than
40nt).
  # the range of acceptable sequence reads is 35-45nt.
cutadaptFwd <- "-i -c 'conda activate cutadaptenv;
+ cutadapt -g TGACACCGTACCTGCTCT -a AAGCACGCCAGGGACTAT -m 35 -M 45 -n 2 -o
/mnt/c/Users/rchan/Documents/R/FASTQ_dada2_processing/10R_sequencing_10Mar23/
PairOut1.fastq
/mnt/c/Users/rchan/Documents/R/FASTQ_dada2_processing/10R_sequencing_10Mar23/
filtNPaired/SELEX10R_S1_L001_R1_001.fastq'"

# For the reverse reads, do the same: select correct primer orientation,
# then removing reads that do not fit our length criteria.
cutadaptRvs <- "-i -c 'conda activate cutadaptenv;
+ cutadapt -g ATAGTCCCTGGCGTGCTT -a AGAGCAGGTACGGTGTCA -m 35 -M 45 -n 2 -o
/mnt/c/Users/rchan/Documents/R/FASTQ_dada2_processing/10R_sequencing_10Mar23/
PairOut2.fastq
/mnt/c/Users/rchan/Documents/R/FASTQ_dada2_processing/10R_sequencing_10Mar23/
filtNPaired/SELEX10R_S1_L001_R2_001.fastq'"


## Part 7: Match pairend reads, using filterAndTrim function
setwd("~/R/FASTQ_dada2_processing/10R_sequencing_10Mar23")
fnFs.filtN <- file.path("./", "RePairing", basename("PairOut1.fastq"))
fnRs.filtN <- file.path("./", "RePairing", basename("PairOut2.fastq"))
filterAndTrim("PairOut1.fastq", fnFs.filtN,
              "PairOut2.fastq", fnRs.filtN,
              maxN = 0, matchIDs = TRUE, multithread = FALSE)
  # visualize primers in sequences, we should expect none
rbind(FWD.ForwardReads = sapply(FWD.orients, primerHits, fn =
fnFs.filtN[[1]]),
       FWD.ReverseReads = sapply(FWD.orients, primerHits, fn =
fnRs.filtN[[1]]),
       REV.ForwardReads = sapply(REV.orients, primerHits, fn =
fnFs.filtN[[1]]),
       REV.ReverseReads = sapply(REV.orients, primerHits, fn =
fnRs.filtN[[1]]))
```

```
  # Plotting data to assess quality of trimming
setwd("~/R/FASTQ_dada2_processing/10R_sequencing_10Mar23/RePairing")
PairedTrimedSeq <- readFastq("PairOut1.fastq")
sread(PairedTrimedSeq)

reads <- sread(PairedTrimedSeq)
widths <- as.data.frame(reads@ranges@width)
ggplot(widths) +
   geom_histogram(aes(x=reads@ranges@width))

# now do the reverse reads
PairedTrimedSeq2 <- readFastq("PairOut2.fastq")
sread(PairedTrimedSeq2)
reads <- sread(PairedTrimedSeq2)
widths <- as.data.frame(reads@ranges@width)
ggplot(widths) +
  geom_histogram(aes(x=reads@ranges@width))
  # The length of prodominant seuquences should be 40nt


## Part 8: assess quality of trim reads
fnFs <- sort(list.files("./", pattern="PairOut1.fastq", full.names = TRUE))
fnRs <- sort(list.files("./", pattern="PairOut2.fastq", full.names = TRUE))
plotQualityProfile(fnFs[1:2])
plotQualityProfile(fnRs[1:2])


## Part 9: learning error rates for sequence merging
errF <- learnErrors(fnFs, multithread = FALSE)
errR <- learnErrors(fnRs, multithread = FALSE)
plotErrors(errF, nominalQ = TRUE)
  # Assess the quality of estimation before proceeding


## Part 10: Dereplicate reads and calculate frequency
derepFs <- derepFastq(fnFs, verbose = TRUE)
derepRs <- derepFastq(fnRs, verbose = TRUE)

# Part 10: inference sample and merging
dadaFs <- dada(derepFs, err = errF, multithread = FALSE)
dadaRs <- dada(derepRs, err = errR, multithread = FALSE)
mergers <- mergePairs(dadaFs, derepFs, dadaRs, derepRs, verbose=TRUE)

# Export top 10 sequences into excel file
library("writexl")
write_xlsx(mergers,"~/R/FASTQ_dada2_processing/10R_sequencing_10Mar23/mergers
.xlsx")
```

8.2. Printed Cutadapt NGS data processing summary

```
=== Forward Read Summary ===

Total reads processed:                 404,548
Reads with adapters:                   396,494 (98.0%)

== Read fate breakdown ==
Reads that were too short:             258,167 (63.8%)
Reads that were too long:              112,575 (27.8%)
Reads written (passing filters):        33,806 (8.4%)

Total basepairs processed:    35,827,144 bp
Total written (filtered):      1,358,055 bp (3.8%)


=== Reverse Read Summary ===

Total reads processed:                 404,548
Reads with adapters:                   333,244 (82.4%)

== Read fate breakdown ==
Reads that were too short:             230,827 (57.1%)
Reads that were too long:              152,720 (37.8%)
Reads written (passing filters):        21,001 (5.2%)

Total basepairs processed:    35,201,746 bp
Total written (filtered):        865,829 bp (2.5%)
```

8.3. Buffer formula

10X TBE Running Buffer:

108 g	tris base
55 g	boric acid
900 ml	Distilled H_2O
40 ml	0.5 M EDTA solution (pH 8.0)

Adjust volume to 1 L.

Chapter Nine: Copyright Permissions

Figure 1. No authorization needed as stated by journal policies.

Figure 2. Copyright clearance is attached.

Figure 3. Copyright clearance is attached.

Figure 4. No authorization needed as stated by journal policies.

SPRINGER NATURE LICENSE
TERMS AND CONDITIONS

Dec 02, 2023

This Agreement between Ms. Rose Chan ("You") and Springer Nature ("Springer Nature") consists of your license details and the terms and conditions provided by Springer Nature and Copyright Clearance Center.

License Number	5681020009029
License date	Dec 02, 2023
Licensed Content Publisher	Springer Nature
Licensed Content Publication	Nature
Licensed Content Title	Structure of the SARS-CoV-2 spike receptor- binding domain bound to the ACE2 receptor
Licensed Content Author	Jun Lan et al
Licensed Content Date	Mar 30, 2020
Type of Use	Thesis/Dissertation
Requestor type	academic/university or research institute
Format	print and electronic
Portion	figures/tables/illustrations

Number of figures/tables/illustrations 1

Would you like a high resolution image with your order?	no
Will you be translating?	no
Circulation/distribution	500 - 999
Author of this Springer Nature content	no
Title of new work	Development and analysis of SARS-CoV-2 spike receptor binding domain-targeting aptamer
Institution name	University of Manitoba
Expected presentation	Feb 2024
Portions	Figure 1 (A)
Requestor Location	Ms. Rose Chan [redacted] [redacted] Attn: University of Manitoba
Total	0.00 CAD

Terms and Conditions

Springer Nature Customer Service Centre GmbH Terms and Conditions

The following terms and conditions ("Terms and Conditions") together with the terms specified in your [RightsLink] constitute the License ("License") between you as Licensee and Springer Nature Customer Service Centre GmbH as Licensor. By clicking 'accept' and completing the transaction for your use of the material ("Licensed Material"), you confirm your acceptance of and obligation to be bound by these Terms and Conditions.

1. Grant and Scope of License

1. 1. The Licensor grants you a personal, non-exclusive, non-transferable, non-sublicensable, revocable, world-wide License to reproduce, distribute, communicate to the public, make available, broadcast, electronically transmit or create derivative works using the Licensed Material for the purpose(s) specified in your RightsLink Licence Details only. Licenses are granted for the specific use requested in the order and for no other use, subject to these Terms and Conditions. You acknowledge and agree that the rights granted to you under this License do not include the right to modify, edit, translate, include in collective works, or create derivative works of the Licensed Material in whole or in part unless expressly stated in your RightsLink Licence Details. You may use the Licensed Material only as permitted under this Agreement and will not reproduce, distribute, display, perform, or otherwise use or exploit any Licensed Material in any way, in whole or in part, except as expressly permitted by this License.

1. 2. You may only use the Licensed Content in the manner and to the extent permitted by these Terms and Conditions, by your RightsLink Licence Details and by any applicable laws.

1. 3. A separate license may be required for any additional use of the Licensed Material, e.g. where a license has been purchased for print use only, separate permission must be obtained for electronic re-use. Similarly, a License is only valid in the language selected and does not apply for editions in other languages unless additional translation rights have been granted separately in the License.

1. 4. Any content within the Licensed Material that is owned by third parties is expressly excluded from the License.

1. 5. Rights for additional reuses such as custom editions, computer/mobile applications, film or TV reuses and/or any other derivative rights requests require additional permission and may be subject to an additional fee. Please apply to journalpermissions@springernature.com or bookpermissions@springernature.com for these rights.

2. Reservation of Rights

Licensor reserves all rights not expressly granted to you under this License. You acknowledge and agree that nothing in this License limits or restricts Licensor's rights in or use of the Licensed Material in any way. Neither this License, nor any act, omission, or statement by Licensor or you, conveys any ownership right to you in any Licensed Material, or to any element or portion thereof. As between Licensor and you, Licensor owns and retains all right, title, and interest in and to the Licensed Material subject to the license granted in Section 1.1. Your permission to use the Licensed Material is expressly conditioned on you not impairing Licensor's or the applicable copyright owner's rights in the Licensed Material in any way.

3. Restrictions on use

3. 1. Minor editing privileges are allowed for adaptations for stylistic purposes or formatting purposes provided such alterations do not alter the original meaning or intention of the Licensed Material and the new figure(s) are still accurate and representative of the Licensed Material. Any other changes including but not limited to, cropping, adapting, and/or omitting material that affect the meaning, intention or moral rights of the author(s) are strictly prohibited.

3. 2. You must not use any Licensed Material as part of any design or trademark.

3. 3. Licensed Material may be used in Open Access Publications (OAP), but any such reuse must include a clear acknowledgment of this permission visible at the same time as the figures/tables/illustration or abstract and which must indicate that the Licensed Material is not part of the governing OA license but has been reproduced with permission. This may be indicated according to any standard referencing system but must include at a minimum 'Book/Journal title, Author, Journal Name (if applicable), Volume (if applicable), Publisher, Year, reproduced with permission from SNCSC'.

4. STM Permission Guidelines

4. 1. An alternative scope of license may apply to signatories of the STM Permissions Guidelines ("STM PG") as amended from time to time and made available at https://www.stm-assoc.org/intellectual-property/permissions/permissions-guidelines/.

4. 2. For content reuse requests that qualify for permission under the STM PG, and which may be updated from time to time, the STM PG supersede the terms and conditions contained in this License.

4. 3. If a License has been granted under the STM PG, but the STM PG no longer apply at the time of publication, further permission must be sought from the Rightsholder. Contact journalpermissions@springernature.com or bookpermissions@springernature.com for these rights.

5. Duration of License

5. 1. Unless otherwise indicated on your License, a License is valid from the date of purchase ("License Date") until the end of the relevant period in the below table:

Reuse in a medical communications project	Reuse up to distribution or time period indicated in License
Reuse in a dissertation/thesis	Lifetime of thesis
Reuse in a journal/magazine	Lifetime of journal/magazine
Reuse in a book/textbook	Lifetime of edition

Reuse on a website	1 year unless otherwise specified in the License
Reuse in a presentation/slide kit/poster	Lifetime of presentation/slide kit/poster. Note: publication whether electronic or in print of presentation/slide kit/poster may require further permission.
Reuse in conference proceedings	Lifetime of conference proceedings
Reuse in an annual report	Lifetime of annual report
Reuse in training/CME materials	Reuse up to distribution or time period indicated in License
Reuse in newsmedia	Lifetime of newsmedia
Reuse in coursepack/classroom materials	Reuse up to distribution and/or time period indicated in license

6. Acknowledgement

6. 2. The Licensor's permission must be acknowledged next to the Licensed Material in print. In electronic form, this acknowledgement must be visible at the same time as the figures/tables/illustrations or abstract and must be hyperlinked to the journal/book's homepage.

6. 2. Acknowledgement may be provided according to any standard referencing system and at a minimum should include "Author, Article/Book Title, Journal name/Book imprint, volume, page number, year, Springer Nature".

7. Reuse in a dissertation or thesis

7. 1. Where 'reuse in a dissertation/thesis' has been selected, the following terms apply: Print rights of the Version of Record are provided for; electronic rights for use only on institutional repository as defined by the Sherpa guideline (www.sherpa.ac.uk/romeo/) and only up to what is required by the awarding institution.

7. 2. For theses published under an ISBN or ISSN, separate permission is required. Please contact journalpermissions@springernature.com or bookpermissions@springernature.com for these rights.

7. 3. Authors must properly cite the published manuscript in their thesis according to current citation standards and include the following acknowledgement: '*Reproduced with permission from Springer Nature*'.

8. License Fee

You must pay the fee set forth in the License Agreement (the "License Fees"). All amounts payable by you under this License are exclusive of any sales, use,

withholding, value added or similar taxes, government fees or levies or other assessments. Collection and/or remittance of such taxes to the relevant tax authority shall be the responsibility of the party who has the legal obligation to do so.

9. Warranty

9. 1. The Licensor warrants that it has, to the best of its knowledge, the rights to license reuse of the Licensed Material. **You are solely responsible for ensuring that the material you wish to license is original to the Licensor and does not carry the copyright of another entity or third party (as credited in the published version).** If the credit line on any part of the Licensed Material indicates

that it was reprinted or adapted with permission from another source, then you should seek additional permission from that source to reuse the material.

9. 2. EXCEPT FOR THE EXPRESS WARRANTY STATED HEREIN AND TO THE EXTENT PERMITTED BY APPLICABLE LAW, LICENSOR PROVIDES THE LICENSED MATERIAL "AS IS" AND MAKES NO OTHER REPRESENTATION OR WARRANTY. LICENSOR EXPRESSLY DISCLAIMS ANY LIABILITY FOR ANY CLAIM ARISING FROM OR OUT OF THE CONTENT, INCLUDING BUT NOT LIMITED TO ANY ERRORS, INACCURACIES, OMISSIONS, OR DEFECTS CONTAINED THEREIN, AND ANY IMPLIED OR EXPRESS WARRANTY AS TO MERCHANTABILITY OR FITNESS FOR A PARTICULAR PURPOSE. IN NO EVENT SHALL LICENSOR BE LIABLE TO YOU OR ANY OTHER PARTY OR ANY OTHER PERSON OR FOR ANY SPECIAL, CONSEQUENTIAL, INCIDENTAL, INDIRECT, PUNITIVE, OR EXEMPLARY DAMAGES, HOWEVER CAUSED, ARISING OUT OF OR IN CONNECTION WITH THE DOWNLOADING, VIEWING OR USE OF THE LICENSED MATERIAL REGARDLESS OF THE FORM OF ACTION, WHETHER FOR BREACH OF CONTRACT, BREACH OF WARRANTY, TORT, NEGLIGENCE, INFRINGEMENT OR OTHERWISE (INCLUDING, WITHOUT LIMITATION, DAMAGES BASED ON LOSS OF PROFITS, DATA, FILES, USE, BUSINESS OPPORTUNITY OR CLAIMS OF THIRD PARTIES), AND WHETHER OR NOT THE PARTY HAS BEEN ADVISED OF THE POSSIBILITY OF SUCH DAMAGES. THIS LIMITATION APPLIES NOTWITHSTANDING ANY FAILURE OF ESSENTIAL PURPOSE OF ANY LIMITED REMEDY PROVIDED HEREIN.

10. Termination and Cancellation

10. 1. The License and all rights granted hereunder will continue until the end of the applicable period shown in Clause 5.1 above. Thereafter, this license will be terminated and all rights granted hereunder will cease.

10. 2. Licensor reserves the right to terminate the License in the event that payment is not received in full or if you breach the terms of this License.

11. General

11. 1. The License and the rights and obligations of the parties hereto shall be construed, interpreted and determined in accordance with the laws of the Federal Republic of Germany without reference to the stipulations of the CISG (United Nations Convention on Contracts for the International Sale of Goods) or to Germany´s choice-of-law principle.

11. 2. The parties acknowledge and agree that any controversies and disputes arising out of this License shall be decided exclusively by the courts of or having jurisdiction for Heidelberg, Germany, as far as legally permissible.

11. 3. This License is solely for Licensor's and Licensee's benefit. It is not for the

benefit of any other person or entity.

Questions? For questions on Copyright Clearance Center accounts or website issues please contact springernaturesupport@copyright.com or +1-855-239-3415 (toll free in the US) or +1-978-646-2777. For questions on Springer Nature licensing please visit https://www.springernature.com/gp/partners/rights-permissions-third-party-distribution

Other Conditions:

Version 1.4 - Dec 2022

Questions? customercare@copyright.com.

SPRINGER NATURE LICENSE
TERMS AND CONDITIONS

Dec 03, 2023

This Agreement between Ms. Rose Chan ("You") and Springer Nature ("Springer Nature") consists of your license details and the terms and conditions provided by Springer Nature and Copyright Clearance Center.

License Number	5681510690414
License date	Dec 03, 2023
Licensed Content Publisher	Springer Nature
Licensed Content Publication	Nature Reviews Microbiology
Licensed Content Title	Coronavirus biology and replication: implications for SARS-CoV-2
Licensed Content Author	Philip V'kovski et al
Licensed Content Date	Oct 28, 2020
Type of Use	Thesis/Dissertation
Requestor type	academic/university or research institute
Format	print and electronic
Portion	figures/tables/illustrations
Number of figures/tables/illustrations	1

Would you like a high resolution image with your order?	no
Will you be translating?	no
Circulation/distribution	500 - 999
Author of this Springer Nature content	no
Title of new work	Development and analysis of SARS-CoV-2 spike receptor binding domain-targeting aptamer
Institution name	University of Manitoba
Expected presentation date	Feb 2024
Portions	Fig 1 A and B
Requestor Location	Ms. Rose Chan [redacted] [redacted] [redacted] [redacted]
Total	0.00 CAD
Terms and Conditions	

Springer Nature Customer Service Centre GmbH Terms and Conditions

The following terms and conditions ("Terms and Conditions") together with the terms specified in your [RightsLink] constitute the License ("License") between you as Licensee and Springer Nature Customer Service Centre GmbH as Licensor. By clicking 'accept' and completing the transaction for your use of the material ("Licensed Material"), you confirm your acceptance of and obligation to be bound by these Terms and Conditions.

1. Grant and Scope of License

1. 1. The Licensor grants you a personal, non-exclusive, non-transferable, non-sublicensable, revocable, world-wide License to reproduce, distribute, communicate to the public, make available, broadcast, electronically transmit or create derivative works using the Licensed Material for the purpose(s) specified in your RightsLink Licence Details only. Licenses are granted for the specific use requested in the order and for no other use, subject to these Terms and Conditions. You acknowledge and agree that the rights granted to you under this License do not include the right to modify, edit, translate, include in collective works, or create derivative works of the Licensed Material in whole or in part unless expressly stated in your RightsLink Licence Details. You may use the Licensed Material only as permitted under this Agreement and will not reproduce, distribute, display, perform, or otherwise use or exploit any Licensed Material in any way, in whole or in part, except as expressly permitted by this License.

1. 2. You may only use the Licensed Content in the manner and to the extent permitted by these Terms and Conditions, by your RightsLink Licence Details and by any applicable laws.

1. 3. A separate license may be required for any additional use of the Licensed Material, e.g. where a license has been purchased for print use only, separate permission must be obtained for electronic re-use. Similarly, a License is only valid in the language selected and does not apply for editions in other languages unless additional translation rights have been granted separately in the License.

1. 4. Any content within the Licensed Material that is owned by third parties is expressly excluded from the License.

1. 5. Rights for additional reuses such as custom editions, computer/mobile applications, film or TV reuses and/or any other derivative rights requests require additional permission and may be subject to an additional fee. Please apply to journalpermissions@springernature.com or bookpermissions@springernature.com for these rights.

2. Reservation of Rights

Licensor reserves all rights not expressly granted to you under this License. You acknowledge and agree that nothing in this License limits or restricts Licensor's rights in or use of the Licensed Material in any way. Neither this License, nor any act, omission, or statement by Licensor or you, conveys any ownership right to you in any Licensed Material, or to any element or portion thereof. As between Licensor and you, Licensor owns and retains all right, title, and interest in and to the Licensed Material subject to the license granted in Section 1.1. Your permission to use the Licensed Material is expressly conditioned on you not impairing Licensor's or the applicable copyright owner's rights in the Licensed Material in any way.

3. Restrictions on use

3. 1. Minor editing privileges are allowed for adaptations for stylistic purposes or formatting purposes provided such alterations do not alter the original meaning or intention of the Licensed Material and the new figure(s) are still accurate and representative of the Licensed Material. Any other changes including but not limited to, cropping, adapting, and/or omitting material that affect the meaning, intention or moral rights of the author(s) are strictly prohibited.

3. 2. You must not use any Licensed Material as part of any design or trademark.

3. 3. Licensed Material may be used in Open Access Publications (OAP), but any such reuse must include a clear acknowledgment of this permission visible at the same time as the figures/tables/illustration or abstract and which must indicate that the Licensed Material is not part of the governing OA license but has been reproduced with permission. This may be indicated according to any standard referencing system but must include at a minimum 'Book/Journal title, Author, Journal Name (if applicable), Volume (if applicable), Publisher, Year, reproduced with permission from SNCSC'.

4. STM Permission Guidelines

4. 1. An alternative scope of license may apply to signatories of the STM Permissions Guidelines ("STM PG") as amended from time to time and made available at https://www.stm-assoc.org/intellectual-property/permissions/permissions-guidelines/.

4. 2. For content reuse requests that qualify for permission under the STM PG, and which may be updated from time to time, the STM PG supersede the terms and conditions contained in this License.

4. 3. If a License has been granted under the STM PG, but the STM PG no longer apply at the time of publication, further permission must be sought from the Rightsholder. Contact journalpermissions@springernature.com or bookpermissions@springernature.com for these rights.

5. Duration of License

5. 1. Unless otherwise indicated on your License, a License is valid from the date of purchase ("License Date") until the end of the relevant period in the below table:

Reuse in a medical communications project	Reuse up to distribution or time period indicated in License
Reuse in a dissertation/thesis	Lifetime of thesis
Reuse in a journal/magazine	Lifetime of journal/magazine
Reuse in a book/textbook	Lifetime of edition

Reuse on a website	1 year unless otherwise specified in the License
Reuse in a presentation/slide kit/poster	Lifetime of presentation/slide kit/poster. Note: publication whether electronic or in print of presentation/slide kit/poster may require further permission.
Reuse in conference proceedings	Lifetime of conference proceedings

Reuse in an annual report	Lifetime of annual report
Reuse in training/CME materials	Reuse up to distribution or time period indicated in License
Reuse in newsmedia	Lifetime of newsmedia
Reuse in coursepack/classroom materials	Reuse up to distribution and/or time period indicated in license

6. Acknowledgement

6. 1. The Licensor's permission must be acknowledged next to the Licensed Material in print. In electronic form, this acknowledgement must be visible at the same time as the figures/tables/illustrations or abstract and must be hyperlinked to the journal/book's homepage.

6. 2. Acknowledgement may be provided according to any standard referencing system and at a minimum should include "Author, Article/Book Title, Journal name/Book imprint, volume, page number, year, Springer Nature".

7. Reuse in a dissertation or thesis

7. 1. Where 'reuse in a dissertation/thesis' has been selected, the following terms apply: Print rights of the Version of Record are provided for; electronic rights for use only on institutional repository as defined by the Sherpa guideline (www.sherpa.ac.uk/romeo/) and only up to what is required by the awarding institution.

7. 2. For theses published under an ISBN or ISSN, separate permission is required. Please contact journalpermissions@springernature.com or bookpermissions@springernature.com for these rights.

7. 3. Authors must properly cite the published manuscript in their thesis according to current citation standards and include the following acknowledgement: '*Reproduced with permission from Springer Nature*'.

8. License Fee

You must pay the fee set forth in the License Agreement (the "License Fees"). All amounts payable by you under this License are exclusive of any sales, use, withholding, value added or similar taxes, government fees or levies or other assessments. Collection and/or remittance of such taxes to the relevant tax authority shall be the responsibility of the party who has the legal obligation to do so.

9. Warranty

9. 1. The Licensor warrants that it has, to the best of its knowledge, the rights to license reuse of the Licensed Material. **You are solely responsible for ensuring that the material you wish to license is original to the Licensor and does not carry the copyright of another entity or third party (as credited in the published version).** If the credit line on any part of the Licensed Material indicates

that it was reprinted or adapted with permission from another source, then you should seek additional permission from that source to reuse the material.

9. 2. EXCEPT FOR THE EXPRESS WARRANTY STATED HEREIN AND TO THE EXTENT PERMITTED BY APPLICABLE LAW, LICENSOR PROVIDES THE LICENSED MATERIAL "AS IS" AND MAKES NO OTHER REPRESENTATION OR WARRANTY. LICENSOR EXPRESSLY DISCLAIMS ANY LIABILITY FOR ANY CLAIM ARISING FROM OR OUT OF THE CONTENT, INCLUDING BUT NOT LIMITED TO ANY ERRORS, INACCURACIES, OMISSIONS, OR DEFECTS CONTAINED THEREIN, AND ANY IMPLIED OR EXPRESS WARRANTY AS TO MERCHANTABILITY OR FITNESS FOR A PARTICULAR PURPOSE. IN NO EVENT SHALL LICENSOR BE LIABLE TO YOU OR ANY OTHER PARTY OR ANY OTHER PERSON OR FOR ANY SPECIAL, CONSEQUENTIAL, INCIDENTAL, INDIRECT, PUNITIVE, OR EXEMPLARY DAMAGES, HOWEVER CAUSED, ARISING OUT OF OR IN CONNECTION WITH THE DOWNLOADING, VIEWING OR USE OF THE LICENSED MATERIAL REGARDLESS OF THE FORM OF ACTION, WHETHER FOR BREACH OF CONTRACT, BREACH OF WARRANTY, TORT, NEGLIGENCE, INFRINGEMENT OR OTHERWISE (INCLUDING, WITHOUT LIMITATION, DAMAGES BASED ON LOSS OF PROFITS, DATA, FILES, USE, BUSINESS OPPORTUNITY OR CLAIMS OF THIRD PARTIES), AND WHETHER OR NOT THE PARTY HAS BEEN ADVISED OF THE POSSIBILITY OF SUCH DAMAGES. THIS LIMITATION APPLIES NOTWITHSTANDING ANY FAILURE OF ESSENTIAL PURPOSE OF ANY LIMITED REMEDY PROVIDED HEREIN.

10. Termination and Cancellation

10. 1. The License and all rights granted hereunder will continue until the end of the applicable period shown in Clause 5.1 above. Thereafter, this license will be terminated and all rights granted hereunder will cease.

10. 2. Licensor reserves the right to terminate the License in the event that payment is not received in full or if you breach the terms of this License.

11. General

11. 1. The License and the rights and obligations of the parties hereto shall be

construed, interpreted and determined in accordance with the laws of the Federal Republic of Germany without reference to the stipulations of the CISG (United Nations Convention on Contracts for the International Sale of Goods) or to Germany´s choice-of-law principle.

11. 2. The parties acknowledge and agree that any controversies and disputes arising out of this License shall be decided exclusively by the courts of or having jurisdiction for Heidelberg, Germany, as far as legally permissible.

11. 3. This License is solely for Licensor's and Licensee's benefit. It is not for the benefit of any other person or entity.

Questions? For questions on Copyright Clearance Center accounts or website issues please contact springernaturesupport@copyright.com or +1-855-239-3415 (toll free in the US) or +1-978-646-2777. For questions on Springer Nature licensing please visit https://www.springernature.com/gp/partners/rights-permissions-third-party-distribution

Other Conditions:

Version 1.4 - Dec 2022

Questions? customercare@copyright.com.